II Data

Organic crystals, liquid crystals and polymers

50 $SC(NH_2)_2$ family

50A Pure compound

No. 50A-1 $SC(NH_2)_2$, Thiourea

(M = 76.12; [D: 80.15])

1a Ferroelectricity in $SC(NH_2)_2$ was discovered by Solomon in 1956. 56Sol

b	phase [*])	V [a])	V' [f]) [**])	IV [a])	III [a])	II [a])	I [a])
	state	F [b])	F [f])		F [a])		P [b])
	crystal system	orthorhombic [a])					orthorhombic [c]) [d])
	space group	$Pb2_1m - C_{2v}^2$ [a])					$Pbnm - D_{2h}^{16}$ [c]) [d]) [e])
	Θ [K]	161	169	176	180	202	
		[D:	185	192	196	213] [***])	

[a]) 59Gol
[b]) 56Sol
[c]) 28Dem
[d]) 32Wyc
[e]) 28Hen
[f]) 96Mag

[*]) The phases are numbered from the high-temperature phase obeying the general rule adopted in this volume (cf. IC of Introduction). Thus the names of phases here are different from those in volumes III/3 and III/9, where the phases were numbered from the low-temperature phase following Goldsmith and White. 59Gol

[**]) Recent studies make clear gradually the transition region between phases V and IV. The region depends on the small crystalline field very much. At present $\Theta_{V'\text{-}IV}$ is considered to be the ferroelectric transition temperature, however, many papers published before disregarded the existence of phase V'.

[***]) D: data on deuterated thiourea $SC(ND_2)_2$.

Phase and successive phase transition temperatures: see also 96Mag
P_s || [010] in phases III and V. 59Gol
Two kinds of settings are currently used for the choice of the unit cell vectors:
1: (***a***, ***b***, ***c***), ***b*** || $\boldsymbol{P}_s$. Space group of phase I: Pbnm. 59Gol
2: (***a′***, ***b′***, ***c′***), ***a′*** || $\boldsymbol{P}_s$. Space group of phase I: Pnma. 68Elc
In the following, the choice of the setting is additionally written when the case 2 is used.
$\rho = 1.406 \cdot 10^3$ kg m^{-3} at RT. 10Gro
Transparent, colorless. 56Sol
Cleavage plane: (010). 59Gol
There is a report that the phase IV is not a single phase but contains a ferroelectric region in it; see subsection 5c. 62Fut
See also 96Mag
High pressure phase VI is centrosymmetric from SHG and pyroelectric measurement. 82Ori

2a Crystal growth: evaporation method from a saturated solution in methanol. 56Sol
b Crystal form: Fig. 50A-1-001.

3a Unit cell parameters: Table 50A-1-001, Table 50A-1-002.

b	$Z = 4$ in phases I [a]) and V [b]).	[a]) 32Wyc, 28Dem [b]) 59Gol
	Crystal structure of phase I: Table 50A-1-003, Table 50A-1-004, Table 50A-1-005; Fig. 50A-1-002, Fig. 50A-1-003, Fig. 50A-1-004.	
	See also	32Wyc, 28Dem, 58Kun, 60Dvo, 61Vai, 67Tru, 78Mul1
	Crystal structure of phase V: Table 50A-1-003, Table 50A-1-004, Table 50A-1-005, Table 50A-1-006; Fig. 50A-1-004, Fig. 50A-1-005, Fig. 50A-1-006.	
	Libration of molecules in phases I and V: Table 50A-1-007; Fig. 50A-1-007, Fig. 50A-1-008.	
	Electron density distributions in phase V at 123 K: see	78Mul2, 82Kut, 82Mul
	In phases II, III, and IV, crystal structure is modulated by a sinusoidal wave along the c axis. The amplitudes of the modulation wave are given as follows:	71Shi
	$\alpha_j = a_j(\Theta_{I-II} - T)$ $a_S = 0.0008$ $a_C = 0.0010$ $a_N = 0.0013$	
	$\beta_j = b_j(\Theta_{I-II} - T)^{1/2}$ $b_S = 0.0067$ $b_C = 0.0015$ $b_N = 0.0005$	
	$M = 8.0 + 0.0018\ (\Theta_{I-II} - T)^2$ α_j, β_j: x, y components of the amplitude of the modulation wave. Θ_{II-I}: transition temperature between phase I and phase II. M: period of the modulation wave. $M = 1/\delta$.	
	Structure of incommensurately modulated phases: Table 50A-1-008, Table 50A-1-009, Table 50A-1-010; Fig. 50A-1-009, Fig. 50A-1-010.	
	See also	87Tak, 88Gao
	Crystal structure with $M = 9$: Table 50A-1-011, Table 50A-1-012, Table 50A-1-013, Table 50A-1-014, Table 50A-1-015; Fig. 50A-1-011, Fig. 50A-1-012, Fig. 50A-1-013, Fig. 50A-1-014.	
	See also	88Sim, 90Mad, 91Mas
	Review of the modulated structure: see See subsection 14a about modulation wave vector and diffraction phenomena related with structural modulation.	89Zun
	Superstructure with $3c$ appears in phase VI induced at high pressure.	61Kab, 80Mou1
4	Lattice distortions: Fig. 50A-1-015; see also	78Jak

5a, b	Dielectric constants in wide temperature range: Fig. 50A-1-016, Fig. 50A-1-017, Fig. 50A-1-018, Fig. 50A-1-019, Fig. 50A-1-020, Fig. 50A-1-021, Fig. 50A-1-022, Fig. 50A-1-023, Fig. 50A-1-024, Fig. 50A-1-025, Fig. 50A-1-026, Fig. 50A-1-027, Fig. 50A-1-028, Fig. 50A-1-029, Fig. 50A-1-030.	
	$\kappa_b = C/(T - \Theta_p)$ $T > \Theta_{II-I}$, where $C = 3.7 \cdot 10^3$ K, $\Theta_p = 185$ K, $\Theta_{II-I} = 202$ K.	59Gol
	κ_a, $\kappa_c \approx 3$ ($f = 1$ kHz). Their temperature variations are negligible in the temperature range from 77 K to RT.	
	Dielectric constant around Θ_{II-I} and in phase II: Fig. 50A-1-031, Fig. 50A-1-032; as for time dependence of dielectric constant in phase II, see	94Ono1
	Dielectric constant around phase III: Fig. 50A-1-033, Fig. 50A-1-034, Fig. 50A-1-035, Fig. 50A-1-036, Fig. 50A-1-037.	
	See also	82Jam, 92Che, 93Kan
	Dielectric constant in phase V: Fig. 50A-1-038, Fig. 50A-1-039, Fig. 50A-1-040, Fig. 50A-1-041, Fig. 50A-1-042, Fig. 50A-1-043, Fig. 50A-1-044, Fig. 50A-1-045, Fig. 50A-1-046.	
	See also	94Kan
	Phase diagram in regard to biasing field: Table 50A-1-016; Fig. 50A-1-047, Fig. 50A-1-048, Fig. 50A-1-049, Fig. 50A-1-050, Fig. 50A-1-051, Fig. 50A-1-052, Fig. 50A-1-053, Fig. 50A-1-054.	
	Effects of hydrostatic pressure on κ_b: Fig. 50A-1-055.	
	Phase diagram in regard to hydrostatic pressure: Table 50A-1-017; Fig. 50A-1-056, Fig. 50A-1-057, Fig. 50A-1-058.	
	Effect of uniaxial stress on dielectric constant: see	92Gla
c	Spontaneous polarization: Fig. 50A-1-059, Fig. 50A-1-060, Fig. 50A-1-061.	
	Coercive field: Fig. 50A-1-062.	
	In phases II, III, and IV, double, single-double, double-double hysteresis loops are observed. According to Futama there is a very narrow ferroelectric region at about 171 K within the phase IV.	62Fut
	Effect of hydrostatic pressure on P_s and E_c: Fig. 50A-1-063, Fig. 50A-1-064.	
d	Pyroelectricity: Fig. 50A-1-065.	
6a	Transition heats and transition entropies: Table 50A-1-018.	
	Heat capacity: Fig. 50A-1-066, Fig. 50A-1-067, Fig. 50A-1-068.	
	Effect of electric field on heat capacity: see	89Lee
	Critical behavior of heat capacity in $SC(ND_2)_2$: see	94Ono2
	Complex heat capacity at $f = 1$ Hz: see	96Noz
8a	Velocity of ultrasonic wave: Fig. 50A-1-069.	
	Elastic constants:	
	from ultrasonic measurements: Fig. 50A-1-070, Fig. 50A-1-071, Fig. 50A-1-072;	
	from Brillouin scattering: Fig. 50A-1-073, Fig. 50A-1-074, Fig. 50A-1-075.	
	Elastic constants and thermoelastic constants: Table 50A-1-019.	
	Effects of electric field on elastic constant: Fig. 50A-1-076.	
	Effects of pressure on elastic constant: Fig. 50A-1-077, Fig. 50A-1-078, Fig. 50A-1-079.	
	Attenuation coefficient of ultrasonic wave: Fig. 50A-1-080, Fig. 50A-1-081, Fig. 50A-1-082.	
b	Third order elastic constants: Table 50A-1-020.	
9a	Optical axial plane is normal to ***a***.	71Jef
	Optical axial angle: $(-)2V = 36°$ for white light.	71Jef
	Refractive indices: $n_a = 1.789$, $n_b = 1.634$, $n_c = 1.806$ at $\lambda = 514$ nm, $T = 20$ °C.	54Win
	Birefringence: Fig. 50A-1-083, Fig. 50A-1-084, Fig. 50A-1-085.	

	Birefringence under electric field: Fig. 50A-1-086, Fig. 50A-1-087.	
	Infrared reflection spectra: Fig. 50A-1-088; see also	80Sia, 80Win2
d	Optical activity: see	94Bil
10a	Spectra of Raman scattering: Fig. 50A-1-089, Fig. 50A-1-090, Fig. 50A-1-091, Fig. 50A-1-092, Fig. 50A-1-093, Fig. 50A-1-094, Fig. 50A-1-095. Frequencies of lattice vibrations obtained by Raman spectra: Table 50A-1-021; Fig. 50A-1-089, Fig. 50A-1-096, Fig. 50A-1-097, Fig. 50A-1-098.	
	See also	80Win2
	For the assignment of the lattice vibration in Raman, IR and far IR studies: see	67Tak, 70McK, 72Lau, 72Ban
	Effects of electric field on the LO soft mode: see	85Far
	Effects of hydrostatic pressure on Raman spectra: Fig. 50A-1-099; see also	82Ori
11	Resistivity of a pressed powder sample can be expressed as $\rho = \exp(\Delta U/kT)$ with the activation energy $\Delta U = 1.35$ eV. Carrier mobility: Fig. 50A-1-100. Seebeck coefficient: Fig. 50A-1-101.	70Yog
	Crystals X-ray irradiated at low temperature emit a broad spectrum of thermoluminescence with peaks centered at about 490 and 530 nm. Activation energy of this process is 0.55(5) eV.	74Ruc, 75Mac
13a	NMR: Table 50A-1-022, Table 50A-1-023; Fig. 50A-1-102, Fig. 50A-1-103, Fig. 50A-1-104; see also	61Ems2
	Effects of hydrostatic pressure on NMR: Fig. 50A-1-105; see also	91Hol
	NQR: Table 50A-1-024.	
14a	X-ray and neutron Bragg reflections due to lattice modulation: Fig. 50A-1-106, Fig. 50A-1-107, Fig. 50A-1-108, Fig. 50A-1-109, Fig. 50A-1-110, Fig. 50A-1-111, Fig. 50A-1-112, Fig. 50A-1-116.	
	See also Fig. 50B-1-014, Fig. 50B-1-015 in No. 50B-1 and	79Tak
	Temperature dependence of lattice modulation wave vector: Fig. 50A-1-113, Fig. 50A-1-114, Fig. 50A-1-115, Fig. 50A-1-116.	
	See also	71Shi, 79Tak, 67Fut
	Electric field dependence of modulated structure: Fig. 50A-1-117, Fig. 50A-1-118, Fig. 50A-1-119, Fig. 50A-1-120, Fig. 50A-1-121, Fig. 50A-1-122, Fig. 50A-1-123, Fig. 50A-1-124, Fig. 50A-1-125, Fig. 50A-1-126, Fig. 50A-1-127.	
	See also	90Ono
	Pressure dependence of modulated structure: Fig. 50A-1-128, Fig. 50A-1-129.	
	See also	81Den
b	Diffuse scattering of X-ray: Fig. 50A-1-130, Fig. 50A-1-131, Fig. 50A-1-132, Fig. 50A-1-133, Fig. 50A-1-134, Fig. 50A-1-135. Diffuse scattering of neutrons: Fig. 50A-1-136, Fig. 50A-1-137.	
	X-ray and neutron diffuse scattering: see also	78Mou2, 80Den
	Inelastic neutron scattering and phonon dispersion: Fig. 50A-1-138, Fig. 50A-1-139, Fig. 50A-1-140, Fig. 50A-1-141.	
	Softening of τ_4 mode: see	80Den
	Elastic stiffness constants estimated by inelastic neutron scattering: see	75McK2

15a	Domain structure: striped domains parallel to the (001) plain were observed by dew method [a]) and powder pattern technique [b]) in phase V. X-ray topographic study: see Effect of sample thickness on domain wall spacing: Fig. 50A-1-142.	[a]) 65Kop [b]) 73Hat 92Aoy, 94Tak
b	Effect of electric field on switching: see Switching time: Fig. 50A-1-143, Fig. 50A-1-144.	59Gol, 90Ham
16	X-ray radiation damage effects on dielectric constant: Fig. 50A-1-145, Fig. 50A-1-146, Fig. 50A-1-147. γ-ray radiation damage effects on dielectric properties: see X-ray radiation damage effects on the modulated structure: Fig. 50A-1-148, Fig. 50A-1-149; see also Memory effect observed by X-ray diffraction: see Observation of defects by X-ray topography: see	 79Wan 84Dur 94Bag, 87And 72Kla1, 72Kla2, 76Kla

Table 50A-1-001. $SC(NH_2)_2$. Unit cell parameters *a*, *b*, *c* of phases I and V determined by X-ray diffraction.

Phase	*T* [°C]	*a* [Å]	*b* [Å]	*c* [Å]	Ref.
I	RT	5.520	7.655	8.537	67Tru
V	–153	5.494(5)	7.516(7)	8.519(10)	59Gol

Table 50A-1-002. $SC(NH_2)_2$. Unit cell parameters *a*, *b*, *c* of phases I and V determined by X-ray diffraction [90Tak]. Parameter: *T*.

	Phase V				Phase I		
T [K]	119	139	149	159	221	257	295
a [Å]	5.464(4)	5.468(3)	5.465(3)	5.468(3)	5.464(2)	5.472(3)	5.488(3)
b [Å]	7.500(5)	7.524(3)	7.527(4)	7.540(4)	7.593(3)	7.633(3)	7.663(4)
c [Å]	8.535(5)	8.538(4)	8.542(4)	8.537(5)	8.553(3)	8.565(6)	8.564(4)

Table 50A-1-003. $SC(NH_2)_2$ and $SC(ND_2)_2$. Structure of phases I and V determined by neutron diffraction [68Elc]. Fractional coordinates and temperature parameters at RT and 110 K. b_{ij} is defined by Eq. (b) in Introduction.

	x	y	z	b_{11}	b_{22}	b_{33}	b_{12}	b_{13}	b_{23}
	$[10^{-4}]$								
$SC(NH_2)_2$, phase I at RT									
S	1148(13)	–0073(12)	2500	185(24)	227(17)	100(11)	–1(18)	0	0
C	–1635(6)	0906(4)	2500	298(13)	148(6)	81(5)	49(7)	0	0
N	–2773(5)	1307(3)	3829(2)	488(11)	328(5)	95(4)	192(6)	11(5)	–0(3)
H(1)	–4405(18)	1842(13)	3761(9)	706(39)	614(26)	154(10)	351(27)	48(16)	10(12)
H(2)	–2054(10)	0955(8)	4870(6)	498(22)	353(73)	95(9)	71(17)	–1(11)	–0(8)
$SC(ND_2)_2$, phase I at RT									
S	1144(11)	–0061(10)	2500	239(19)	244(14)	122(9)	6(14)	0	0
C	–1628(5)	0911(4)	2500	340(10)	165(5)	122(4)	43(6)	0	0
N	–2755(4)	1305(2)	3830(2)	497(8)	328(4)	137(3)	178(5)	24(4)	–8(3)
D(1)	–4386(7)	1870(6)	3797(4)	668(14)	611(12)	168(5)	412(12)	34(7)	–16(7)
D(2)	–2046(5)	0930(4)	4866(3)	503(13)	325(7)	116(4)	116(7)	–7(5)	–4(4)
$SC(NH_2)_2$, phase V at 110 K									
S(1)	3454(19)	0062(16)	0000	52(30)	99(21)	26(12)	–20(19)	0	0
C(1)	0455(7)	0733(10)	0000	54(13)	73(10)	19(5)	6(8)	0	0
N(1)	–0756(4)	1000	1337(3)	94(8)	113(4)	36(4)	33(7)	5(4)	1(5)
H(1)	–2506(13)	1365(12)	1305(10)	151(26)	242(25)	70(10)	94(17)	14(11)	–3(11)
H(2)	0052(14)	0772(18)	2378(8)	198(20)	183(17)	50(9)	34(18)	–7(12)	14(13)
S(2)	1215(17)	0272(16)	5000	34(27)	86(17)	35(12)	–14(18)	0	0
C(2)	3860(8)	–0985(9)	5000	61(13)	51(7)	49(7)	9(9)	0	0
N(2)	4912(6)	–1475(5)	3656(3)	117(8)	84(4)	40(4)	37(5)	3(5)	–9(5)
H(3)	6506(14)	–2169(13)	3698(9)	189(25)	174(14)	85(10)	118(20)	15(13)	–9(11)
H(4)	4271(13)	–1028(16)	2614(10)	217(23)	133(13)	66(12)	40(14)	21(12)	–5(11)
$SC(ND_2)_2$, phase V at 110 K									
S(1)	3412(21)	0113(17)	0000	133(34)	70(21)	75(15)	6(22)	0	0
C(1)	0427(8)	0744(9)	0000	111(15)	70(10)	66(6)	14(11)	0	0
N(1)	–0785(5)	1000	1333(3)	160(9)	128(5)	50(4)	47(7)	–1(4)	–2(5)
D(1)	–2569(8)	1358(9)	1323(5)	173(14)	241(13)	105(7)	92(11)	15(8)	–5(8)
D(2)	0013(8)	0777(10)	2381(5)	215(11)	146(10)	81(6)	28(12)	10(8)	–6(7)
S(2)	1217(20)	0328(16)	5000	123(32)	69(19)	64(14)	13(21)	0	0
C(2)	3852(10)	–0956(9)	5000	168(15)	62(8)	54(7)	19(11)	0	0
N(2)	4863(6)	–1463(6)	3659(3)	184(9)	94(4)	67(4)	36(5)	3(6)	1(5)
D(3)	6441(8)	–2191(8)	3690(6)	191(13)	159(8)	98(6)	89(9)	–6(8)	–4(7)
D(4)	4232(8)	–0999(8)	2622(6)	241(14)	130(9)	79(7)	43(10)	1(7)	6(7)

Table 50A-1-004. $SC(NH_2)_2$ and $SC(ND_2)_2$. Structure of phases I and V [68Elc]. Intermolecular N–H…S distances and angles. The atoms with asterisks are related by the symmetry elements to those given in Table 50A-1-003. They can be identified in Fig. 50A-1-002, Fig. 50A-1-005 where all the N–S distances in $SC(NH_2)_2$ are given. (I): the H atom involved is noncoplanar with its molecule. (II), (III): the H atom involved is planar with its molecule.

Substance and phase	Atoms			Distances [Å]		Angles [deg]
				N–S	H...S	
$SC(NH_2)_2$, I	(I) N	H(2)	S*	3.394(4)	2.397(6)	168.9(5)
$SC(ND_2)_2$, I	N	D(2)	S*	3.393(3)	2.398(3)	169.1(3)
$SC(NH_2)_2$, V	N(1)	H(2)	S(2)	3.348(4)	2.354(8)	169.5(6)
$SC(ND_2)_2$, V	N(1)	D(2)	S(2)	3.350(5)	2.352(5)	170.4(5)
$SC(NH_2)_2$, V	N(2)	H(4)	S(1)	3.417(6)	2.415(10)	170.4(7)
$SC(ND_2)_2$, V	N(2)	D(4)	S(1)	3.429(6)	2.427(7)	170.6(5)
$SC(NH_2)_2$, I	(II) N*	H(1)*	S*	3.526(8)	2.767(12)	133.7(7)
$SC(ND_2)_2$, I	N*	D(1)*	S*	3.539(7)	2.772(8)	133.9(4)
$SC(NH_2)_2$, V	N(1)*	H(1)*	S(1)*	3.580(11)	3.038(13)	115.2(6)
$SC(ND_2)_2$, V	N(1)*	D(1)*	S(1)*	3.596(12)	3.074(13)	113.0(4)
$SC(NH_2)_2$, V	N(2)*	H(3)*	S(2)	3.438(10)	2.549(13)	145.4(7)
$SC(ND_2)_2$, V	N(2)*	D(3)*	S(2)	3.429(12)	2.526(11)	146.7(5)
$SC(NH_2)_2$, I	(III) N*	H(1)*	S	3.696(7)	3.055(12)	123.5(7)
$SC(ND_2)_2$, I	N*	D(1)*	S	3.705(6)	3.082(8)	121.6(3)
$SC(NH_2)_2$, V	N(1)*	H(1)*	S(1)	3.452(10)	2.669(12)	135.3(7)
$SC(ND_2)_2$, V	N(1)*	D(1)*	S(1)	3.449(11)	2.649(12)	135.5(5)
$SC(NH_2)_2$, V	N(2)	H(3)	S(2)*	3.876(10)	3.360(13)	113.2(6)
$SC(ND_2)_2$, V	N(2)	D(3)	S(2)*	3.912(11)	3.423(12)	111.2(4)

Table 50A-1-005. $SC(NH_2)_2$. Fractional coordinates and equivalent isotropic temperature parameters in phase I (T = 295 K) and phase V (T = 119 K) [90Tak]. $U_{eq} = \frac{1}{3}\Sigma U_{ij}\, a_i^*\, a_j^*\, \boldsymbol{a}_i \cdot \boldsymbol{a}_j$. U_{ij} is defined by Eq. (d) in Introduction.

	x	y	z	U_{eq} [10^{-4}]
Phase I 295 K				
S	0.1142(1)	–0.0075(1)	0.25	551(4)
C	–0.1616(6)	0.0904(4)	0.25	514(16)
N	–0.2748(5)	0.1311(3)	0.3822(2)	762(14)
H(1)	–0.430(6)	0.182(4)	0.381(3)	657(93)
H(2)	–0.218(5)	0.097(3)	0.468(3)	393(67)
Phase V 119 K				
S(1)	0.3466(1)	0.0036(3)	0.0	208(2)
C(1)	0.0487(4)	0.0734(4)	0.0	187(7)
N(1)	–0.0715(3)	0.1	0.1335(2)	267(6)
H(11)	–0.225(4)	0.129(4)	0.131(3)	133(61)
H(12)	–0.002(5)	0.078(4)	0.228(2)	30(43)
S(4)	0.1230(1)	0.0230(3)	0.5	195(2)
C(4)	0.3866(4)	–0.0994(4)	0.5	185(7)
N(4)	0.4923(3)	–0.1486(3)	0.3659(1)	255(5)
H(41)	0.626(4)	–0.206(3)	0.368(3)	82(60)
H(42)	0.434(4)	–0.110(3)	0.283(3)	77(56)

Table 50A-1-006. $SC(NH_2)_2$. Fractional coordinates and equivalent isotropic temperature parameters in phase V [88Tan]. $T = 153$ K. $B_{eq} = \frac{4}{3} \Sigma b_{ij} \boldsymbol{a}_i \cdot \boldsymbol{a}_j$. b_{ij} is defined by Eq. (b) in Introduction.

	x	y	z	B_{eq} [Å^2]
S1	0.0998(1)	0.0265 (fixed)	0.25 (fixed)	1.77(1)
S2	–0.1255(1)	0.0457(2)	0.75 (fixed)	1.69(1)
C1	–0.1959(5)	0.1014(5)	0.25 (fixed)	1.63(4)
C2	0.1403(6)	–0.0731(4)	0.75 (fixed)	1.60(4)
N1	–0.3158(4)	0.1295(4)	0.3829(2)	2.46(4)
N2	0.2471(5)	–0.1219(4)	0.6164(2)	2.36(4)

Table 50A-1-007. $SC(NH_2)_2$. Fractional coordinates of the center of libration in phases I and V [90Tak]. See Table 50A-1-005 for numbering of molecules.

T [K]	(x, y, z)
295	(–0.06, 0.02, 0.25)
257	(–0.06, 0.01, 0.25)
221	(–0.06, 0.01, 0.25)
159 (mol. 1)	(0.16, 0.02, 0.00)
159 (mol. 4)	(0.30, –0.03, 0.50)
149 (mol. 1)	(0.17, 0.02, 0.00)
149 (mol. 4)	(0.29, –0.03, 0.50)
139 (mol. 1)	(0.16, 0.02, 0.00)
139 (mol. 4)	(0.30, –0.03, 0.50)
119 (mol. 1)	(0.16, 0.02, 0.00)
119 (mol. 4)	(0.29, –0.03, 0.50)

Table 50A-1-008. $SC(NH_2)_2$. Parameters concerning sinusoidal structural modulation in phase II determined at –86 °C [71Shi]. The structural modulation can be described as a transverse wave with the propagation vector parallel to the c axis. x, y: fractional coordinates of atoms in the unit cell without the structural perturbation. α, β: x and y components of the amplitude of the modulation wave. ϕ_x, ϕ_y: relative phases of the modulation wave concerning each atom.

	x	α	ϕ_x	y	β	ϕ_y
S	0.115	0.012	π	–0.009	0.026	0
C	–0.165	0.015	π	0.106	0.006	0
N	–0.292	0.019	π	0.131	0.002	π

Table 50A-1-009. $SC(NH_2)_2$. Fractional coordinates and anisotropic temperature parameters of the mean structure of the modulated phase [88Tak]. $T = 175$ K. $\delta = 0.126(2)$. Definition of the anisotropic temperature parameter b_{ij} is given by Eq. (b) in Introduction.

Atom	x	y	z	b_{11}	b_{22}	b_{33}	b_{12}	b_{13}	b_{23}
				[10^{-4}]					
S	0.1149(4)	–0.0065(5)	0.2500	108(5)	152(6)	61(2)	12(25)	0	0
C	–0.1658(17)	0.0873(12)	0.2500	171(34)	60(14)	87(11)	78(64)	0	0
N	–0.2814(13)	0.1289(10)	0.3850(6)	252(25)	177(13)	64(6)	143(49)	50(27)	1(20)

Table 50A-1-010. $SC(NH_2)_2$. Amplitudes R, T and phases ϕ of the lattice modulation wave components determined at T = 175 K, δ = 0.126(2) [88Tak]. R: rotational mode, T: translational mode.

R_c	0.090(5) rad		
T_a	0.138(4) Å	ϕ_a	π rad
T_b	0.116(8) Å	ϕ_b	0 rad
T_c	0.0085(42) Å	ϕ_c	–π/2 rad

Table 50A-1-011. $SC(NH_2)_2$. Fractional coordinates and equivalent isotropic temperature parameters at 170 K [88Tan]. $B_{eq} = \frac{4}{3} \Sigma b_{ij} \boldsymbol{a}_i \boldsymbol{a}_j$. b_{ij} is defined by Eq. (b) in Introduction. The structure is commensurately modulated with M = 9. The difference between the two models is the shift of molecules by Δz = 1/18 along the c axis.

	x	y	z	B_{eq} [Å^2]
Model 1				
S1	0.1016(4)	0.0253(3)	0.25 (fixed)	2.33(5)
S2	0.1028(3)	0.0217(2)	0.36103(2)	2.11(3)
S3	0.1139(3)	–0.0004(2)	0.47224(2)	2.17(3)
S4	0.1228(3)	–0.0280(2)	0.58329(2)	2.28(3)
S5	0.1253(2)	–0.0426(2)	0.69433(3)	2.02(3)
C1	–0.1940(15)	0.1024(10)	0.25 (fixed)	1.94(18)
C2	–0.1921(11)	0.0985(7)	0.36110(8)	2.05(13)
C3	–0.1742(12)	0.0939(7)	0.47256(8)	2.24(14)
C4	–0.1520(11)	0.0828(7)	0.58356(8)	2.12(13)
C5	–0.1436(9)	0.0761(6)	0.69457(11)	1.97(10)
N1	–0.3121(10)	0.1305(7)	0.26476(7)	2.83(12)
N2	–0.3099(10)	0.1295(8)	0.34657(7)	3.17(14)
N3	–0.3087(10)	0.1273(8)	0.37616(7)	3.08(13)
N4	–0.2912(10)	0.1302(8)	0.45790(7)	3.04(13)
N5	–0.2841(11)	0.1306(8)	0.48745(7)	3.19(13)
N6	–0.2578(12)	0.1293(7)	0.56883(7)	3.13(13)
N7	–0.2555(11)	0.1274(7)	0.59838(7)	2.86(12)
N8	–0.2508(11)	0.1225(7)	0.67966(7)	2.60(12)
N9	–0.2455(11)	0.1236(7)	0.70931(7)	2.81(12)
Model 2				
S1	0.1018(2)	0.0239(2)	0.30555(3)	2.12(3)
S2	0.1069(3)	0.0142(2)	0.41663(2)	2.41(3)
S3	0.1196(3)	–0.0141(2)	0.52774(2)	2.05(3)
S4	0.1243(3)	–0.0370(2)	0.63883(2)	2.19(3)
S5	0.1257(4)	–0.0456(3)	0.75 (fixed)	1.95(4)
C1	–0.1944(9)	0.1011(6)	0.30563(11)	2.01(11)
C2	–0.1853(11)	0.0961(7)	0.41685(8)	2.03(13)
C3	–0.1605(12)	0.0891(7)	0.52809(8)	2.38(14)
C4	–0.1478(11)	0.0783(7)	0.63902(8)	1.90(12)
C5	–0.1415(16)	0.0754(10)	0.75 (fixed)	2.05(18)
N1	–0.3115(10)	0.1311(8)	0.29077(7)	2.92(13)
N2	–0.3125(10)	0.1286(8)	0.32032(7)	3.00(13)
N3	–0.3030(10)	0.1285(8)	0.40228(7)	3.11(14)
N4	–0.2993(10)	0.1283(8)	0.43191(7)	3.10(14)
N5	–0.2739(11)	0.1315(8)	0.51345(7)	3.17(13)
N6	–0.2672(11)	0.1302(7)	0.54287(7)	3.10(13)
N7	–0.2534(11)	0.1245(7)	0.62427(7)	2.87(12)
N8	–0.2493(12)	0.1249(7)	0.65390(7)	2.80(12)
N9	–0.2460(11)	0.1228(7)	0.73515(7)	2.66(12)

Table 50A-1-012. $SC(NH_2)_2$. Fourier coefficients (in 10^{-4}) for the positional parameters of model 1 in Table 50A-1-011 [88Tan]. T = 170 K. The coefficients are defined by

$X = \bar{X} + \sum_{n=1}^{4} [A_n \cos(2\pi n\zeta) + B_n \sin(2\pi n\zeta)]$, where ζ is the nominal height parameter (e.g. $\zeta = \frac{1}{4} + \frac{2}{9}$ for S3).

The center of mass of molecule is denoted by G. θ, ϕ: polar and azimuth angles [°] of the molecular direction.

		Mean	A_1	B_1	A_2	B_2	A_3	B_3	A_4	B_4
G	y	–983	0	–248	4	0	0	–33	1	0
G	x	658	0	194	12	0	0	3	5	0
G	z	0.0	–1.8	0	0	–0.3	–0.7	0	0	–0.3
	θ	90.0	0.77	0	0	–0.24	0.01	0	0	0.21
	ϕ	–25.43	0	6.55	–0.02	0	0	0.57	–0.38	0
S	x	1146	0	–132	1.7	0	0	–12	8	0
S	y	–81	0	370	8	0	0	21	–6	0
C	x	–1687	0	–282	3	0	0	–27	5	0
C	y	894	0	133	13	0	0	1	11	0
N1	x	–2795	26	–362	6	–4	1	–44	–2	17
N1	y	1279	–5	29	22	–2	3	–12	7	9
N2	x	–2795	–26	–362	6	4	–1	–44	–2	–17
N2	y	1279	5	29	22	2	–3	–12	7	–9

Table 50A-1-013. $SC(NH_2)_2$. Average structure at 168 K [89Zun]. Fractional coordinates and temperature parameters. Although the structure is commensurately modulated with M = 9, the structure was analyzed by superspace-group formalism including up to the third order harmonics. For non-hydrogen atoms, $U_{eq} = \frac{1}{3}\Sigma U_{ii}$, where U_{ii} is defined by Eq. (d) in Introduction. Mean square thermal displacements are listed for hydrogen atoms.

	x	y	z	U_{eq}, $\overline{u^2}$ [Å^2]
S	–0.00760(5)	0.25000	0.11473(7)	0.029
C	0.08812(20)	0.25000	–0.16772(30)	0.028
N	0.12754(14)	0.38277(16)	–0.27982(20)	0.040
H1	0.1606(23)	0.3796(24)	–0.4266(29)	0.031
H2	0.0921(20)	0.4699(25)	–0.2145(27)	0.013

Table 50A-1-014. $SC(NH_2)_2$. Amplitude [10^{-5}] and phases [10^{-3}] of the modulation functions at 168 K [89Zun]. Fixed parameters are denoted by asterisks. Modulation functions are defined as $u_i(t) = \sum_{n=1}^{3} a_{i,n} \cos[2\pi(nt + \phi_{i,n})]$, $i = x, y, z$. See the caption of Table 50A-1-013 for the method of analysis.

		First harmonic		Second harmonic		Third harmonic	
		$a_{i,1}$	$\phi_{i,1}$	$a_{i,2}$	$\phi_{i,2}$	$a_{i,3}$	$\phi_{i,3}$
S	x	3418(19)	0*	139(8)	500*	150(6)	500*
	y	40(6)	250*	28(7)	750*	5(3)	750*
	z	1204(11)	500*	128(7)	500*	97(12)	0*
C	x	1201(29)	0*	135(25)	500*	24(26)	0*
	y	107(24)	750*	1(30)	750*	42(34)	250*
	z	2758(39)	500*	67(35)	500*	235(45)	0*
N	x	320(21)	28(11)	168(18)	431(18)	105(20)	957(33)
	y	318(15)	733(8)	15(18)	620(216)	74(22)	241(63)
	z	3406(31)	493(1)	33(27)	240(103)	343(36)	983(17)
H1	x	688(233)	65(62)	212(234)	825(151)	96(249)	849(401)
	y	346(196)	734(88)	220(243)	835(188)	163(296)	472(287)
	z	4384(217)	504(13)	712(274)	934(71)	820(412)	962(90)
H2	x	653(196)	64(49)	176(176)	382(155)	111(216)	129(304)
	y	209(160)	372(121)	386(193)	404(86)	346(230)	164(141)
	z	3662(281)	469(13)	325(299)	515(126)	322(310)	144(151)

Table 50A-1-015. $SC(NH_2)_2$. Amplitude and phases of the modulation functions corresponding to the rigid-molecule model at 168 K [89Zun]. The values are obtained by fitting the independent atomic displacements of Table 50A-1-014 to a rigid-molecule model. The rotational amplitudes are given in degrees.

		First harmonic		Second harmonic		Third harmonic	
		a	$\phi/2\pi$	a	$\phi/2\pi$	a	$\phi/2\pi$
Rotation	x	0.552	0.75	0.101	0.25	0.169	0.25
	y	0.326	0.00	0.031	0.50	0.552	0.50
	z	0.364	0.75	0.150	0.75	0.000	0.75
Translation	x	0.0185	0.00	0.0015	0.50	0.0003	0.50
	y	0.0012	0.75	0.0002	0.75	0.0003	0.25
	z	0.0234	0.50	0.0005	0.50	0.0022	0.00

Table 50A-1-016. $SC(NH_2)_2$. $d\Theta/dE_{bias}$ obtained from 50 Hz hysteresis loop [62Fut].

$d\Theta_{IV-III}/dE_{bias}$	$-0.5(1) \cdot 10^{-5}$ K m V^{-1}
$d\Theta_{III-II}/dE_{bias}$	$0.50(5) \cdot 10^{-5}$ K m V^{-1}

Table 50A-1-017. $SC(NH_2)_2$. Θ, $d\Theta/dp$ [76Kli].

Transition	Θ [K]	$d\Theta/dp$ [10^{-8} K Pa^{-1}]
II–I	202.3	–16.8
III–II	180	–35.2
IV–III	177.5	–32.2
V–IV	171.4	–25.5
V–II		–35.5

Table 50A-1-018. $SC(NH_2)_2$. Transition heats and transition entropies.

Transition	ΔQ_m [J mol^{-1}]	ΔS_m [J K^{-1} mol^{-1}]	Ref.
V–IV	27.6(4)	0.163(4)	62Fut
	12.5	0.075	63Nak
		0.167	63Cha
V–V'	26.3(1)	0.155(4)	93Iga
V'→IV	0.9(2)	0.005(1)	93Iga
V→IV→III→II		0.042	63Cha
II→I	4.2	0.025	63Nak
		0.710	63Cha
	112.6(3)	0.654(5)	93Iga

Table 50A-1-019. $SC(NH_2)_2$. Elastic constants c_{ij} and thermoelastic constants $T_{ij} = [dc_{ij}/dT]/c_{ij}$ [86Hau]. f = 20 MHz. Used crystallographic axes are (***a′***, ***b′***, ***c′***), the case 2 in 1b.

T [K]	293	273	204	198	175	165	150
Phase	I	I	I	II	IV	V	V
c_{11} [10^{10} N m^{-2}]	1.024(3)	1.053(3)	1.144(5)	1.095(6)	1.120(8)	1.101(8)	1.111(8)
c_{22}	2.595(5)	2.638(6)	2.770(8)	2.790(8)	2.895(10)	2.930(20)	2.980(10)
c_{33}	1.503(3)	1.545(4)	1.650(6)	1.336(10)	1.502(15)	1.470(20)	1.560(10)
c_{44}	0.222(2)	0.230(2)	0.256(2)	0.257(3)	0.274(3)	0.253(4)	0.259(4)
c_{55}	0.608(3)	0.632(3)	0.708(4)	0.709(5)	0.683(6)	0.618(7)	0.620(7)
c_{66}	0.057(1)	0.055(1)	0.052(1)	0.052(1)	0.058(2)	0.066(2)	0.070(3)
c_{12}	0.223(5)	0.208(5)	0.178(7)	0.167(10)	0.264(12)	0.216(15)	0.236(15)
c_{13}	0.567(6)	0.578(7)	0.596(8)	0.502(10)	0.567(10)	0.529(15)	0.563(15)
c_{23}	0.443(6)	0.439(6)	0.428(8)	0.475(10)	0.480(10)	0.499(10)	0.525(10)
T_{11} [10^{-3} K^{-1}]	–1.38(3)	–1.32(4)	0.1(2)	–1.2(2)	–0.3(2)	–0.6(3)	–0.6(1)
T_{22}	–0.82(3)	–0.81(3)	–1.1(1)	–2.8(2)	–0.64(8)	–1.3(2)	–1.2(2)
T_{33}	–1.39(3)	–1.36(3)	6.7(6)	–10.5(8)	–4.7(8)	–6.2(8)	–4(1)
T_{44}	–1.82(8)	–1.62(10)	–0.6(3)	–2.9(5)	–2.4(5)	–2.3(6)	–2.3(5)
T_{55}	–1.92(8)	–1.86(8)	–1.6(3)	1.2(2)	1.6(3)	0.0(3)	–0.2(3)
T_{66}	1.52(6)	1.02(8)	0.0(3)	–5.2(5)	–5.4(5)	–4.4(5)	–3.9(5)
T_{12}	3.0(5)	4.8(10)	16(4)	41(10)	–7(2)	–8(2)	–4(1)
T_{13}	–1.05(9)	–1.04(9)	15(3)	–11(2)	–3.7(10)	–3.3(10)	–2.8(10)
T_{23}	0.38(6)	0.52(8)	10(2)	1.0(3)	–13(4)	–6(2)	–4.5(10)

Table 50A-1-020. $SC(NH_2)_2$. Third order elastic constants c_{ijk} [$\cdot 10^{10}$ N m^{-2}] [86Hau]. T = 293 K (phase I). Used crystallographic axes are (***a′***, ***b′***, ***c′***), the case 2 in 1b.

ijk	c_{ijk}	ijk	c_{ijk}
111	–15.0(7)	223	–3.4(9)
112	–1.1(2)	233	–0.7(2)
113	–5.0(10)	244	–2.3(8)
122	–7.5(8)	255	–4.4(20)
123	–2.5(8)	266	–2.2(7)
133	–4.4(7)	333	–39(2)
144	–2.1(4)	344	–1.9(2)
155	–7.3(17)	355	–4(1)
166	–1.8(9)	366	–0.1
222	–9.4(19)	456	–0.7(4)

Table 50A-1-021. $SC(NH_2)_2$. Frequencies of the lattice vibrations obtained by Raman spectra at RT. $(\partial(\nu/c)/\partial p)_T$ is the rate of the frequency shift due to hydrostatic pressure. 1 $cm^{-1} = 3 \cdot 10^{10}$ Hz.

Ref.	[67Tak]		[72Lau]		[76Iqb]	
Assignment	ν/c [cm^{-1}]	Relative intensity	ν/c [cm^{-1}]	Relative intensity	ν/c [cm^{-1}]	$(\partial(\nu/c)/\partial p)_T$ [cm^{-1} (10^8 Pa)$^{-1}$]
A_g	122	3	118(1)	1.5	116	2.29
			32(1)	0.75		
B_{1g}	101	4	101(1)	3	99.5	2.08
B_{2g}	63	6	62(1)	6	60.0	2.00
B_{3g}	45	2	47(1)	1.87	44.0	1.73

Table 50A-1-022. $SC(ND_2)_2$. Electric field gradient tensors and the direction cosines of their principal axes with respect to crystallographic ***a***, ***b***, ***c*** axes at 300 K [71ORe]. Estimated error is ± 2°.

i	ϕ_{ii} [kHz]	Direction cosines	i	ϕ_{ii} [kHz]	Direction cosines
Inner deuterons			Outer deuterons		
x	–93(3)	(0.000, 0.000, 1.000)	*x*	–21(2)	(0.841, 0.541, 0.000)
y	–104(3)	(–0.406, 0.914, 0.000)	*y*	–114(2)	(–0.541, 0.841, 0.000)
z	197(3)	(0.914, 0.406, 0.000)	*z*	135(2)	(0.000, 0.000, 1.000)

Table 50A-1-023. $SC(ND_2)_2$. Electric field gradient tensors and the direction cosines of their principal axes at 120 K [71ORe]. At $T < 169$ K (phase V) there are two crystallographically inequivalent molecules; the molecular plane of one type (molecule 1) intersects the *a* axis with an angle of 19.6° and the other (molecule 2) with 29.5°.

i	ϕ_{ii} [kHz]	Direction cosines	i	ϕ_{ii} [kHz]	Direction cosines
Inner deuterons, molecule 1			Outer deuterons, molecule 1		
x	–69	(–0.006, 0.036, 0.999)	*x*	–65	(0.829, –0.335, 0.447)
y	–93	(–0.291, 0.956, –0.036)	*y*	–91	(0.288, 0.942, 0.173)
z	162	(0.956, 0.291, –0.005)	*z*	157	(–0.479, –0.015, 0.878)
Inner deuterons, molecule 2			Outer deuterons, molecule 2		
x	–64	(0.000, 0.000, 1.000)	*x*	–62	(0.657, –0.667, 0.350)
y	–93	(–0.504, 0.861, 0.000)	*y*	–91	(0.594, 0.744, 0.305)
z	157	(0.861, 0.504, 0.000)	*z*	153	(–0.464, 0.008, 0.886)

Table 50A-1-024. $SC(NH_2)_2$. e^2qQ/h and η of ^{14}N [64Smi]. $T = 77$ K. For molecules 1 and 2, see caption of Table 50A-1-023.

Molecule	e^2qQ/h [kHz]	η [%]
1	3121.6	39.54
2	3099.6	39.30

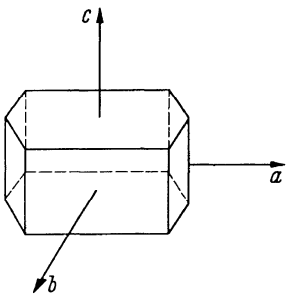

Fig. 50A-1-001. $SC(NH_2)_2$. Crystal form [59Gol].

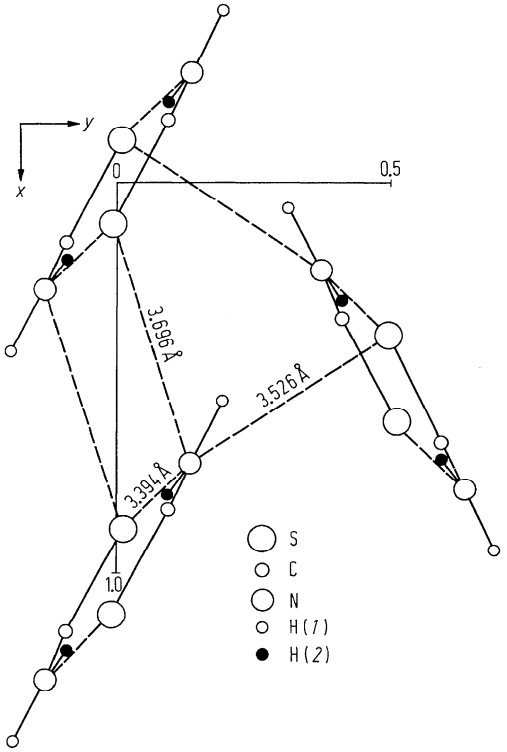

Fig. 50A-1-002. $SC(NH_2)_2$. Structure of phase I determined by neutron diffraction at RT [68Elc]. Projection on (001).

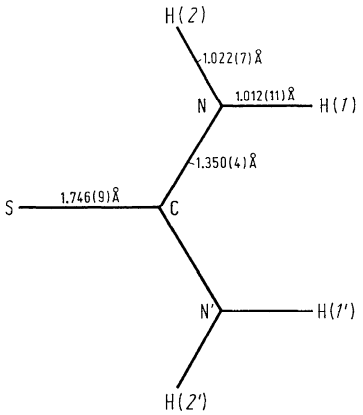

Fig. 50A-1-003. $SC(NH_2)_2$. Structure of phase I [68Elc]. Interatomic distances in thiourea molecule at RT.

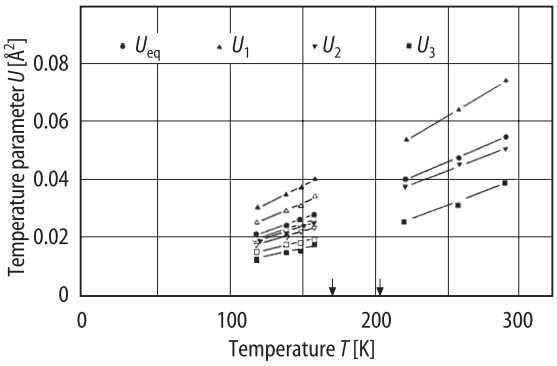

Fig. 50A-1-004. $SC(NH_2)_2$. U_{eq}, U_i (i = 1, 2, 3) vs. T [90Tak]. U_{eq}, U_i (i = 1, 2, 3): isotropic and diagonalized temperature parameter of S atom. Directions of the principal axes are nearly along the *b* axis (i = 1), rigorously along the *c* axis (i = 2), and nearly along the *a* axis (i = 3). Open and closed symbols in phase V correspond to molecules 4 and 1 in Table 50A-1-005.

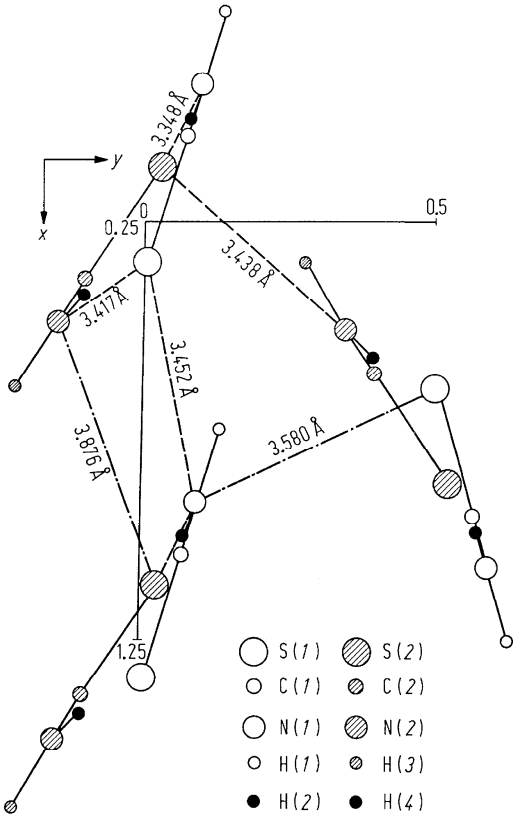

Fig. 50A-1-005. $SC(NH_2)_2$. Structure of phase V determined by neutron diffraction at 110 K [68Elc]. Projection on (001).

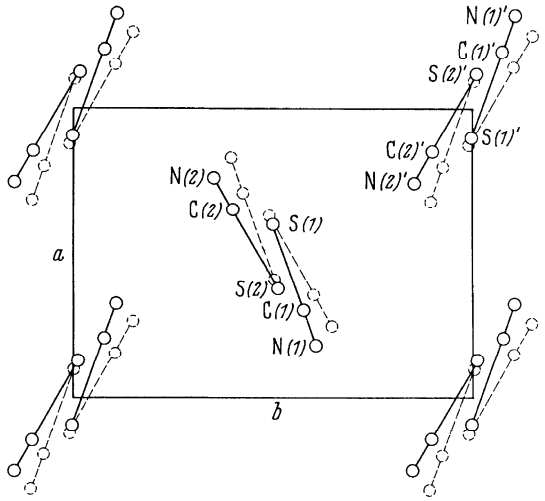

Fig. 50A-1-006. $SC(NH_2)_2$. Structure of phase V [59Gol]. An illustration of the polarization reversal projected on (001). The full circles represent atomic positions for one direction of P_s; the dotted circles represent atomic positions for the opposite direction of P_s.

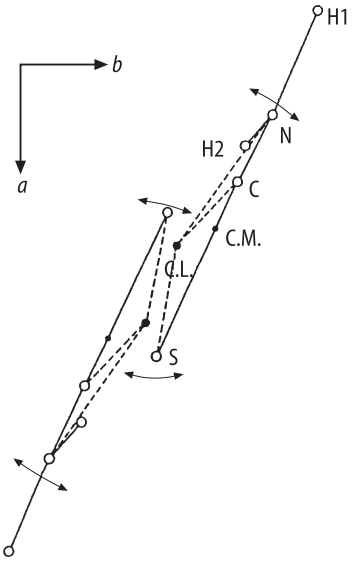

Fig. 50A-1-007. $SC(NH_2)_2$. Projection of molecules 1 and 4 along the *c* axis at 295 K [90Tak]. C.L.: the center of libration, which does not change significantly with temperature. C.M.: center of mass of the molecule.

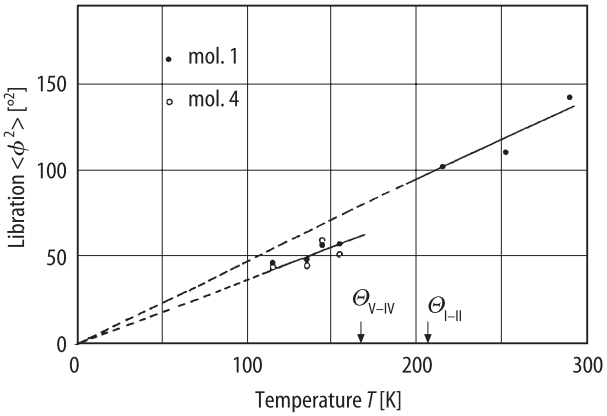

Fig. 50A-1-008. $SC(NH_2)_2$. $\langle\phi^2\rangle$ vs. T [90Tak]. $\langle\phi^2\rangle$: the mean square of the libration along the c axis. See Table 50A-1-005 for numbering of molecules.

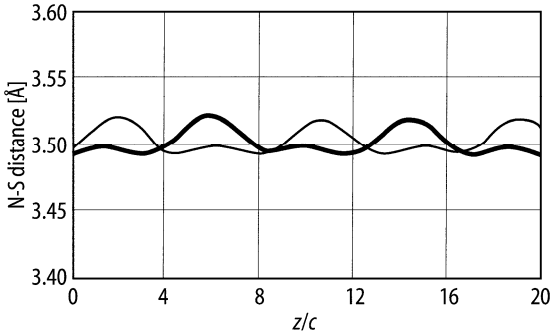

Fig. 50A-1-009. $SC(NH_2)_2$. Modulated structure [88Tak]. Spatial variation of N–S distances (type I in Table 50A-1-004) along c. T = 175 K. Unit of abscissa is the unit cell constant c.

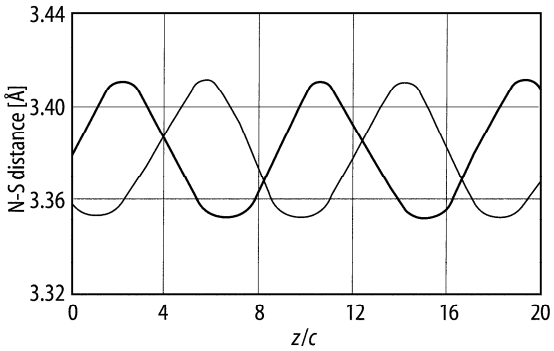

Fig. 50A-1-010. $SC(NH_2)_2$. Modulated structure [88Tak]. Spatial variation of N–S distances (type II in Table 50A-1-004) along c. T = 175 K. Unit of abscissa is the unit cell constant c.

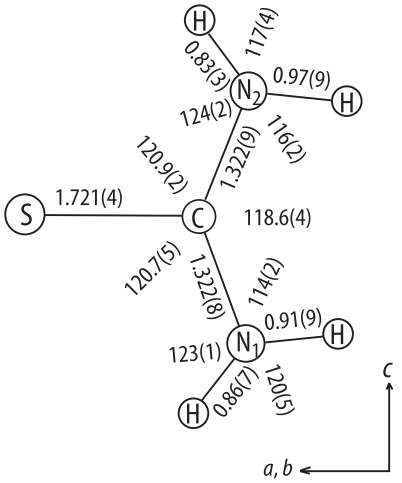

Fig. 50A-1-011. $SC(NH_2)_2$. Mean molecular structure at 170 K [88Tan]. The mean bond lengths [Å] and bond angles [°] are for model 1 in Table 50A-1-011. The values for model 2 are almost the same.

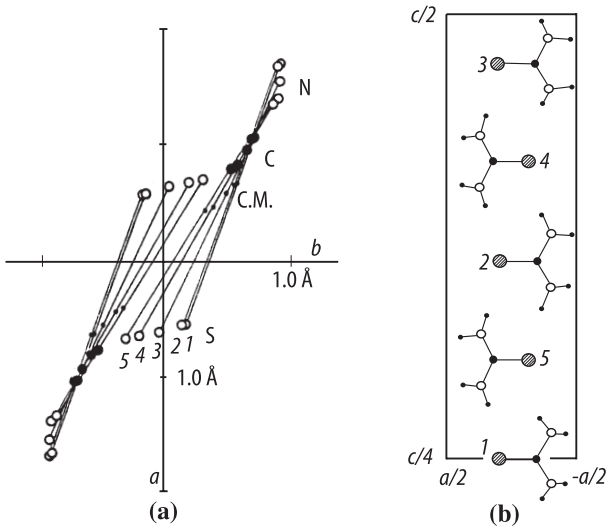

Fig. 50A-1-012. $SC(NH_2)_2$. View of modulated structure at 170 K [88Tan]. Model 1 in Table 50A-1-011 is shown. (**a**) Along the *c* axis. Molecules around $x \cong 0$ and $y \cong 0$ are projected. C.M.: center of mass of the molecules. (**b**) Along the *b* axis. Molecules in one-eighth of the unit cell (–*a*/2 to *a*/2, –*b*/4 to *b*/4, *c*/4 to *c*/2) are shown.

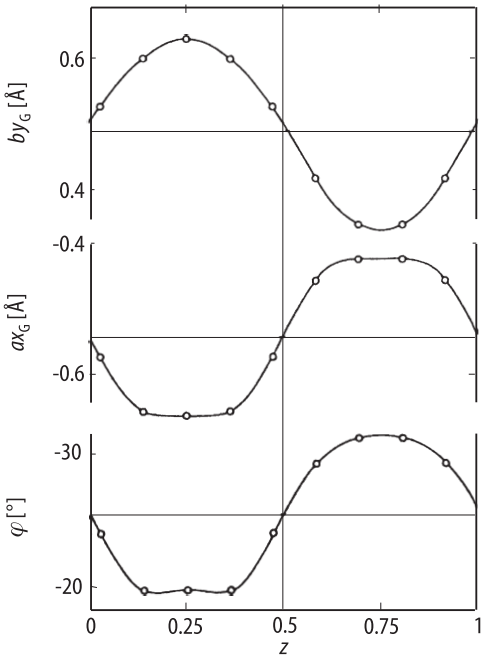

Fig. 50A-1-013. $SC(NH_2)_2$. Translational and rotational modulation waves, ax_G, by_G, φ vs. z [88Tan]. T = 170 K. x_G, y_G: fractional coordinates of the center of mass of molecules. φ: azimuth angle of the molecular direction. Solid lines are drawn by use of coefficients listed in Table 50A-1-012.

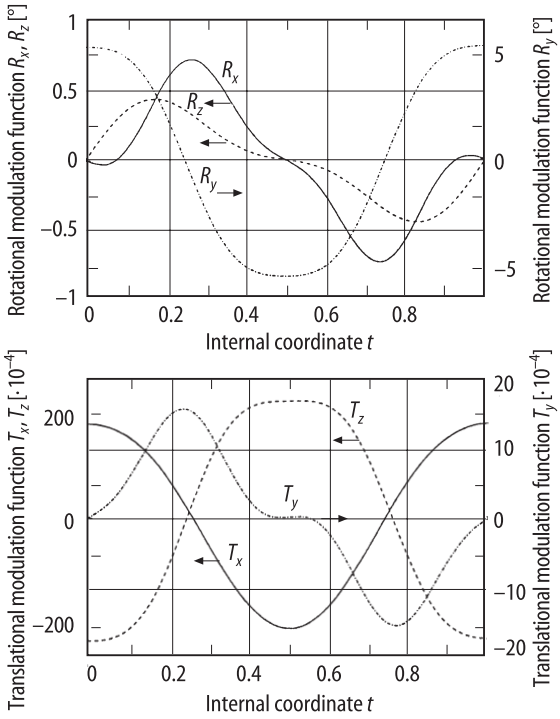

Fig. 50A-1-014. $SC(NH_2)_2$. Rotational and translational modulation functions in rigid-molecule model [89Zun]. R_x, R_y, R_z, T_x, T_y, T_z vs. t. T = 168 K. t: internal coordinate. See the caption of Table 50A-1-015.

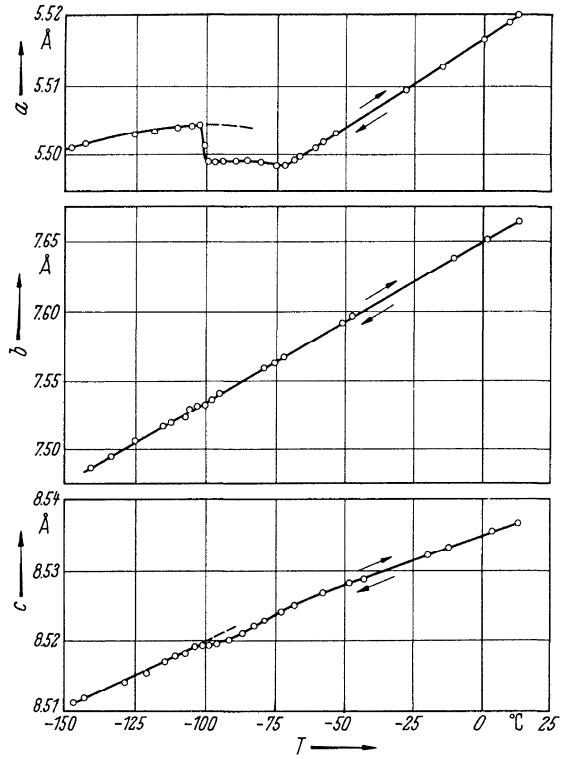

Fig. 50A-1-015. $SC(NH_2)_2$. *a*, *b*, *c* vs. *T* [62Fut]. Values of *a*, *b*, *c* were obtained by measuring thermal elongation of specimens by means of the optical lever method and by using values of *a*, *b*, *c* at 20 °C determined with X-ray.

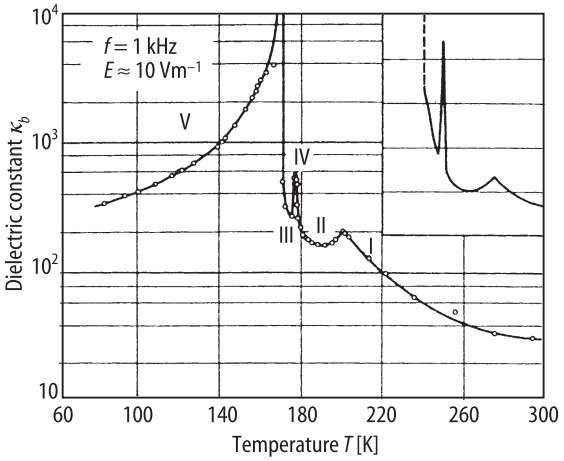

Fig. 50A-1-016. $SC(NH_2)_2$. κ_b vs. *T* [59Gol].

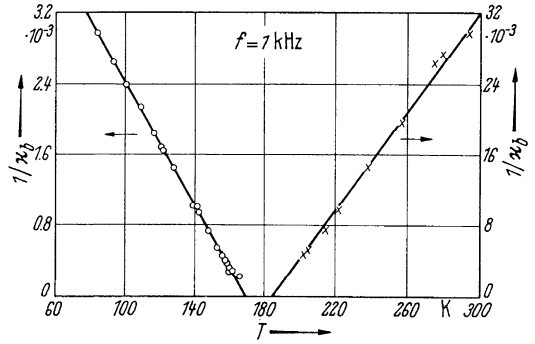

Fig. 50A-1-017. $SC(NH_2)_2$. $1/\kappa_b$ vs. T [59Gol].

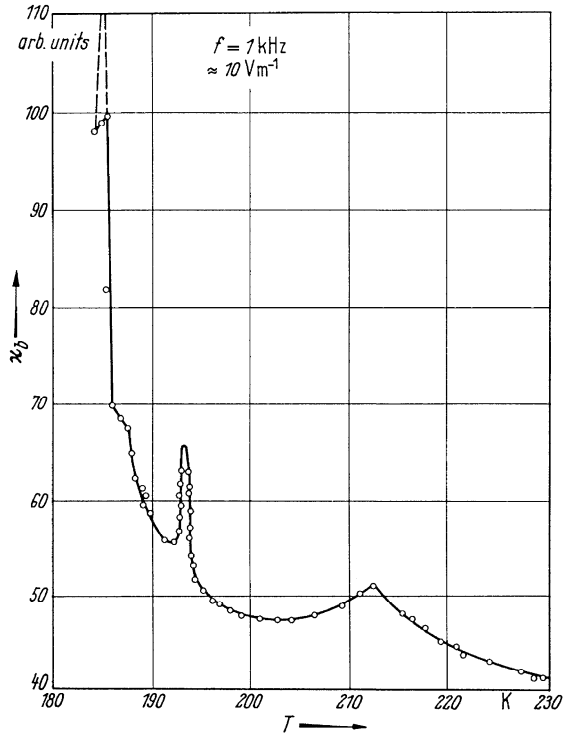

Fig. 50A-1-018. $SC(ND_2)_2$. κ_b vs. T [59Gol].

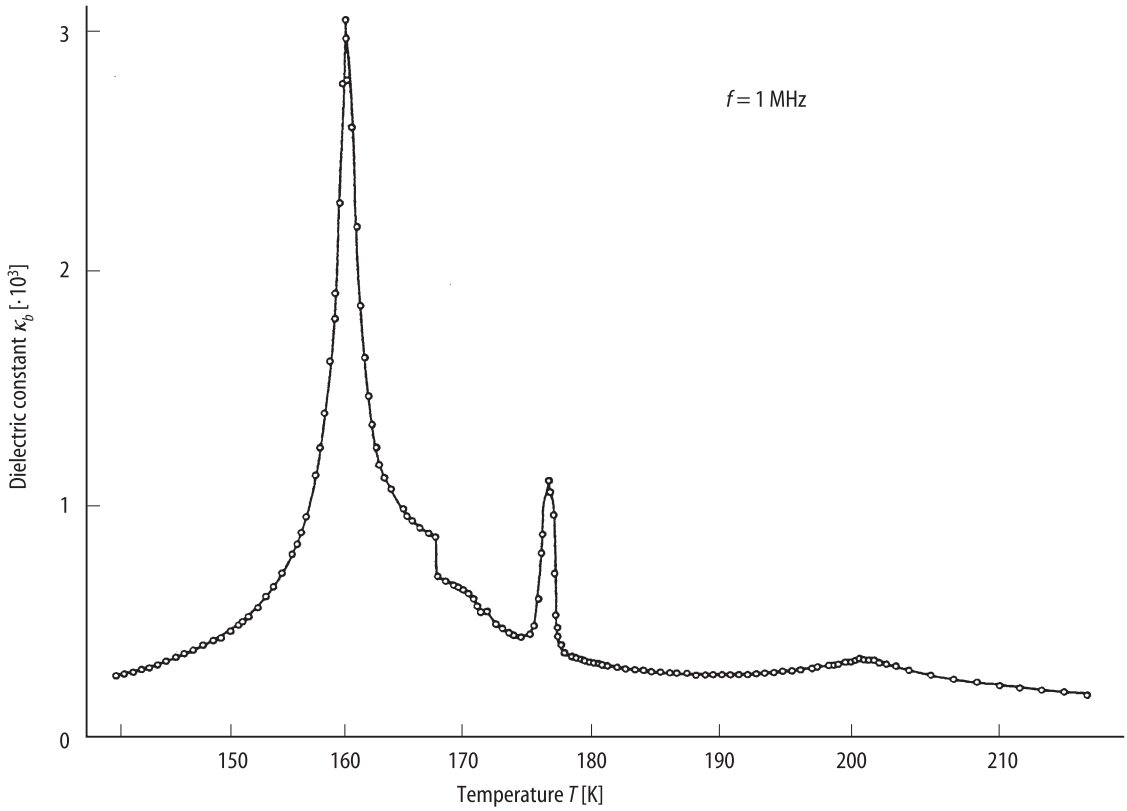

Fig. 50A-1-019. $SC(NH_2)_2$. κ_b vs. T [96Mag].

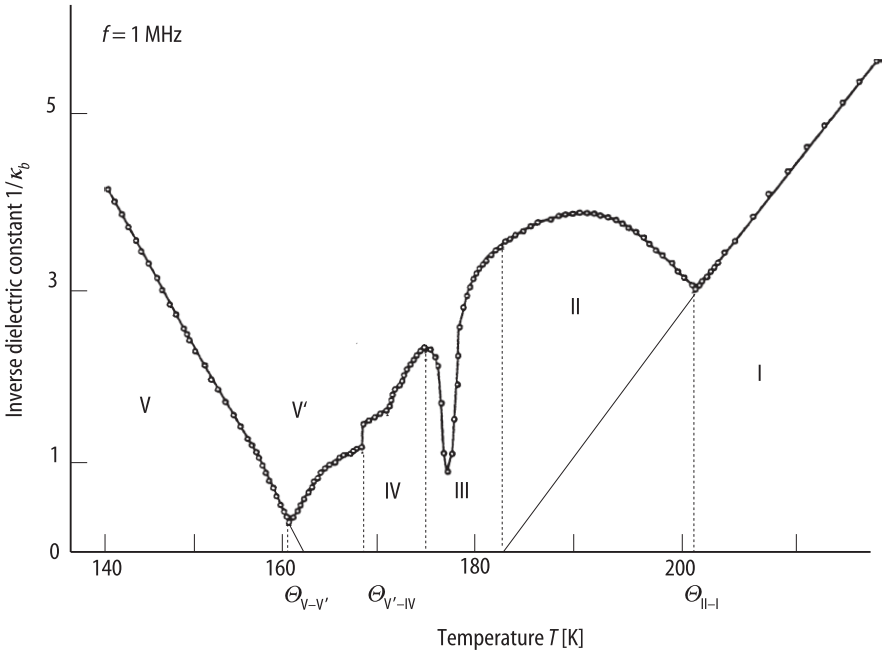

Fig. 50A-1-020. $SC(NH_2)_2$. $1/\kappa_b$ vs. T [96Mag].

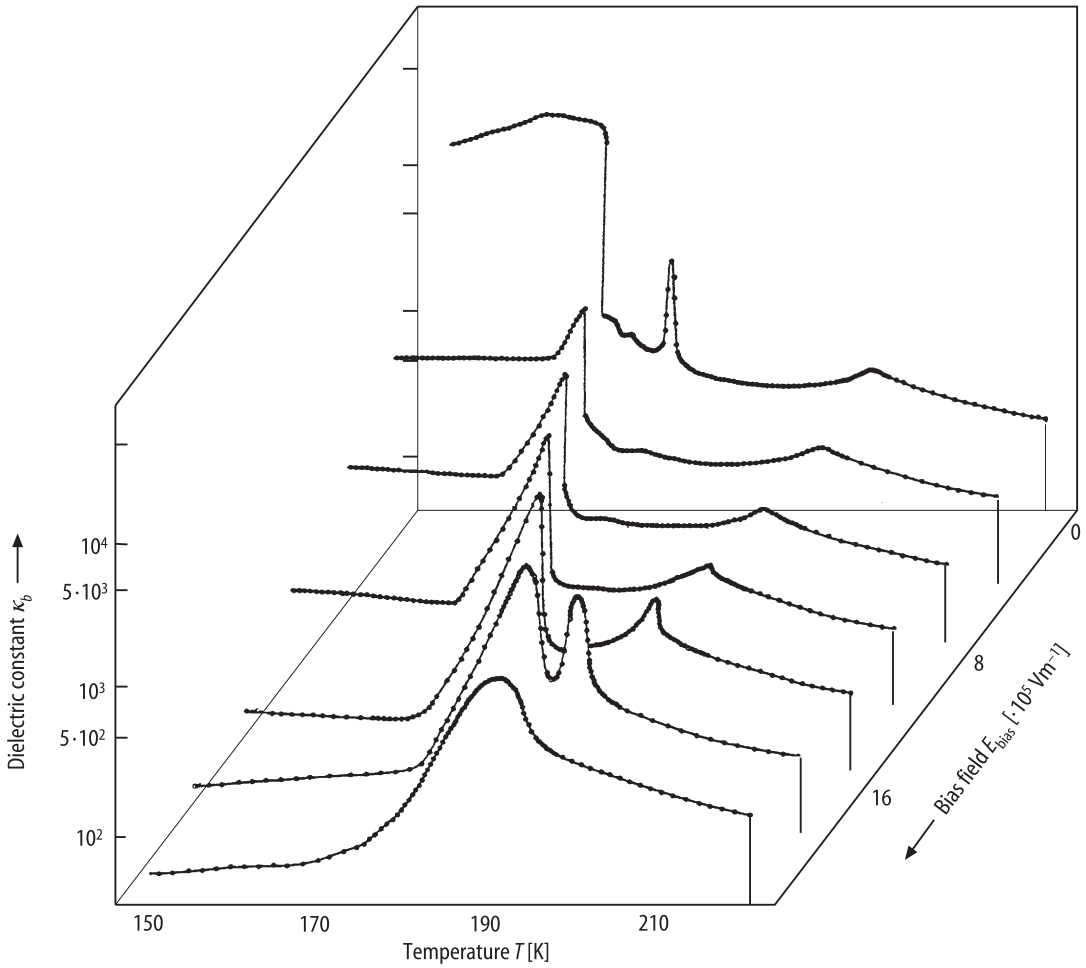

Fig. 50A-1-021. SC(NH$_2$)$_2$. κ_b vs. T [96Mag]. Parameter: E_{bias}.

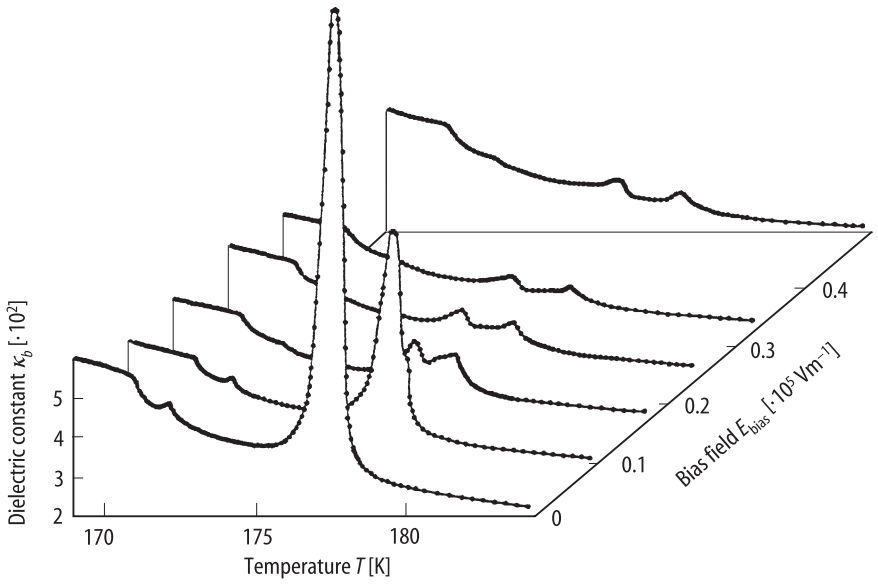

Fig. 50A-1-022. SC(NH$_2$)$_2$. κ_b vs. T [96Mag]. Parameter: E_{bias}.

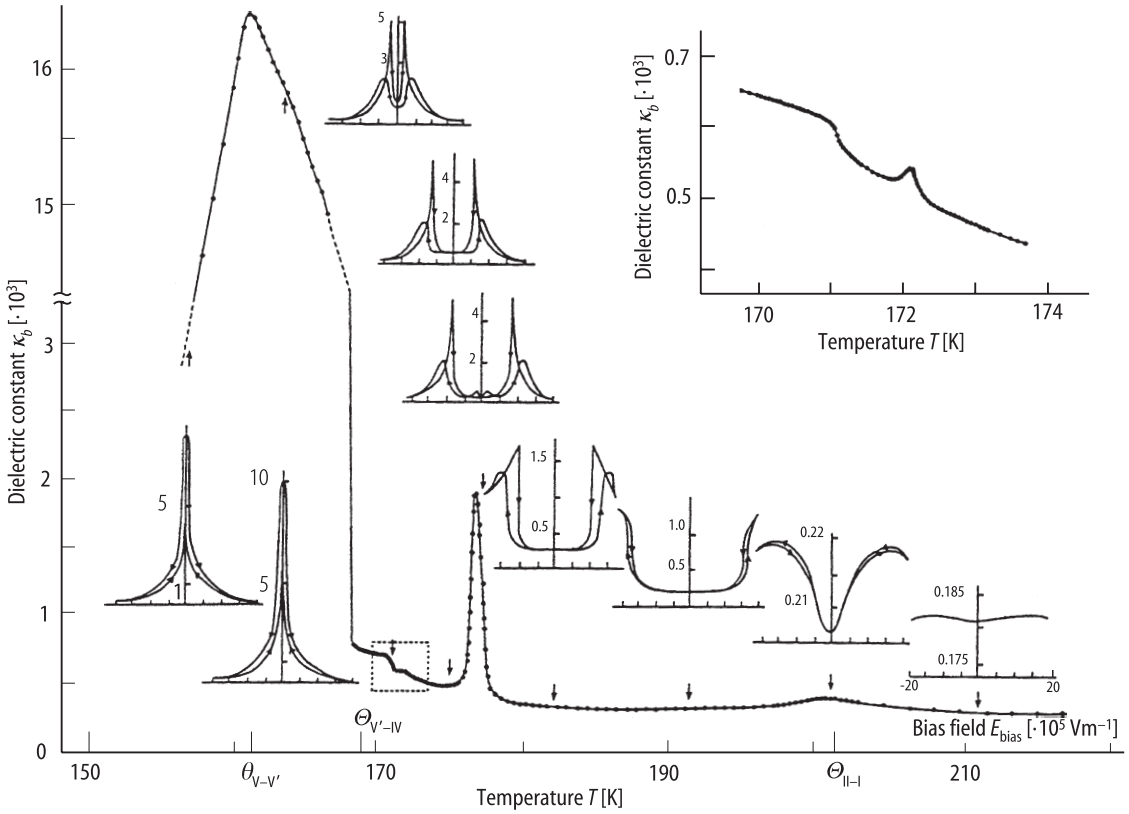

Fig. 50A-1-023. SC(NH$_2$)$_2$. κ_b vs. T [96Mag]. κ_b vs. E_{bias} curves are shown for various temperatures indicated by arrows.

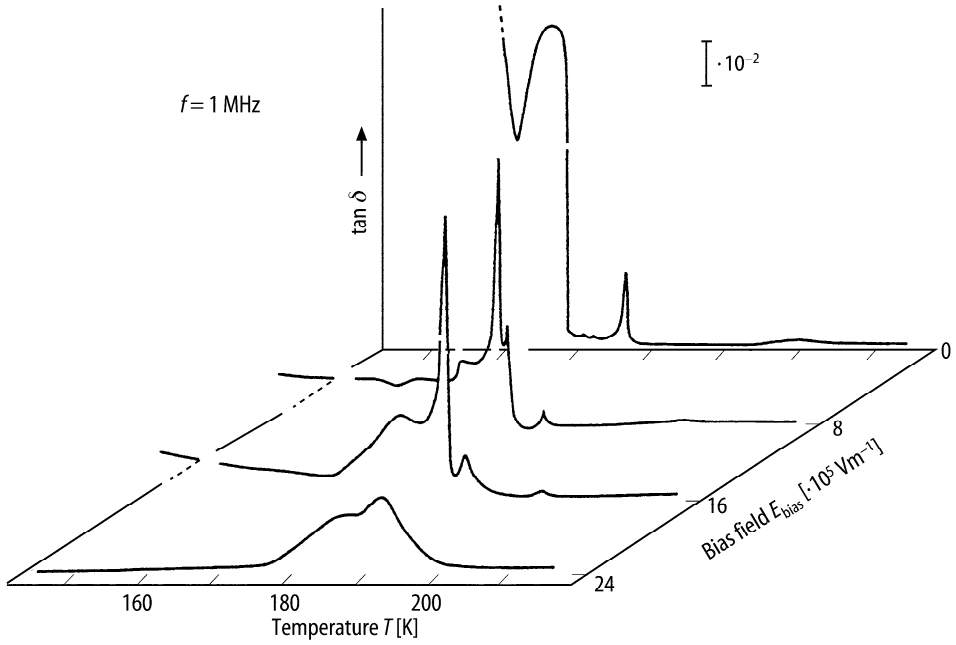

Fig. 50A-1-024. SC(NH$_2$)$_2$. tanδ vs. T [96Mag]. Parameter: E_{bias}.

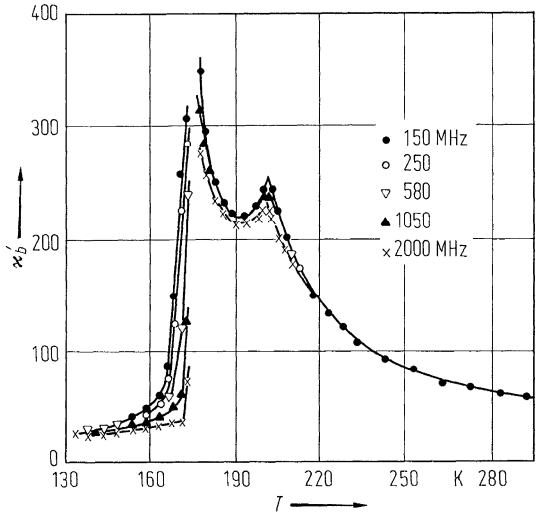

Fig. 50A-1-025. $SC(NH_2)_2$. κ_b' vs. T [75Cza]. Parameter: f.

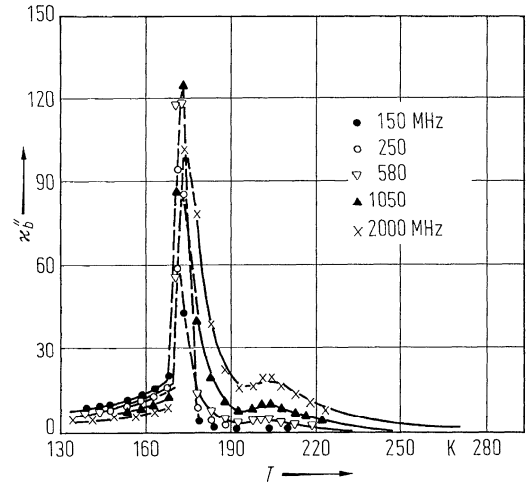

Fig. 50A-1-026. $SC(NH_2)_2$. κ_b'' vs. T [75Cza]. Parameter: f.

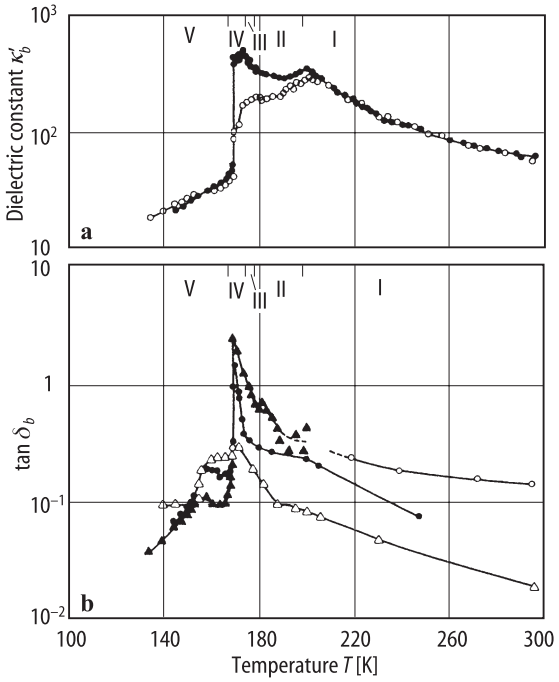

Fig. 50A-1-027. $SC(NH_2)_2$. κ_b' and $\tan\delta_b$ vs. T [76Toe]. Parameter: f. (**a**) For κ_b' in phase I: full circles: measurements from 18.0 to 28.0 GHz, and open circles: measurements from 50.0 to 75.0 GHz. (**b**) Open triangles: 9.0 GHz, full circles: 21.0 GHz, open circles: 56.8 GHz, full triangles: 65.3 GHz.

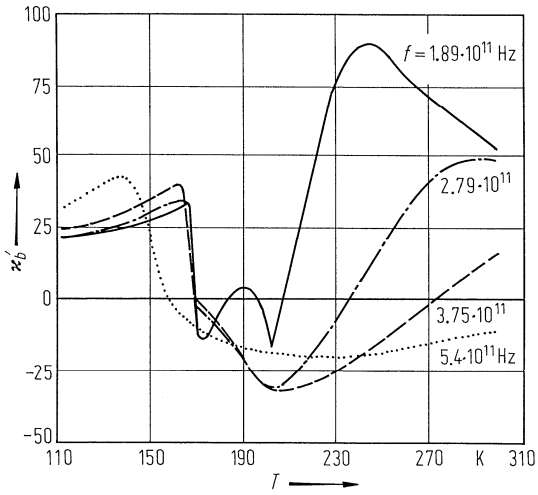

Fig. 50A-1-028. $SC(NH_2)_2$. κ_b' vs. T [80Vol]. Parameter: f.

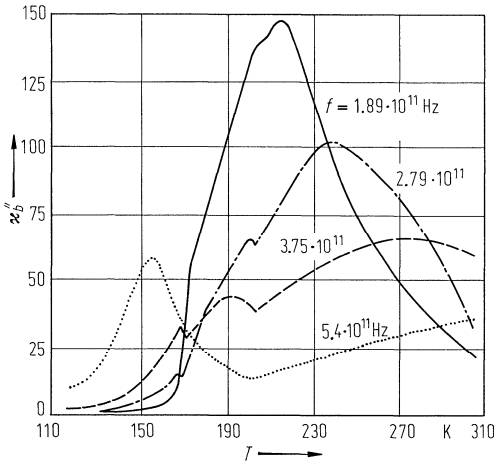

Fig. 50A-1-029. $SC(NH_2)_2$. κ_b'' vs. T [80Vol]. Parameter: f.

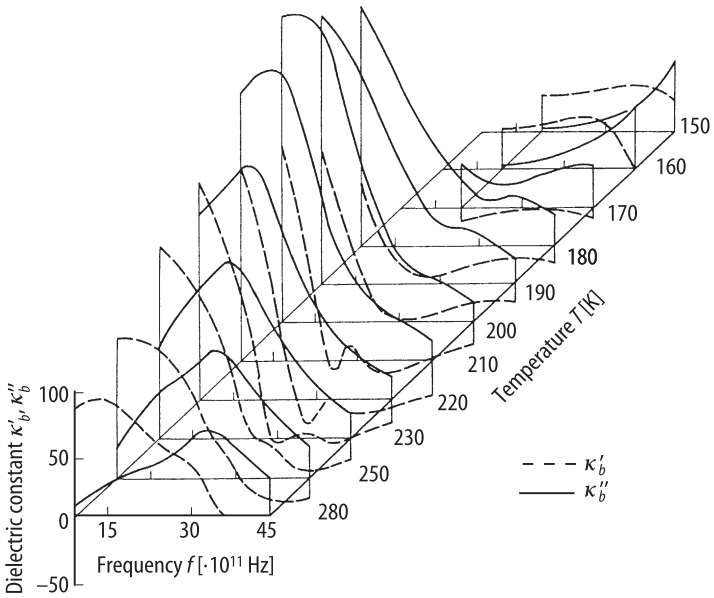

Fig. 50A-1-030. SC(NH$_2$)$_2$. κ_b', κ_b'' vs. f [82Vol]. Parameter: T.

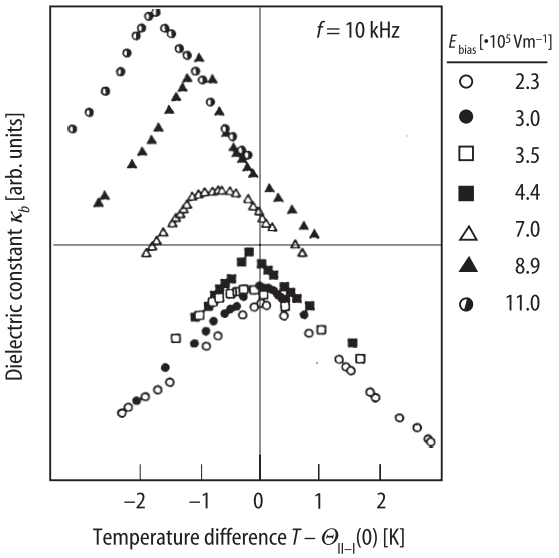

Fig. 50A-1-031. SC(NH$_2$)$_2$. κ_b vs. $T - \Theta_{II-I}(0)$ [88Kim]. Parameter E_{bias}. $\Theta_{II-I}(0)$: II–I transition temperature at zero bias field.

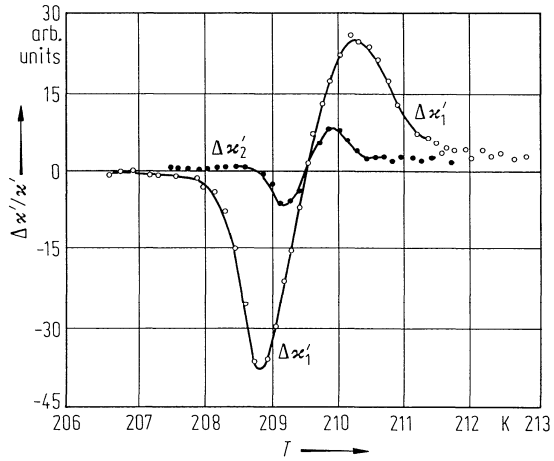

Fig. 50A-1-032. $SC(ND_2)_2$. $\Delta\kappa'/\kappa'$ vs. T after some thermal treatment [86Led]. κ': ordinary dielectric constant. $\Delta\kappa' = \kappa_i' - \kappa'$, κ_i': dielectric constant measured by cooling run after i-th thermal treatment. κ_1' : after 15 h temperature stabilization kept at $T = 209.6$ K. κ_2' : after 12 h temperature stabilization kept at $T = \Theta_{II-I} + 3$ K $\cong$ 220 K continued from the measurement of κ_1' .

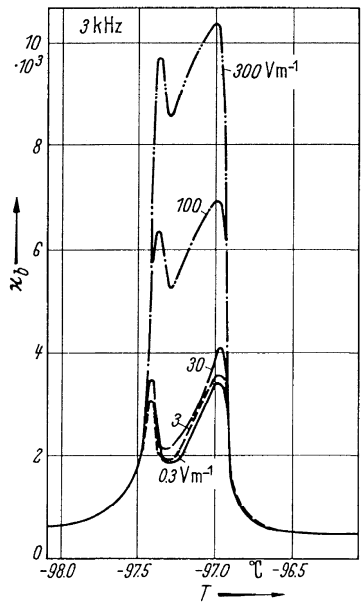

Fig. 50A-1-033. $SC(NH_2)_2$. $\varkappa_b$ vs. T in the vicinity of phase III [67Sug]. Parameter: E, amplitude of measuring ac field.

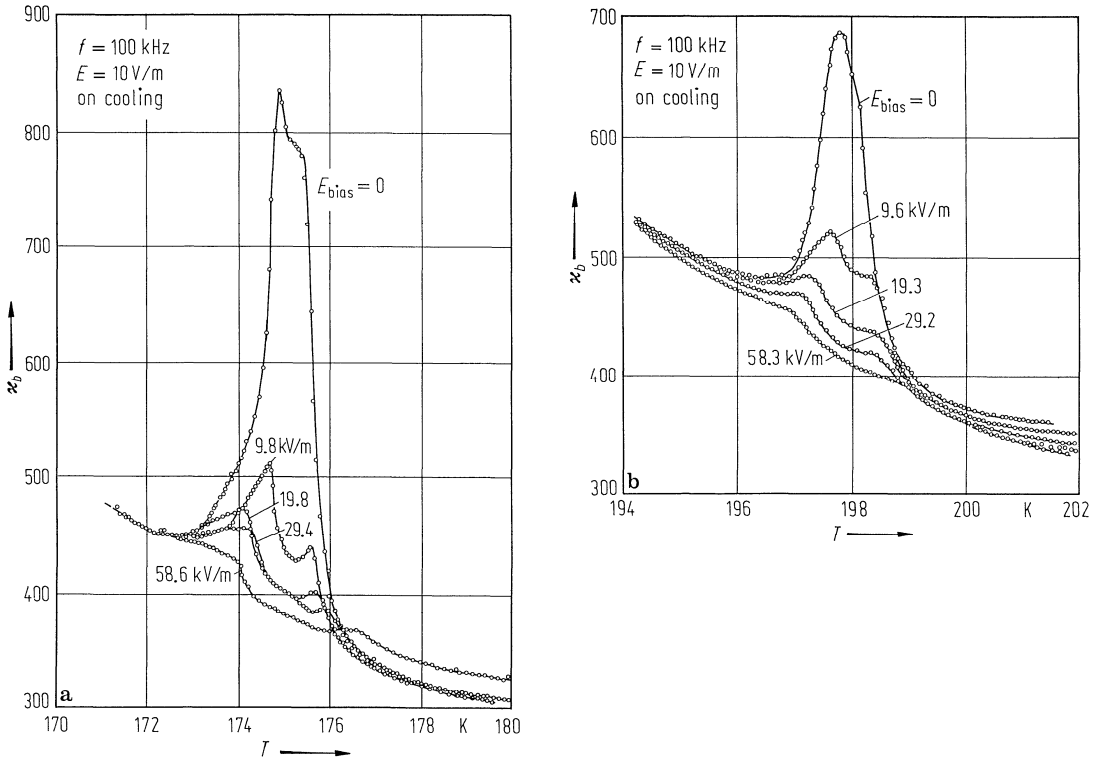

Fig. 50A-1-034. $SC(NH_2)_2$ (**a**), $SC(ND_2)_2$ (**b**). κ_b vs. T in the vicinity of phase III [82Ges1]. Parameter: E_{bias}.

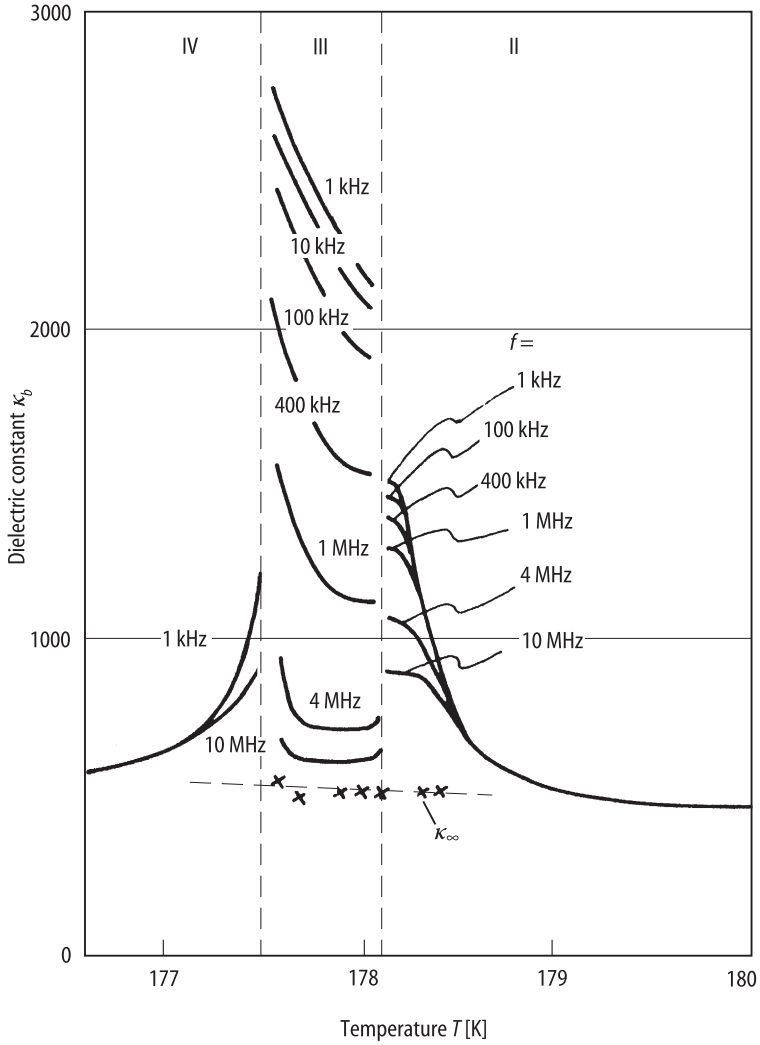

Fig. 50A-1-035. $SC(NH_2)_2$. κ_b vs. T in the vicinity of phase III [89Ham]. Parameter: f. κ_∞: dielectric constant at high frequency limit obtained from the Cole-Cole plot. On heating.

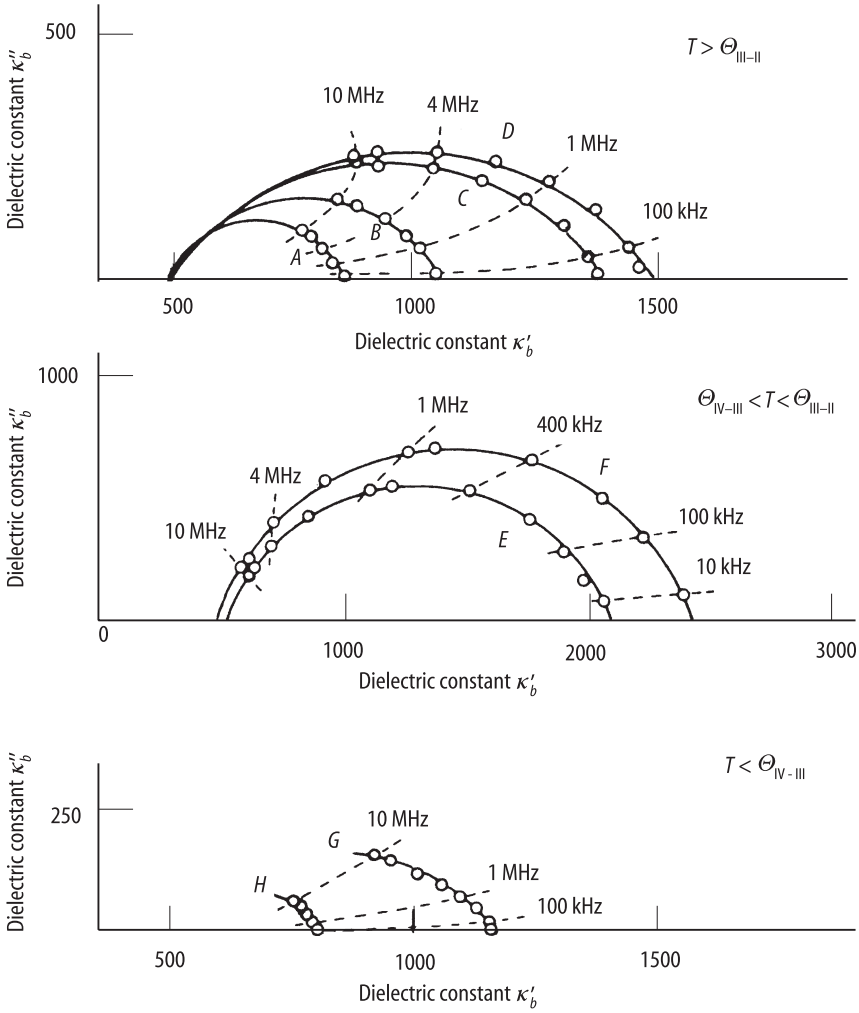

Fig. 50A-1-036. $SC(NH_2)_2$. Cole-Cole diagram of complex dielectric constant [89Ham]. Parameter: *T*; *A*: 178.42 K, *B*: 178.32 K, *C*: 178.24 K, *D*: 178.12 K, *E*: 178.02 K, *F*: 177.77 K, *G*: 177.46 K, *H*: 177.29 K. On heating.

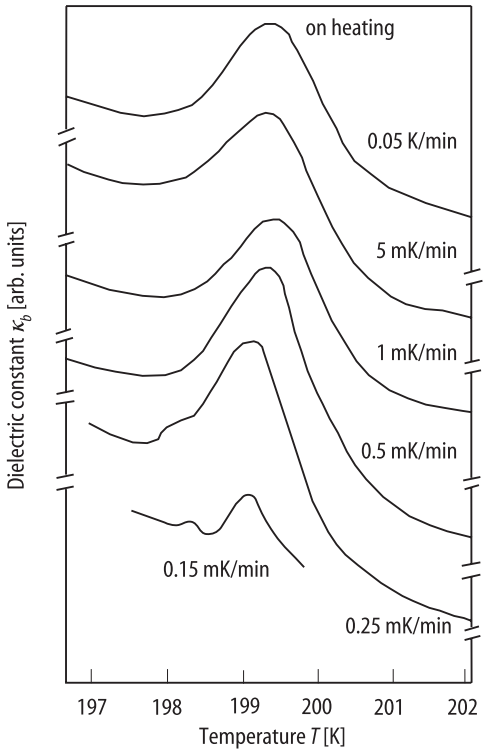

Fig. 50A-1-037. $SC(ND_2)_2$. κ_b vs. T in the vicinity of phase III [94Ono1]. Parameter: heating rate. f = 10 kHz.

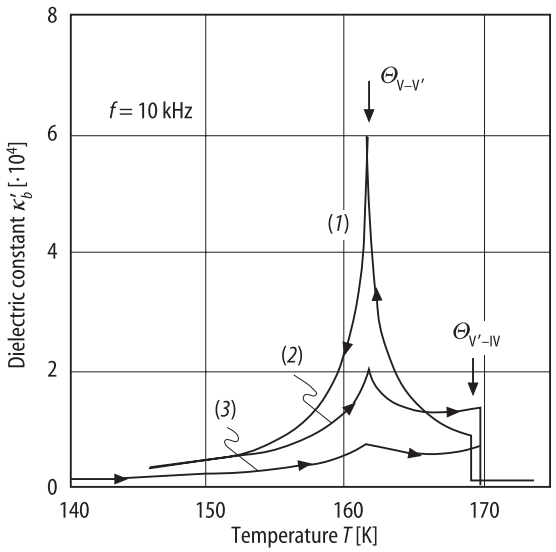

Fig. 50A-1-038. $SC(NH_2)_2$. κ'_b vs. T [90Ham]. Effect of thermal hysteresis is shown. (*1*) first cooling run, (*2*) heating run taken by turning the first cooling run at 146 K, (*3*) heating run after the sample was kept at 100 K for 12 h.

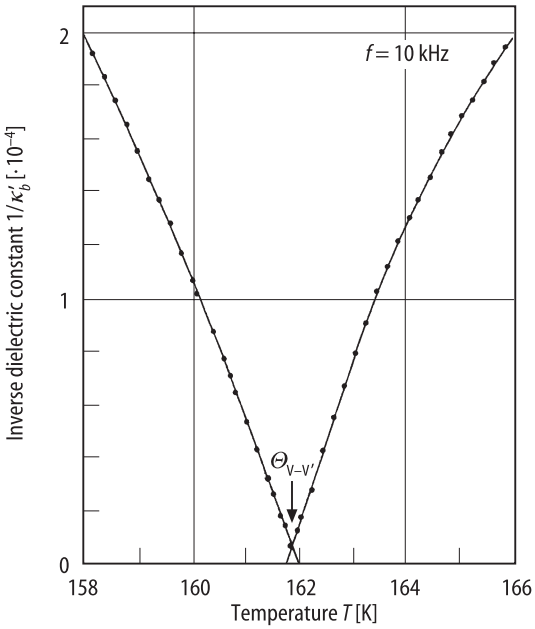

Fig. 50A-1-039. $SC(NH_2)_2$. $1/\kappa'_b$ vs. T in the vicinity of $\Theta_{V-V'}$ [90Ham].

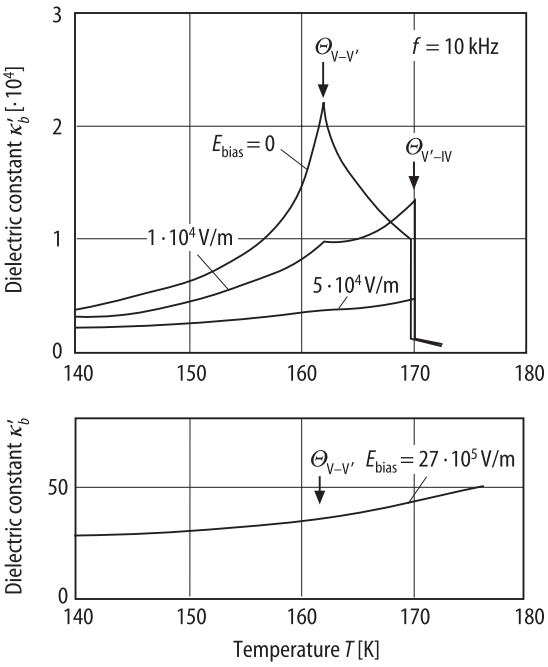

Fig. 50A-1-040. $SC(NH_2)_2$. κ'_b vs. T [90Ham]. Parameter: E_{bias}. On cooling.

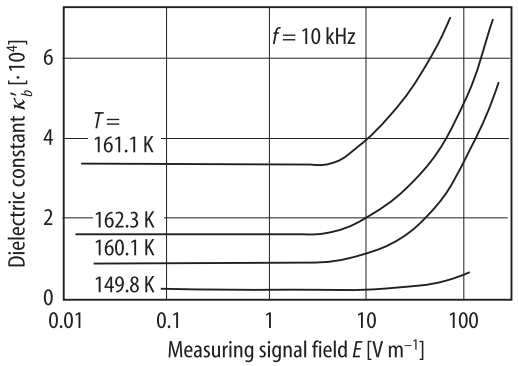

Fig. 50A-1-041. $SC(NH_2)_2$. κ_b' vs. E [90Ham]. Parameter: T. E: measuring signal field.

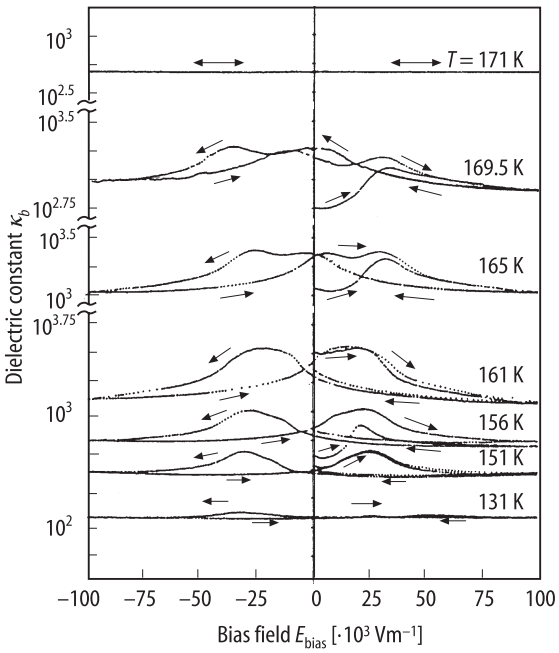

Fig. 50A-1-042. $SC(NH_2)_2$. κ_b vs. E_{bias} [90Mas]. Parameter: T.

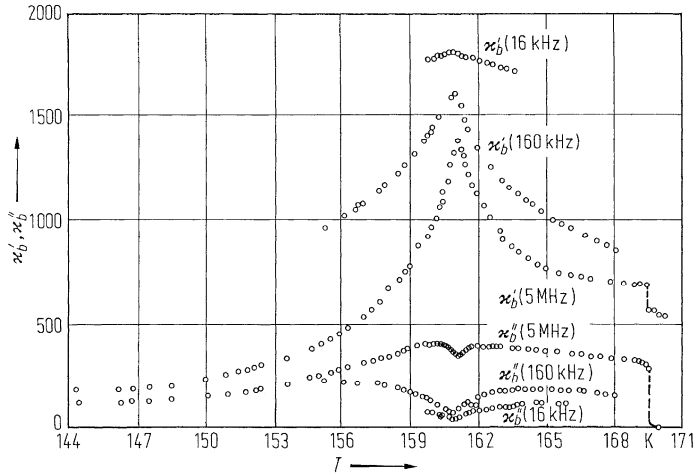

Fig. 50A-1-043. $SC(NH_2)_2$. κ_b', κ_b'' vs. T [73McK]. Parameter: f.

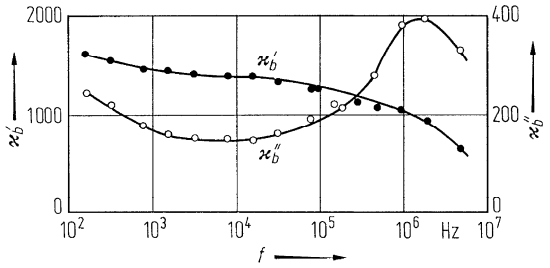

Fig. 50A-1-044. $SC(NH_2)_2$. κ_b', κ_b'' vs. f at 146 K [73McK].

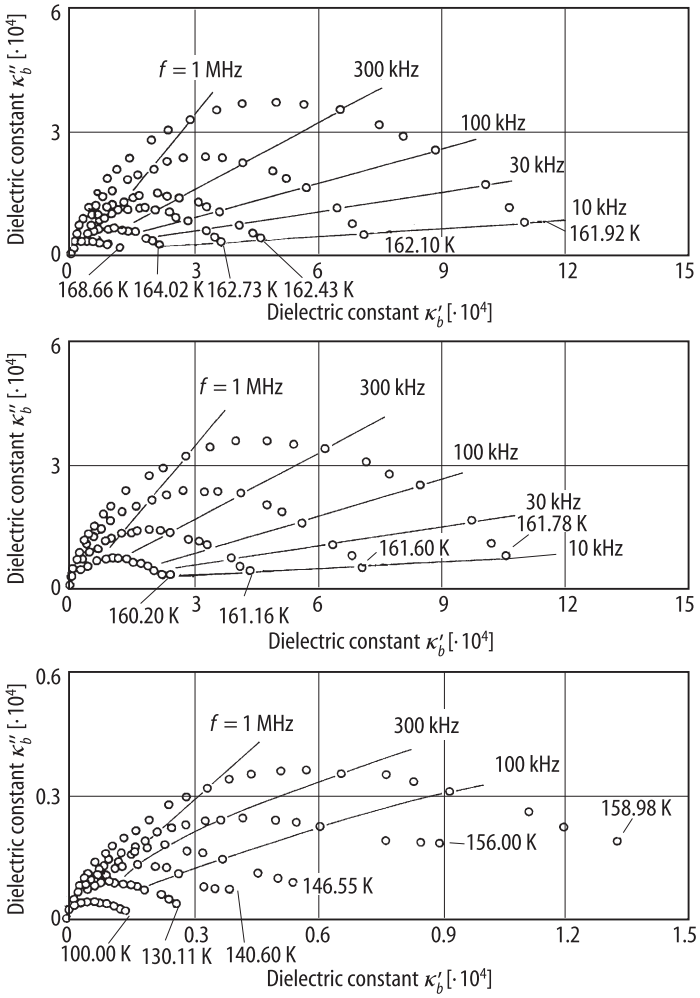

Fig. 50A-1-045. $SC(NH_2)_2$. Cole-Cole diagram of complex dielectric constant [90Ham]. Parameter: *T*. On cooling.

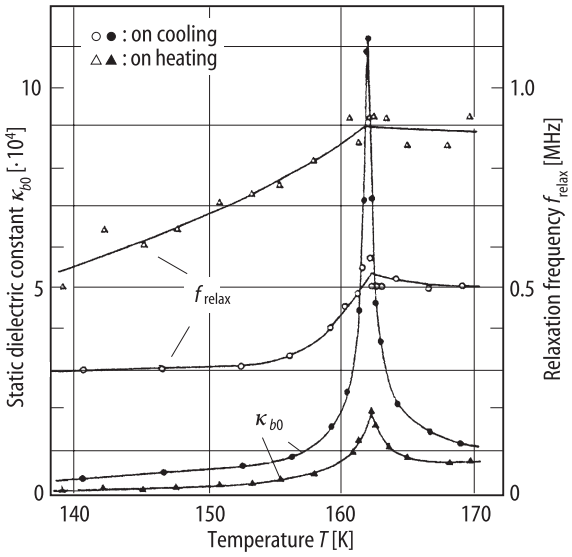

Fig. 50A-1-046. $SC(NH_2)_2$. κ_{b0}, f_{relax} vs. T in the vicinity of $\Theta_{V-V'}$ [90Ham]. κ_{b0}: static dielectric constant, f_{relax}: relaxation frequency.

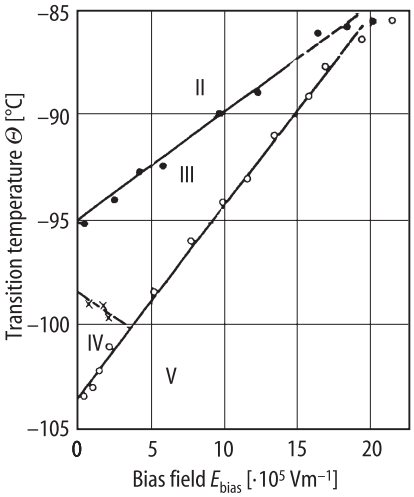

Fig. 50A-1-047. $SC(NH_2)_2$. Θ vs. E_{bias} [62Fut].

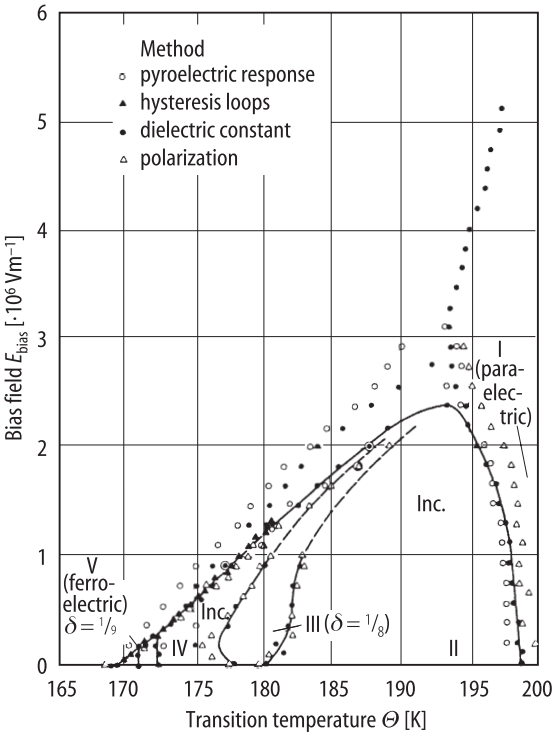

Fig. 50A-1-048. $SC(NH_2)_2$. Θ vs. E_{bias} [87Bou]. Inc.: incommensurate phase.

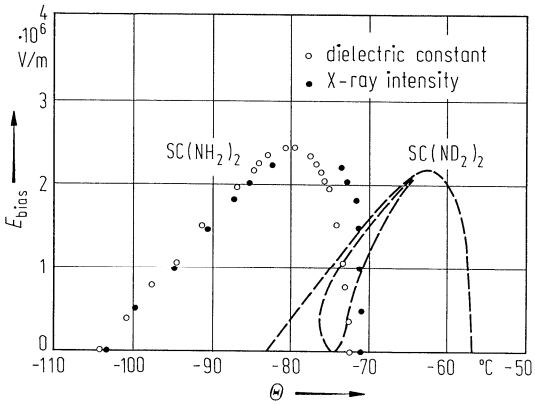

Fig. 50A-1-049. $SC(NH_2)_2$. Θ vs. E_{bias} determined by dielectric and X-ray measurements [85Hat]. Dashed lines show the result for $SC(ND_2)_2$ for comparison [83Bar].

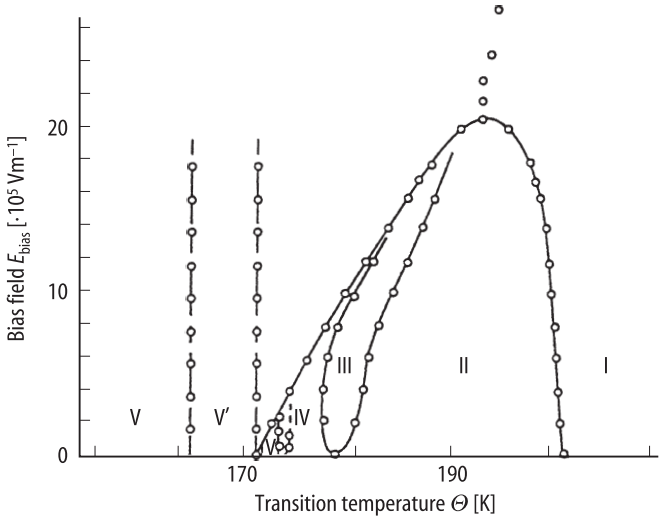

Fig. 50A-1-050. $SC(NH_2)_2$. E_{bias} vs. Θ [96Mag].

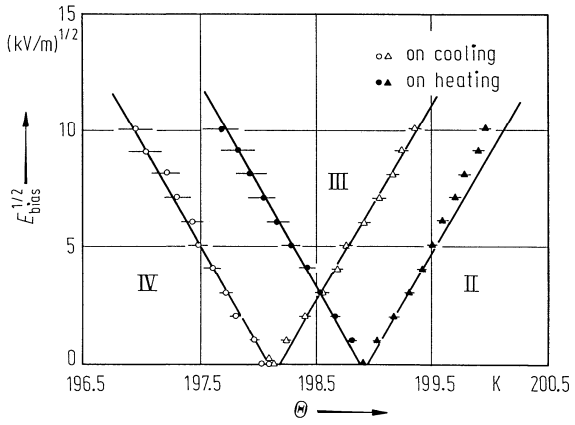

Fig. 50A-1-051. $SC(ND_2)_2$. $E_{bias}^{1/2}$ vs. Θ [82Jam].

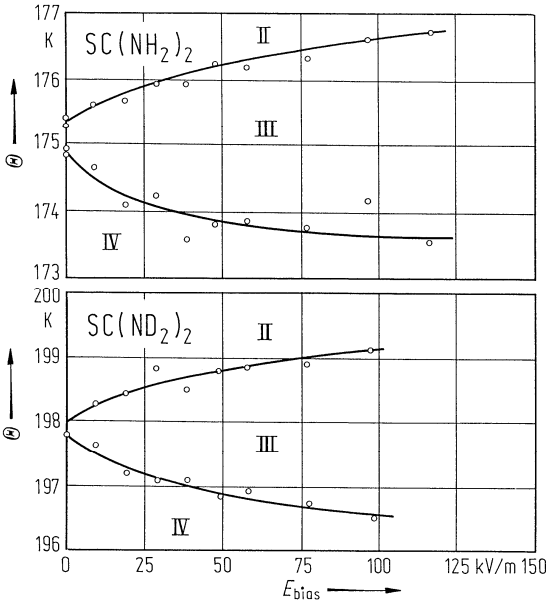

Fig. 50A-1-052. $SC(NH_2)_2$, $SC(ND_2)_2$. Θ vs. E_{bias} in the vicinity of phase III [82Ges1]. On cooling.

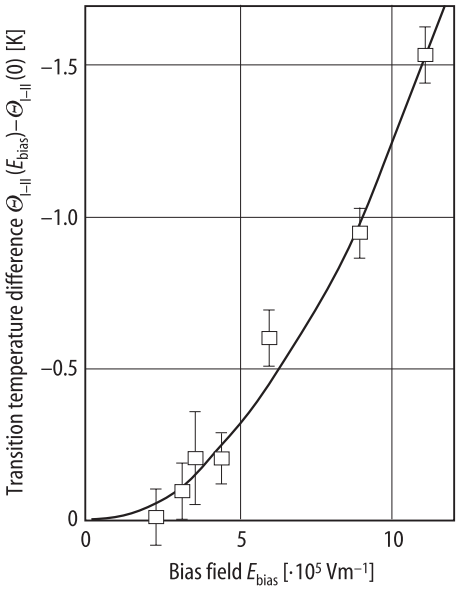

Fig. 50A-1-053. $SC(NH_2)_2$. $\Theta_{II-I}(E_{bias}) - \Theta_{II-I}(0)$ vs. E_{bias} [88Kim]. $\Theta_{II-I}(E_{bias})$: I–II transition temperature at E_{bias}.

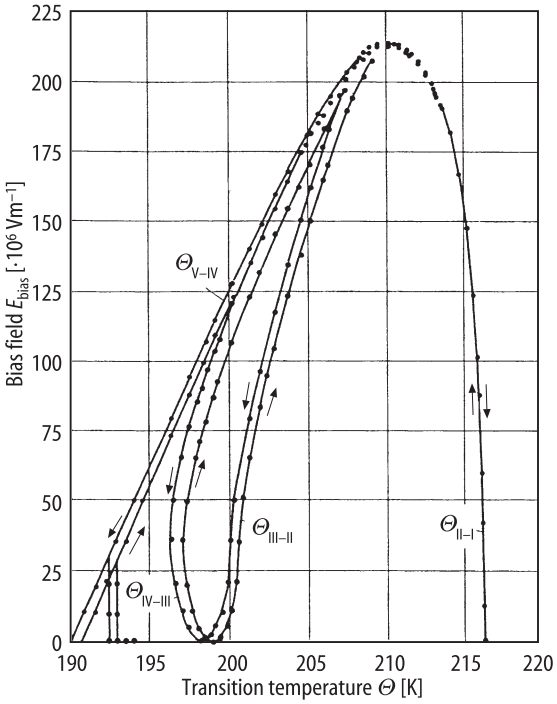

Fig. 50A-1-054. $SC(ND_2)_2$. E_{bias} vs. Θ obtained by birefringence [83Bar].

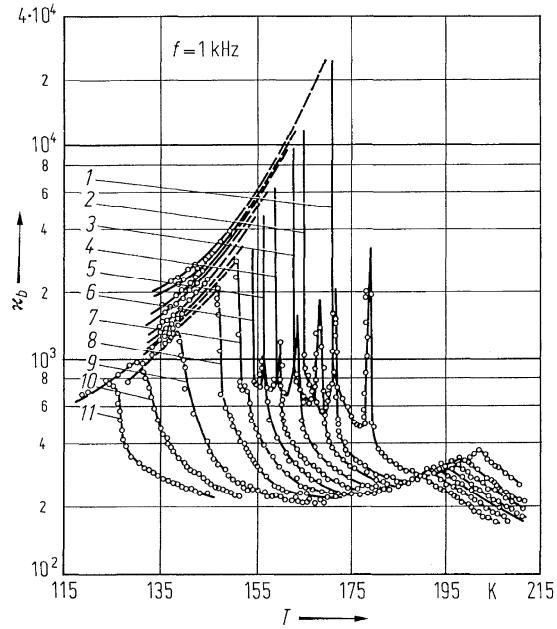

Fig. 50A-1-055. $SC(NH_2)_2$. $\varkappa_b$ vs. T [76Kli]. Parameter: p. Curve *1*: atmospheric pressure, *2*: 0.22, *3*: 0.34, *4*: 0.48, *5*: 0.57, *6*: 0.67, *7*: 0.77, *8*: 0.88, *9*: 1.14, *10*: 1.30, *11*: $1.46 \cdot 10^8$ Pa.

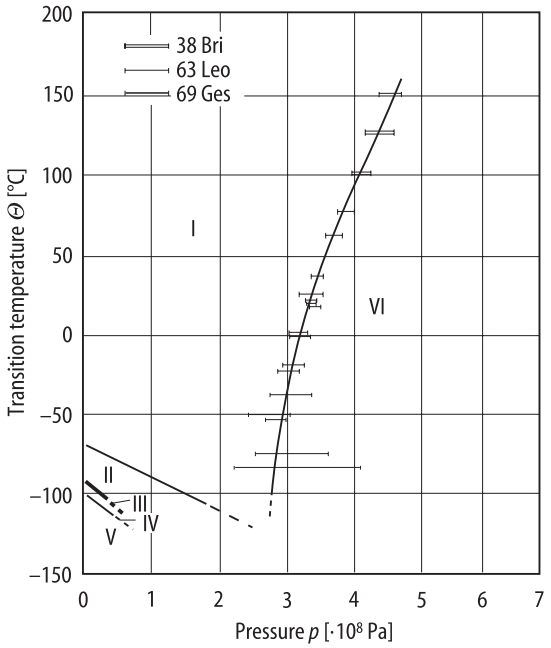

Fig. 50A-1-056. $SC(NH_2)_2$. Θ vs. p [69Ges, 63Leo, 38Bri].

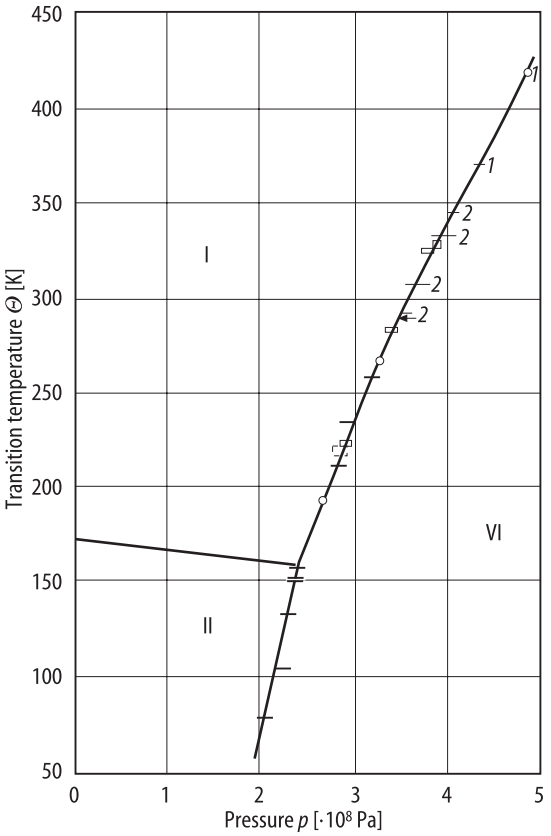

Fig. 50A-1-057. $SC(NH_2)_2$. Θ vs. p [75Fig]. *1*: [38Bri], *2*: [63Leo].

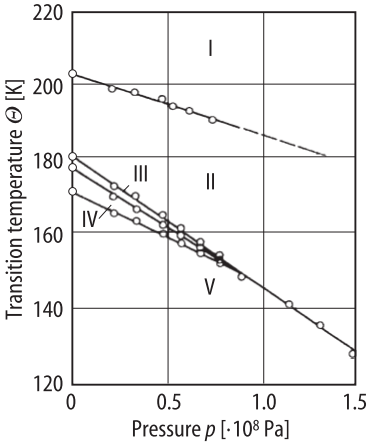

Fig. 50A-1-058. $SC(NH_2)_2$. Θ vs. p [76Kli].

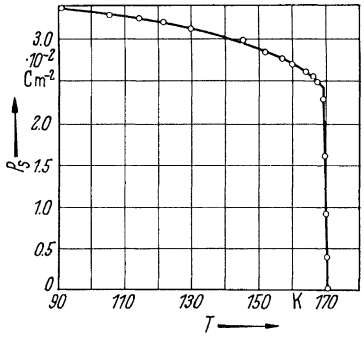

Fig. 50A-1-059. $SC(NH_2)_2$. P_s vs. T in phase V [59Gol].

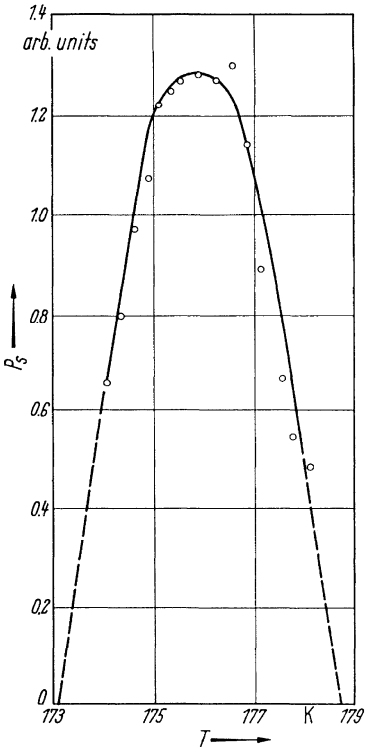

Fig. 50A-1-060. $SC(NH_2)_2$. P_s vs. T in phase III [59Gol]. $E_c \cong 10$ kVm^{-1}.

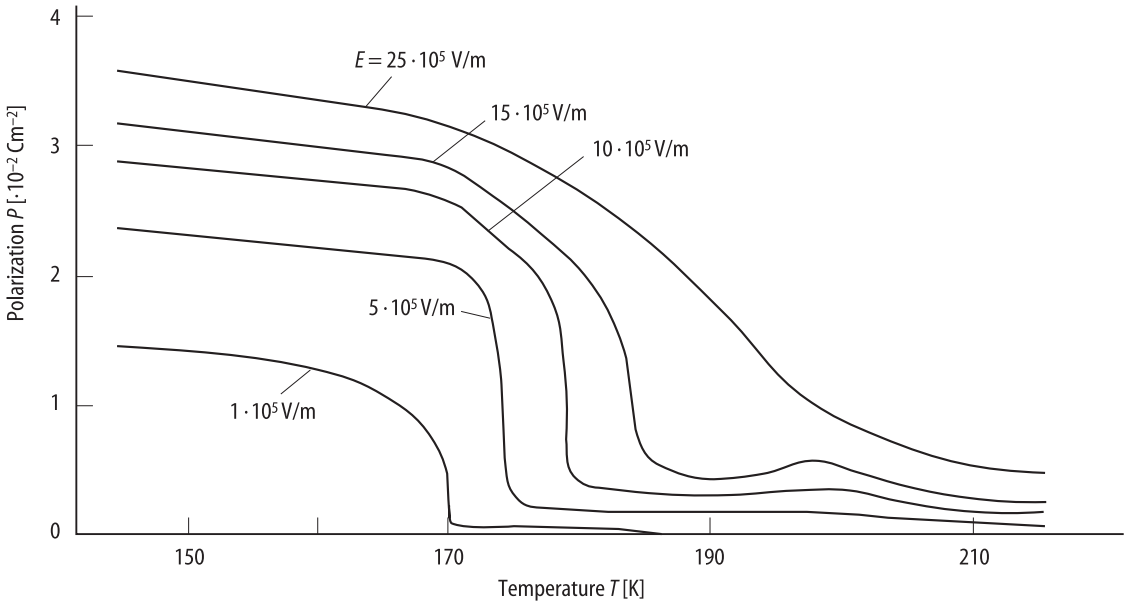

Fig. 50A-1-061. $SC(NH_2)_2$. P vs. T [96Mag]. Parameter: E.

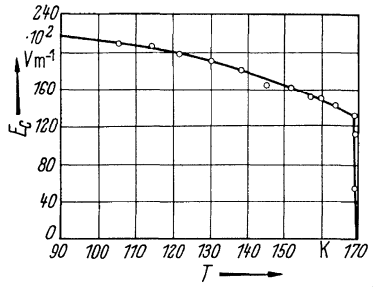

Fig. 50A-1-062. $SC(NH_2)_2$. E_c vs. T in phase V [59Gol].

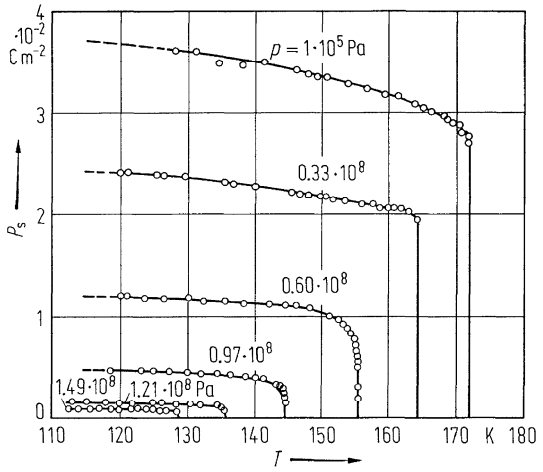

Fig. 50A-1-063. $SC(NH_2)_2$. P_s vs. T [76Kli]. Parameter: p.

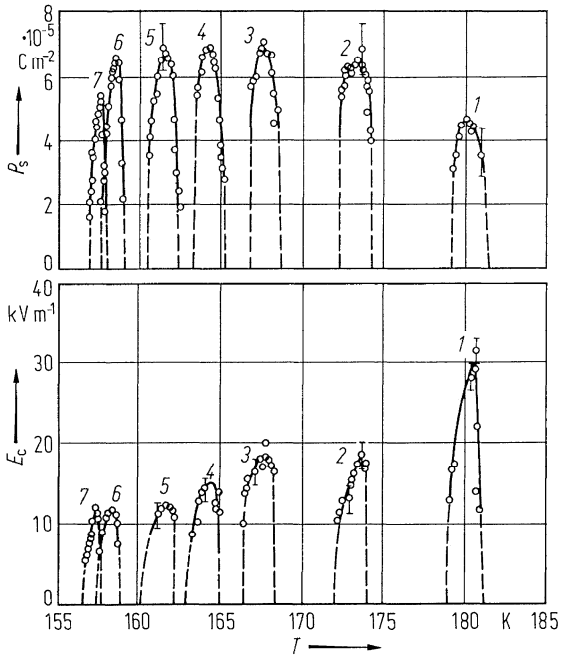

Fig. 50A-1-064. $SC(NH_2)_2$. P_s, E_c vs. T in phase III [76Kli]. Parameter: p. Curve *1*: atmospheric pressure, *2*: 0.18, *3*: 0.37, *4*: 0.45, *5*: 0.54, *6*: 0.65, *7*: $0.70 \cdot 10^8$ Pa.

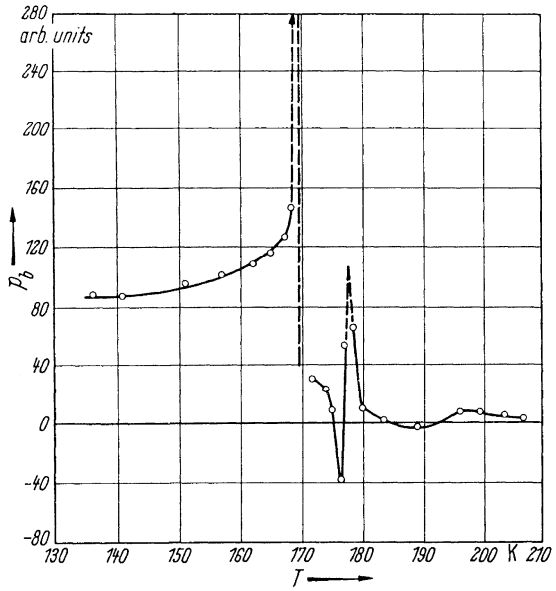

Fig. 50A-1-065. $SC(NH_2)_2$. p_b vs. T [59Gol]. p_b: pyroelectric coefficient along b.

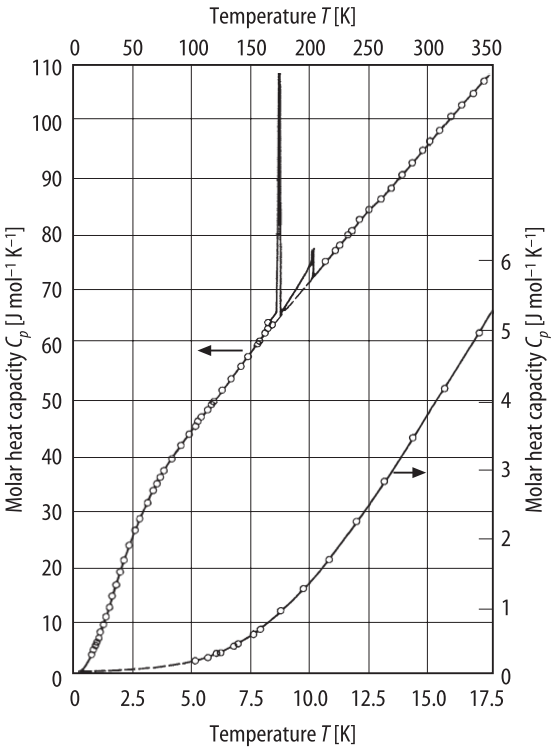

Fig. 50A-1-066. $SC(NH_2)_2$. C_p vs. T [63Cha]. C_p: molar heat capacity at constant pressure. For details in the range between 160 K and 210 K, see Fig. 50A-1-067.

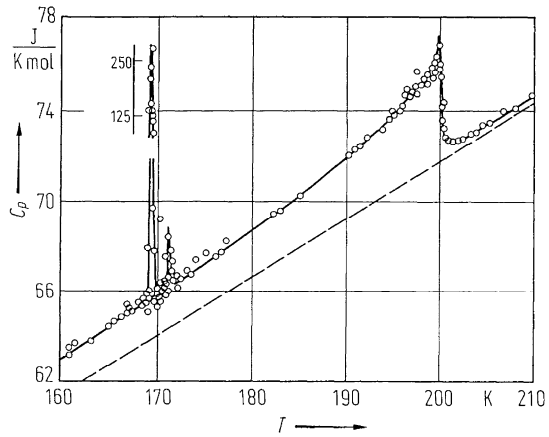

Fig. 50A-1-067. $SC(NH_2)_2$. C_p vs. T [63Cha]. C_p: molar heat capacity at constant pressure. For data in wider range of T, see Fig. 50A-1-066.

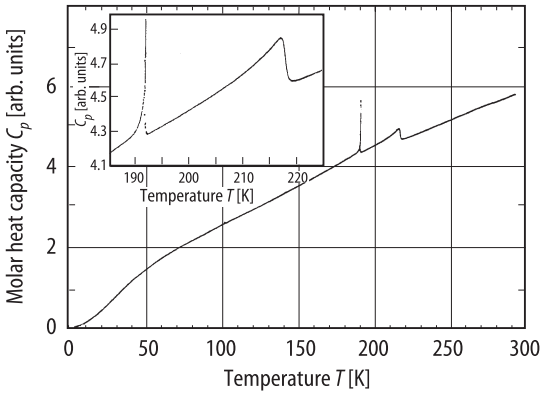

Fig. 50A-1-068. $SC(ND_2)_2$. C_p vs. T [94Ono2]. C_p: molar heat capacity at constant pressure. Obtained by ac calorimetry.

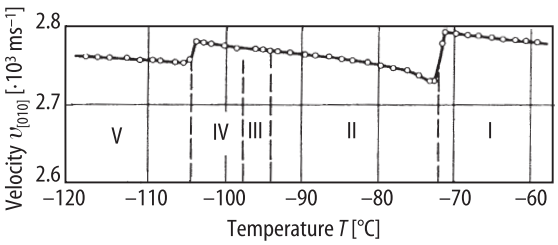

Fig. 50A-1-069. $SC(NH_2)_2$. $v_{[010]}$ vs. T [73Tsu]. ν = 7 MHz. $v_{[010]}$: velocity of the longitudinal ultrasonic wave propagating along [010].

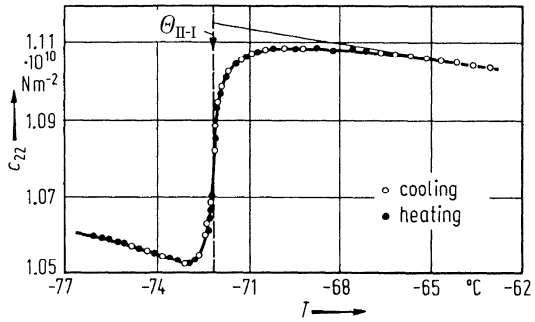

Fig. 50A-1-070. $SC(NH_2)_2$. c_{22} vs. T near Θ_{II-I} [73Tsu]. Ultrasonic measurement at 7 MHz.

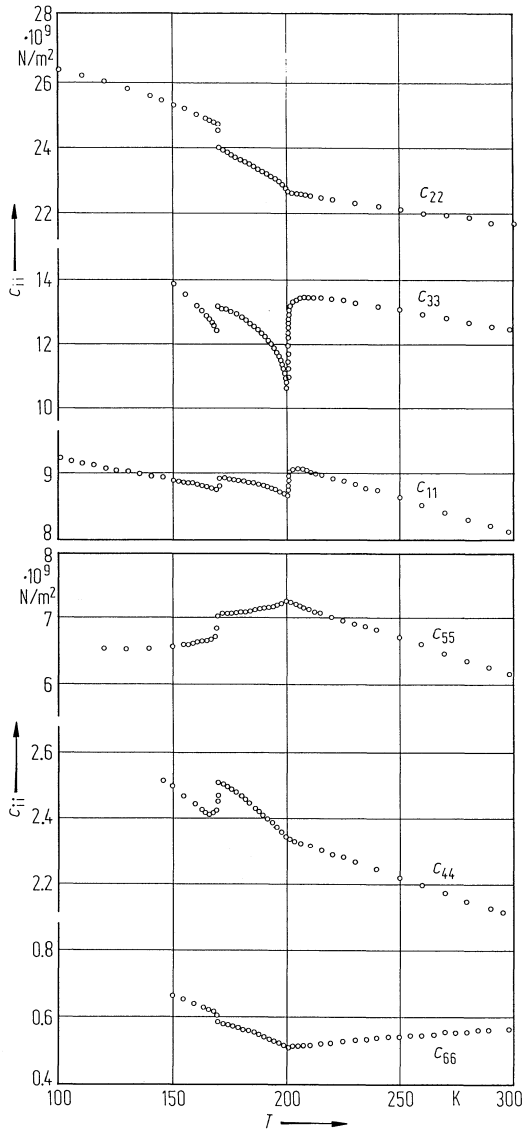

Fig. 50A-1-071. $SC(NH_2)_2$. c_{ii} vs. T [82Reh]. c_{ii}: elastic stiffness constants measured by ultrasonic velocity at 15 MHz. Used crystallographic axes are ($\boldsymbol{a}'$, $\boldsymbol{b}'$, $\boldsymbol{c}'$), the case 2 in 1b.

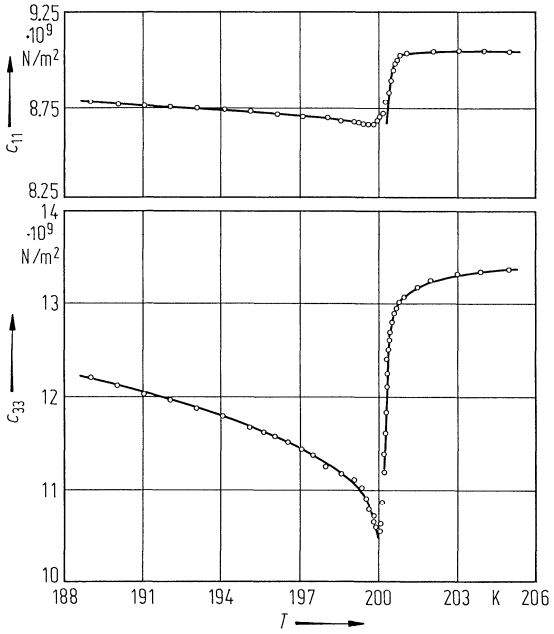

Fig. 50A-1-072. $SC(NH_2)_2$. c_{11}, c_{33} vs. T around Θ_{II-I} [82Reh]. Ultrasonic measurement at 15 MHz. Used crystallographic axes are (***a′***, ***b′***, ***c′***), the case 2 in 1b.

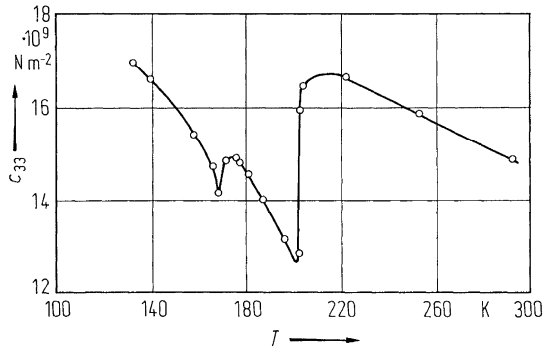

Fig. 50A-1-073. $SC(NH_2)_2$. c_{33} vs. T [74Ben]. Measured by Brillouin scattering. λ = 632.8 nm. Used crystallographic axes are (***a′***, ***b′***, ***c′***), the case 2 in 1b.

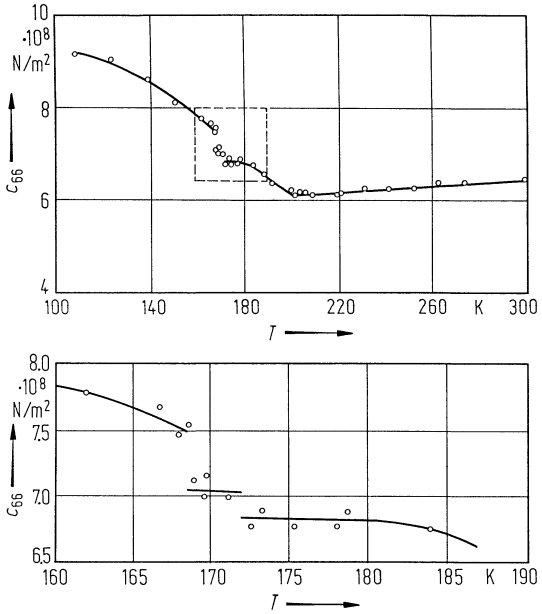

Fig. 50A-1-074. SC(NH$_2$)$_2$. c_{66} vs. T [79Cao]. Measured by Brillouin scattering. λ = 514.5 nm. Used crystallographic axes are (***a***′, ***b***′, ***c***′), the case 2 in 1b.

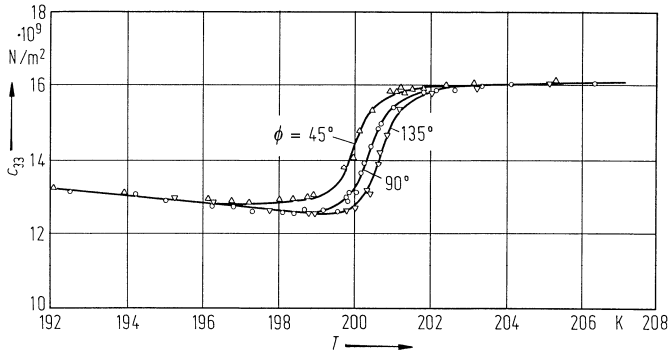

Fig. 50A-1-075. SC(NH$_2$)$_2$. c_{33} vs. T [79Cao]. Parameter: Brillouin scattering angle ϕ. λ = 514.5 nm. Used crystallographic axes are (***a***′, ***b***′, ***c***′), the case 2 in 1b.

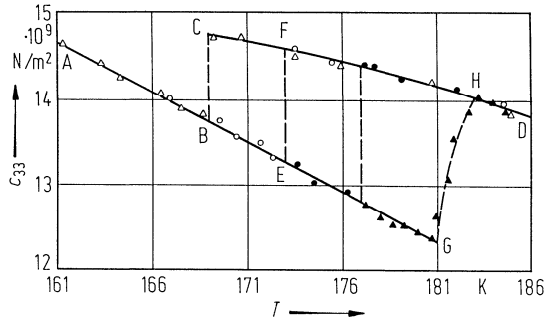

Fig. 50A-1-076. $SC(NH_2)_2$. c_{33} vs. T [82Cao]. Parameter: E_{bias}. Open triangle: E_{bias} = 0 (ABCD), open circle: $E_{bias} = 5 \cdot 10^5$ V m^{-1} (AEFD), full circle: $E_{bias} = 10 \cdot 10^5$ V m^{-1}, full triangle: $E_{bias} = 15 \cdot 10^5$ Vm^{-1} (AGHD). Measured by Brillouin scattering. Used crystallographic axes are (***a***′, ***b***′, ***c***′), the case 2 in 1b.

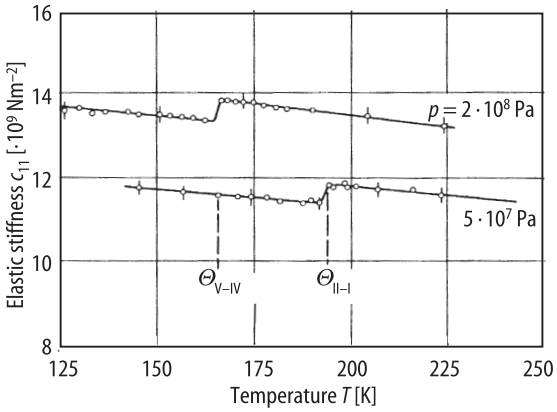

Fig. 50A-1-077. $SC(NH_2)_2$. c_{11} vs. T [84Ben]. Parameter: p. Measured by Brillouin scattering. Used crystallographic axes are (***a***′, ***b***′, ***c***′), the case 2 in 1b.

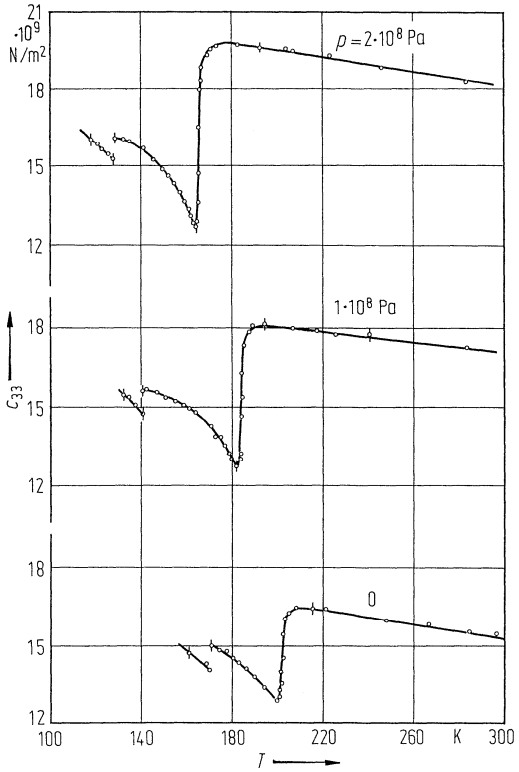

Fig. 50A-1-078. $SC(NH_2)_2$. c_{33} vs. T [84Ben]. Parameter: p. Measured by Brillouin scattering. Used crystallographic axes are (***a′***, ***b′***, ***c′***), the case 2 in 1b.

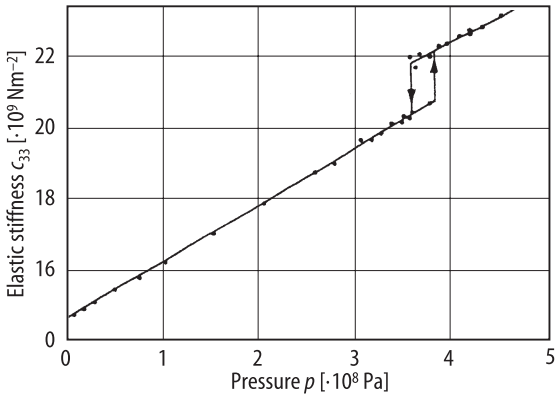

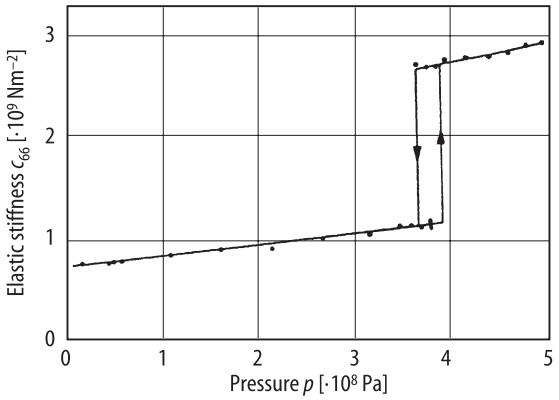

Fig. 50A-1-079. $SC(NH_2)_2$. c_{33}, c_{66} vs. p [83Ben]. T = 293 K. Measured by Brillouin scattering. λ = 514.5 nm. Used crystallographic axes are (***a***′, ***b***′, ***c***′), the case 2 in 1b.

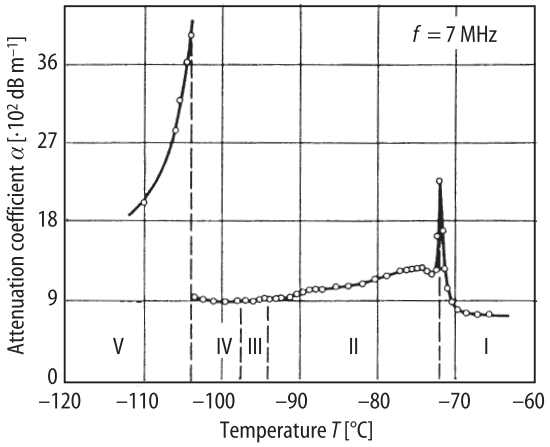

Fig. 50A-1-080. $SC(NH_2)_2$. α vs. T [73Tsu]. α: attenuation coefficient of the longitudinal ultrasonic wave propagating along [010].

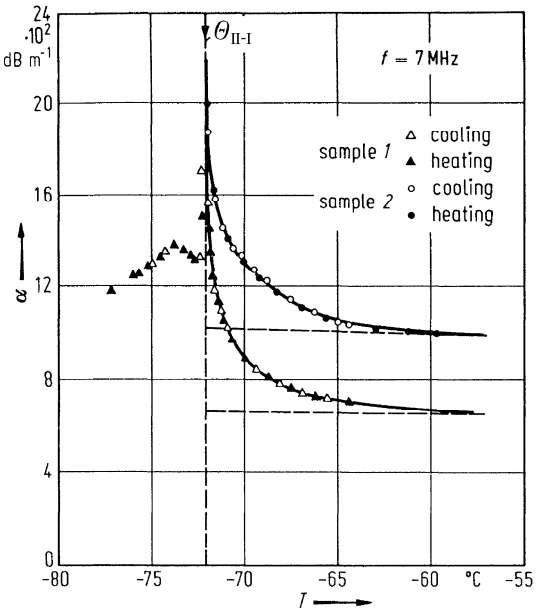

Fig. 50A-1-081. $SC(NH_2)_2$. α vs. T near Θ_{II-I} [73Tsu]. α: attenuation coefficient of the longitudinal ultrasonic wave propagating along [010]. Two specimens were used for this measurement. Absolute values of α differ for the two specimens, but the anomalous parts depend upon temperature in a similar manner.

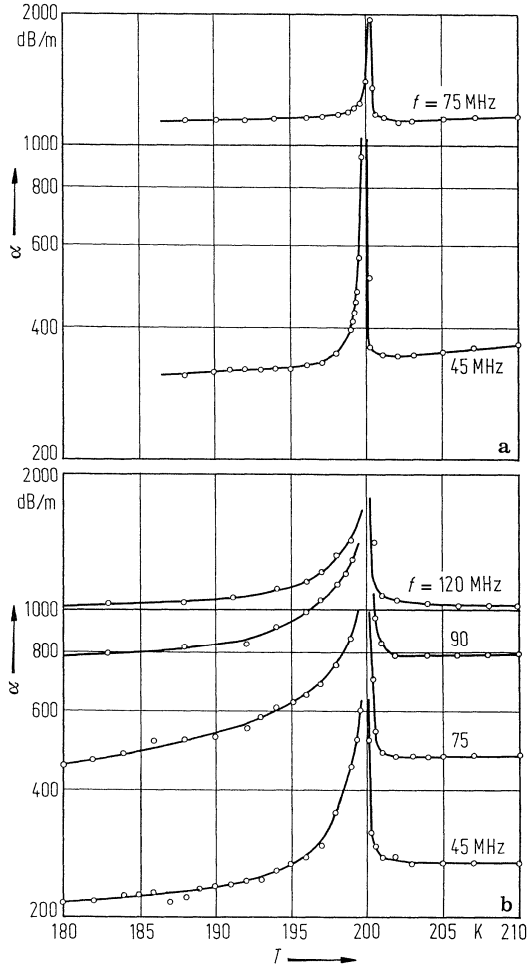

Fig. 50A-1-082. $SC(NH_2)_2$. α vs. T [82Reh]. Parameter: *f.* α: attenuation coefficient of longitudinal ultrasonic waves. (**a**) along $\boldsymbol{a'}$, (**b**) along $\boldsymbol{c'}$. Used crystallographic axes are ($\boldsymbol{a'}$, $\boldsymbol{b'}$, $\boldsymbol{c'}$), the case 2 in 1b.

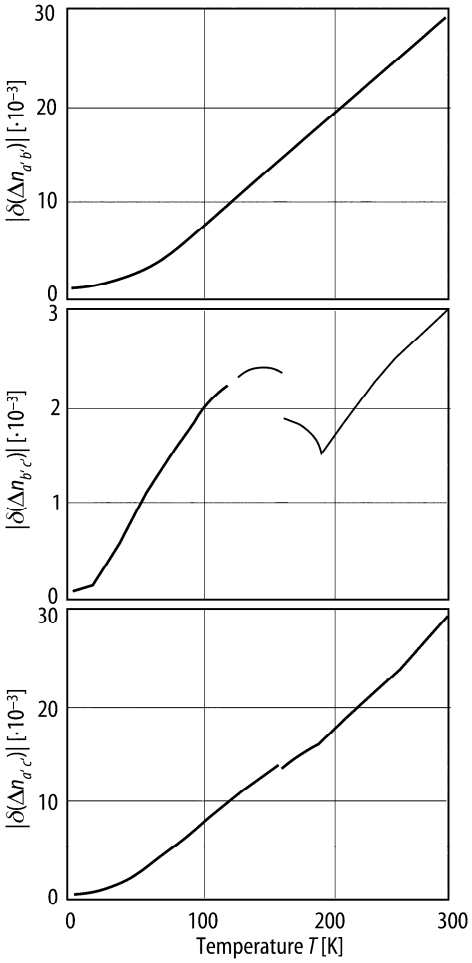

Fig. 50A-1-083. SC(NH$_2$)$_2$. $|\delta(\Delta n_{a'b'})|$, $|\delta(\Delta n_{b'c'})|$, $|\delta(\Delta n_{a'c'})|$ vs. T [90Far]. λ = 589.3 nm. $\delta(\Delta n_{a'b'})$, $\delta(\Delta n_{b'c'})$, $\delta(\Delta n_{a'c'})$: change in birefringence. Used crystallographic axes are ($\boldsymbol{a}'$, $\boldsymbol{b}'$, $\boldsymbol{c}'$), the case 2 in 1b.

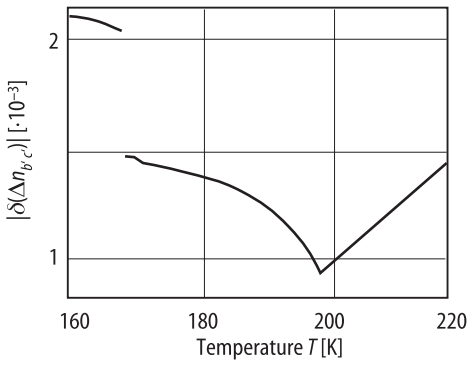

Fig. 50A-1-084. SC(NH$_2$)$_2$. $|\delta(\Delta n_{b'c'})|$ vs. T [90Far]. λ = 589.3 nm. $\delta(\Delta n_{b'c'})$: change in $\Delta n_{b'c'}$. Used crystallographic axes are ($\boldsymbol{a}'$, $\boldsymbol{b}'$, $\boldsymbol{c}'$), the case 2 in 1b.

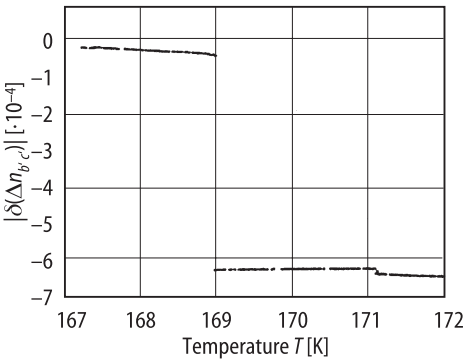

Fig. 50A-1-085. SC(NH$_2$)$_2$. $|\delta(\Delta n_{b'c'})|$ vs. T in the vicinity of Θ_{V-IV} [90Far]. λ = 589.3 nm. $\delta(\Delta n_{b'c'})$: change in $\Delta n_{b'c'}$. Used crystallographic axes are ($\boldsymbol{a}'$, $\boldsymbol{b}'$, $\boldsymbol{c}'$), the case 2 in 1b.

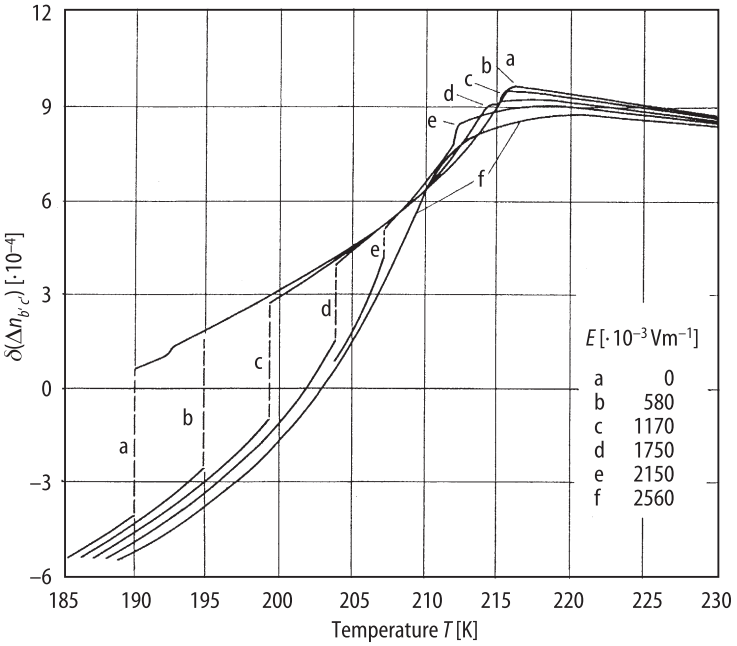

Fig. 50A-1-086. SC(ND$_2$)$_2$. $\delta(\Delta n_{b'c'})$ vs. T [81Jam]. Parameter: E. λ = 632.8 nm. $\delta(\Delta n_{b'c'})$: change in $\Delta n_{b'c'}$. Used crystallographic axes are ($\boldsymbol{a}'$, $\boldsymbol{b}'$, $\boldsymbol{c}'$), the case 2 in 1b.

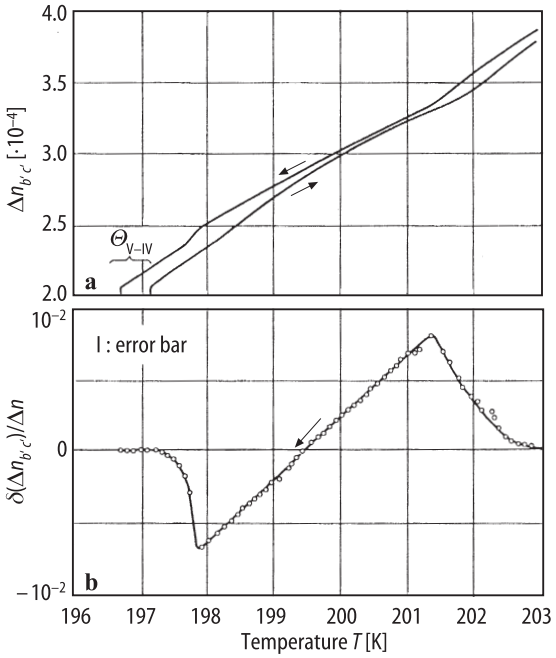

Fig. 50A-1-087. $SC(ND_2)_2$. dc field effects on birefringence [86Led]. (**a**) $\Delta n_{b'c'}$ vs. T. E_{bias} = 750 kV m^{-1}. (**b**) $\delta(\Delta n_{b'c'})/\Delta n$ vs. T. $\delta(\Delta n_{b'c'}) = \Delta n_{b'c'}(E_{bias} = 750 \text{ kV m}^{-1}) - \Delta n$, $\Delta n = \Delta n_{b'c'}(E_{bias} = 0)$. Used crystallographic axes are (***a′***, ***b′***, ***c′***), the case 2 in 1b.

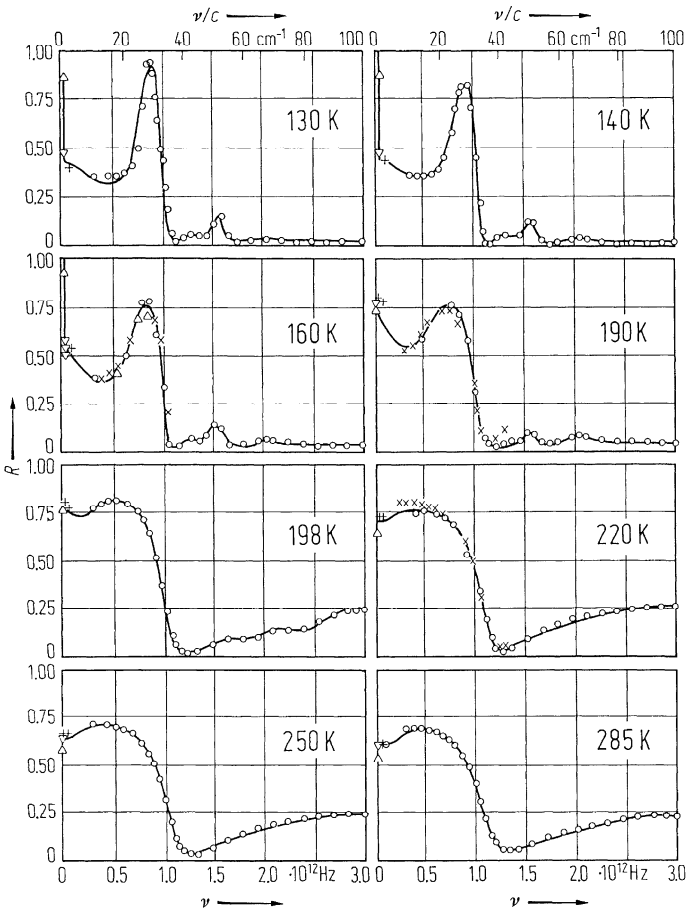

Fig. 50A-1-088. $SC(NH_2)_2$. R vs. ν along [100] at various temperatures [77Khe]. ν: frequency of the infrared radiation, of which polarization is parallel to ***b***. Following data points are shown: empty upside triangle [59Gol], empty downside triangle [75Cza], plus [76Toe], cross [73Fle] and open circle [76Bre]. The full curves represent the best fit reflectivity.

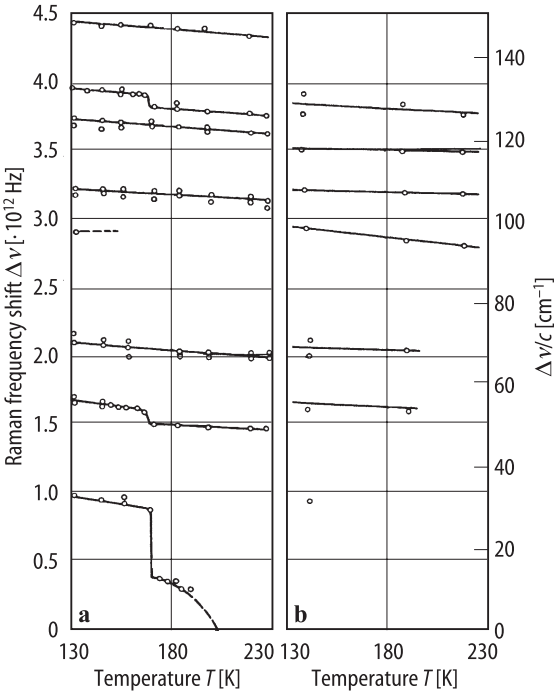

Fig. 50A-1-089. $SC(NH_2)_2$. $\Delta\nu$ vs. T [80Win1]. (**a**) $\Delta\nu$: Raman shift of the various symmetry modes. (**b**) $\Delta\nu$: mode frequencies measured from infrared spectrum.

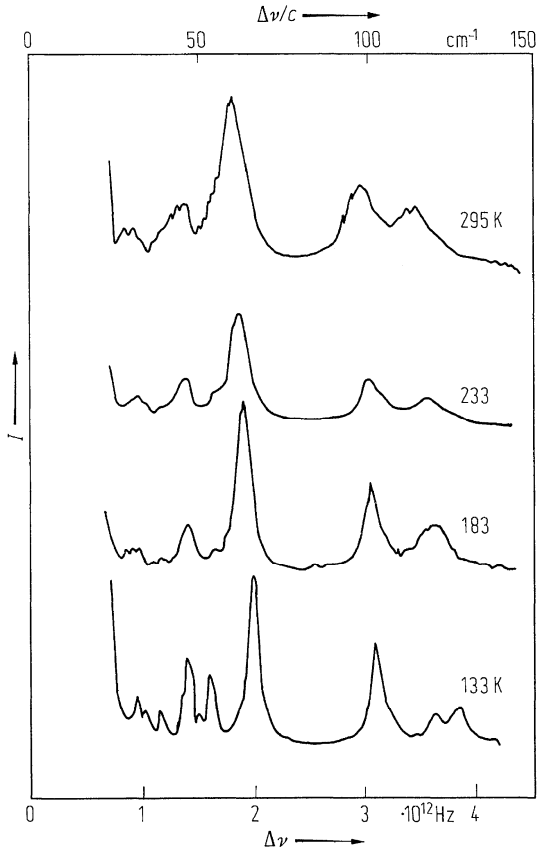

Fig. 50A-1-090. $SC(NH_2)_2$. I vs. $\Delta\nu$ [72Lau]. I: Raman scattering intensity from a powder sample. Parameter: T.

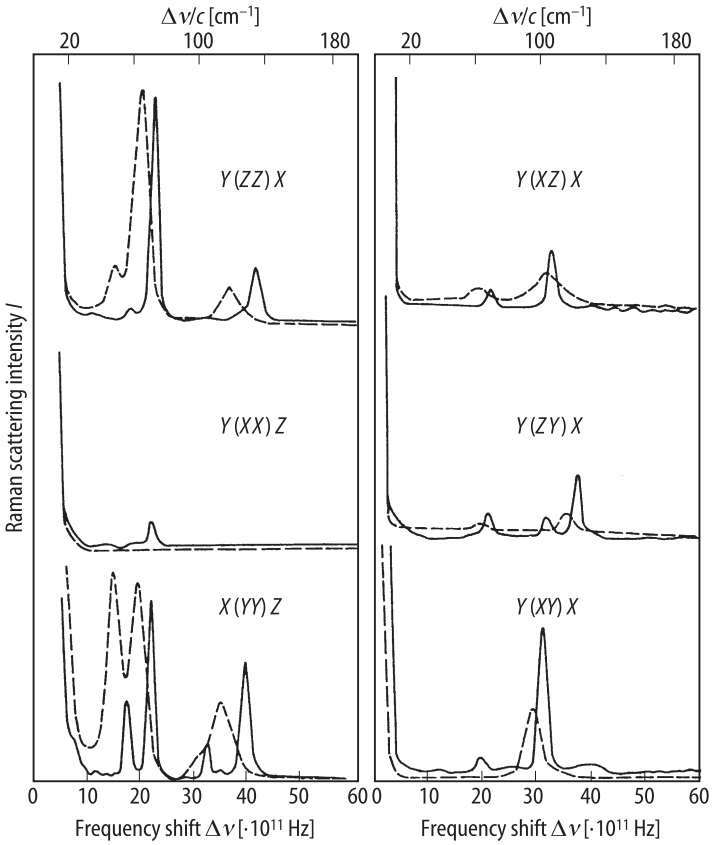

Fig. 50A-1-091. $SC(NH_2)_2$. I vs. $\Delta\nu$ [72Ban]. I: Raman scattering intensity for various scattering geometries. The dashed lines are data at room temperature and the solid lines are at –150 °C. Used crystallographic axes are (***a***′, ***b***′, ***c***′), the case 2 in 1b.

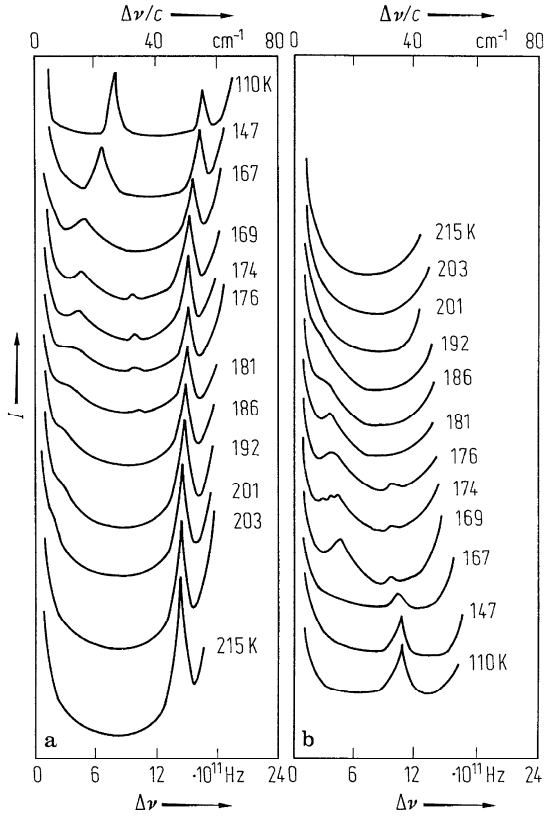

Fig. 50A-1-092. $SC(NH_2)_2$. *I* vs. $\Delta\nu$ [75Del]. *I*: Raman scattering intensity at various temperatures. Spectra (**a**) show transverse optic modes measured in the scattering geometry of $b(cc)\,\bar{b}$. Spectra (**b**) show longitudinal modes measured in the geometry of $a(cc)\,\bar{a}$. Used crystallographic axes are (***a′***, ***b′***, ***c′***), the case 2 in 1b.

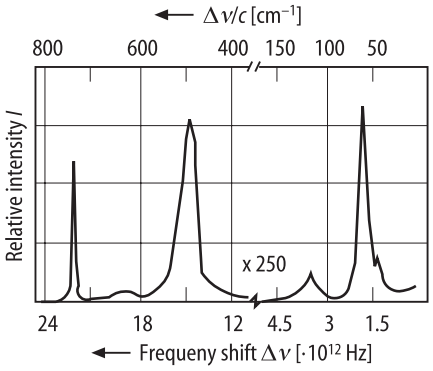

Fig. 50A-1-093. $SC(NH_2)_2$. *I* vs. $\Delta\nu$ [89Kim]. *I*: relative intensity of Ag-mode Raman spectra observed at RT.

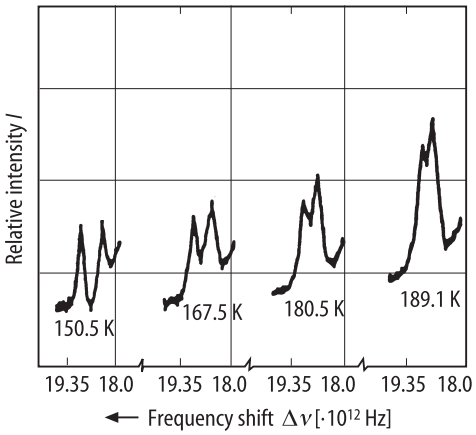

Fig. 50A-1-094. $SC(NH_2)_2$. I vs. $\Delta\nu$ [89Kim]. I: relative intensity of Raman scattering. Parameter: T.

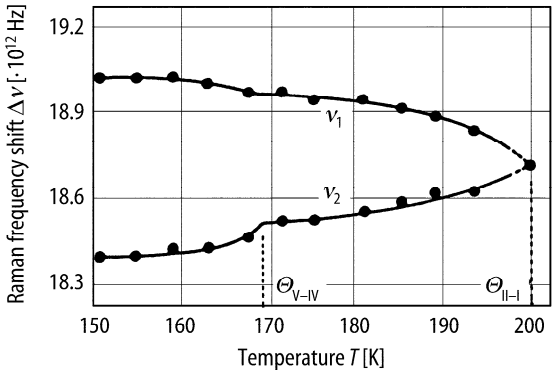

Fig. 50A-1-095. $SC(NH_2)_2$. $\Delta\nu$ vs. T [89Kim]. $\Delta\nu$: Raman frequency shift of ν_1 and ν_2 modes.

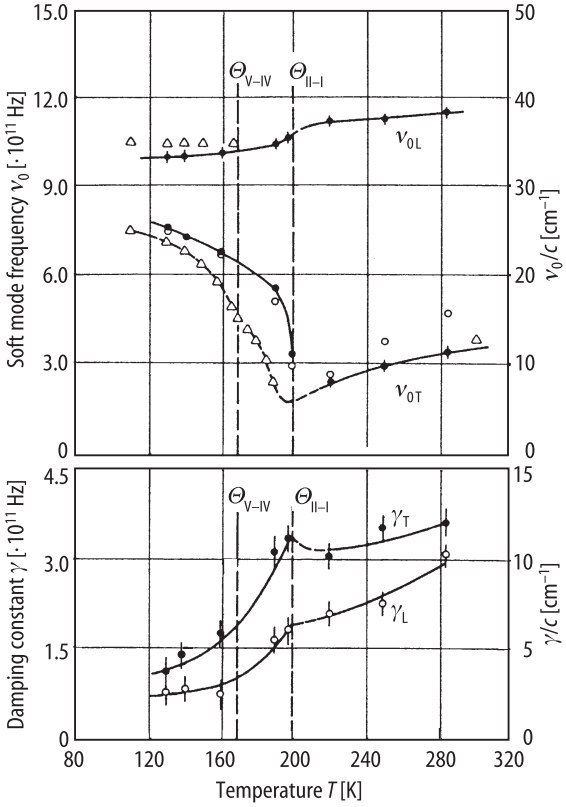

Fig. 50A-1-096. $SC(NH_2)_2$. ν_0, γ vs. T [77Khe]. ν_0: soft mode frequency. γ: damping constant of the soft mode. Subscripts T and L denote transverse and longitudinal modes, respectively. Triangles are the Raman data from [75Del], others are results of the Kramers-Kronig analysis of [76Bre, 73Fle, 77Khe].

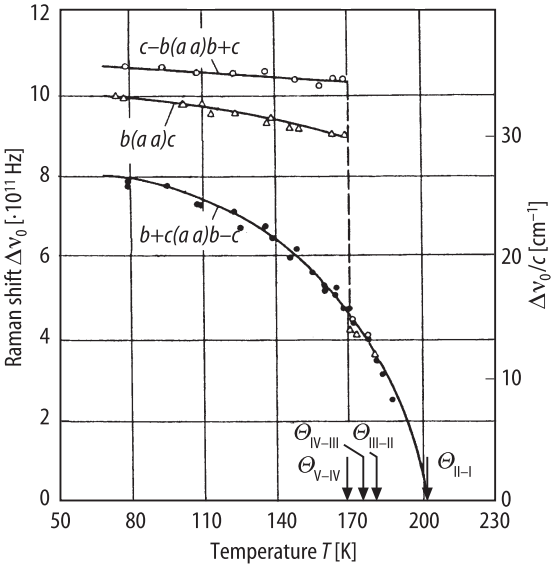

Fig. 50A-1-097. $SC(NH_2)_2$. $\Delta\nu_0$ vs. T [78Wad]. $\Delta\nu_0$: Raman shift of the low frequency modes.

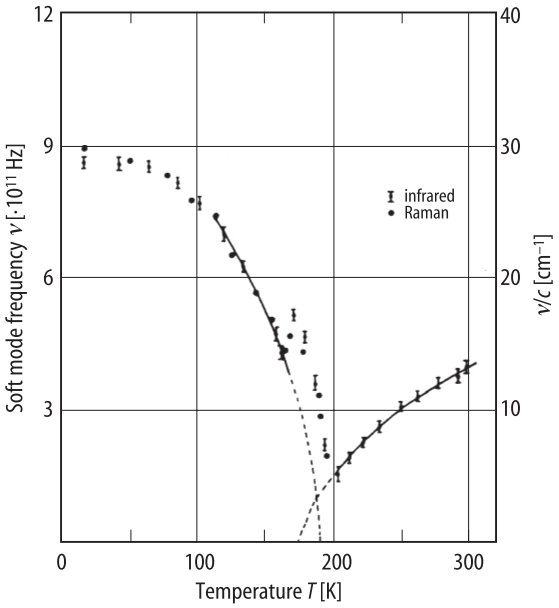

Fig. 50A-1-098. $SC(NH_2)_2$. ν vs. T [80Sia]. ν: soft mode frequency obtained from Raman and infrared reflection spectra.

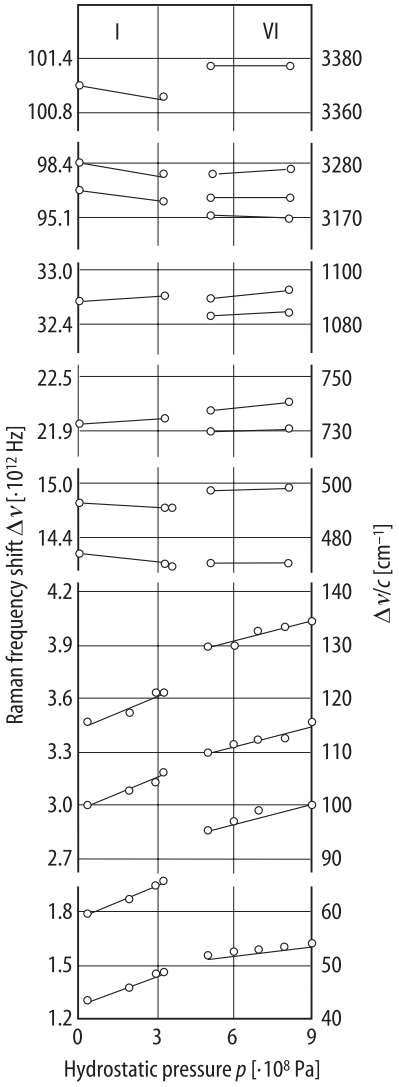

Fig. 50A-1-099. $SC(NH_2)_2$. $\Delta\nu$ vs. p [76Iqb]. $\Delta\nu$: Raman frequency shift at RT. p: hydrostatic pressure. Confer Fig. 50A-1-056, Fig. 50A-1-057.

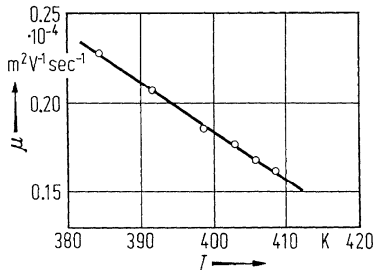

Fig. 50A-1-100. $SC(NH_2)_2$. μ vs. T [70Yog]. μ: carrier mobility.

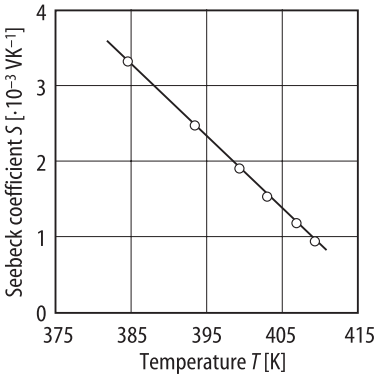

Fig. 50A-1-101. $SC(NH_2)_2$. S vs. T [70Yog]. S: Seebeck coefficient obtained from pressed powder sample.

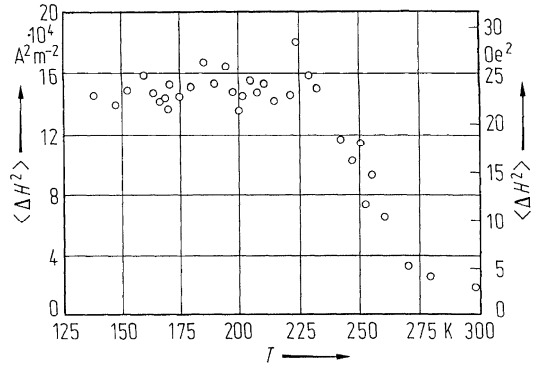

Fig. 50A-1-102. $SC(NH_2)_2$. $\langle \Delta H^2 \rangle$ of proton vs. T [61Ems1]. $\boldsymbol{a} \wedge \boldsymbol{H} = 90°$, $\boldsymbol{b} \wedge \boldsymbol{H} = 40°$. $\langle \Delta H^2 \rangle$: second moment obtained from a single crystal. Used crystallographic axes are ($\boldsymbol{a}'$, $\boldsymbol{b}'$, $\boldsymbol{c}'$), the case 2 in 1b.

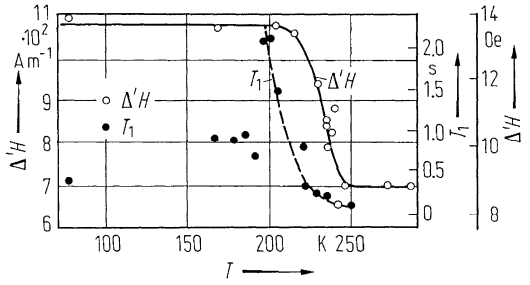

Fig. 50A-1-103. $SC(NH_2)_2$. $\Delta'H$, T_1 vs. T obtained from polycrystalline sample [61Ems1]. $\Delta'H$: separation between maximum and minimum of the derivative of proton NMR curve. T_1: proton spin-lattice relaxation time.

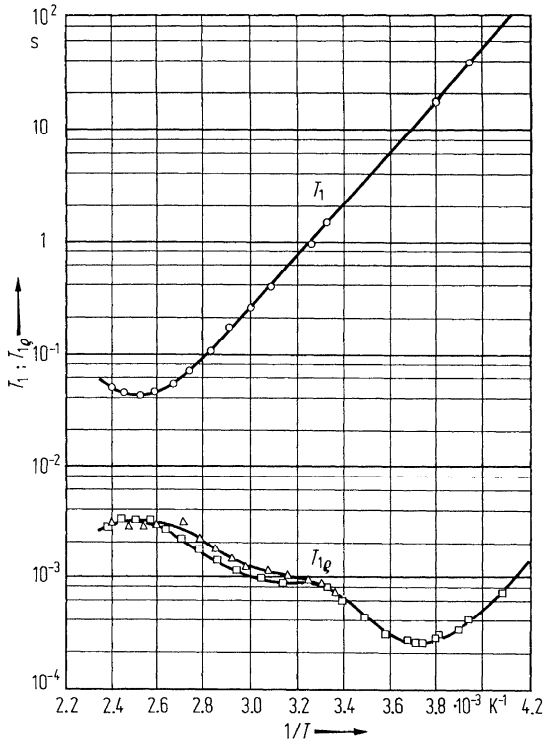

Fig. 50A-1-104. SC(NH$_2$)$_2$. T_1, $T_{1\rho}$ vs. $1/T$ [71ORe]. T_1: proton spin-lattice relaxation time, $T_{1\rho}$: rotating frame relaxation time. Squares: $H_1 = 1.03 \cdot 10^3$ A m^{-1}, triangles: $H_1 = 1.51 \cdot 10^3$ A m^{-1}, where H_1 is the radio frequency magnetic field.

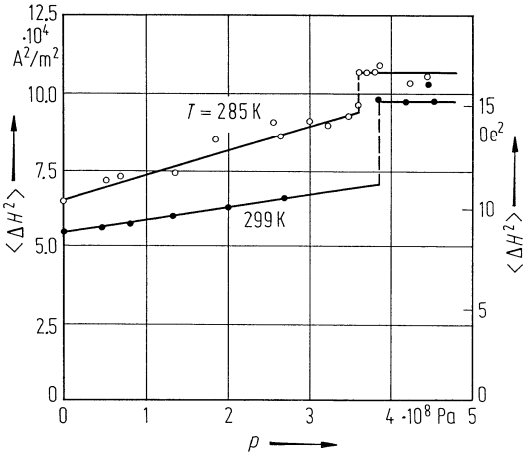

Fig. 50A-1-105. SC(NH$_2$)$_2$. $\langle \Delta H^2 \rangle$ vs. p [80Kli]. Parameter: T. $\langle \Delta H^2 \rangle$: second moment of proton NMR measured by powder sample.

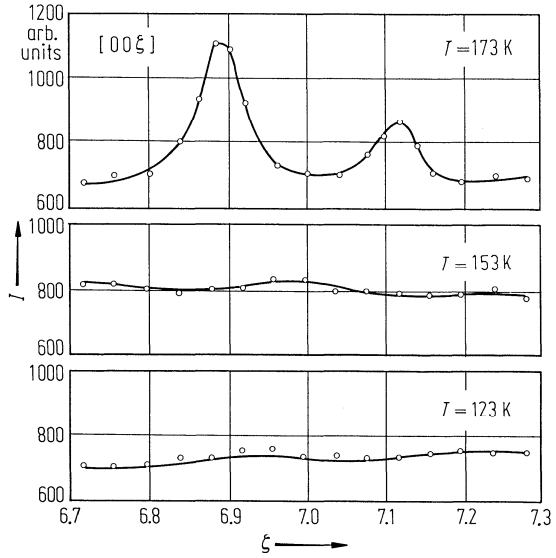

Fig. 50A-1-106. $SC(NH_2)_2$. $I_{(007\pm\delta)}$ vs. ζ [88Tak]. $I_{(007\pm\delta)}$: X-ray satellite intensity due to longitudinal modulation component. δ: reduced wave vector of lattice modulation. Parameter: T. ζ: reduced wave vector coordinate in units of $1/c$.

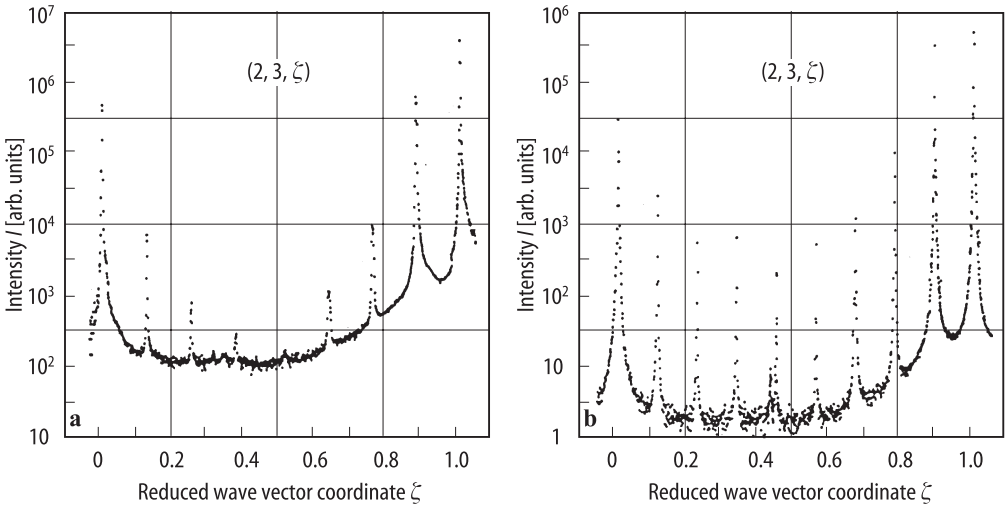

Fig. 50A-1-107. $SC(NH_2)_2$. $I_{(2,3,\zeta)}$ vs. ζ [91Mas]. (**a**) T = 178 K, $\delta \cong 1/8$, (**b**) T = 170.5 K, $\delta \cong 1/9$. ζ: reduced wave vector coordinate in units of $1/c$. δ: reduced wave vector of lattice modulation.

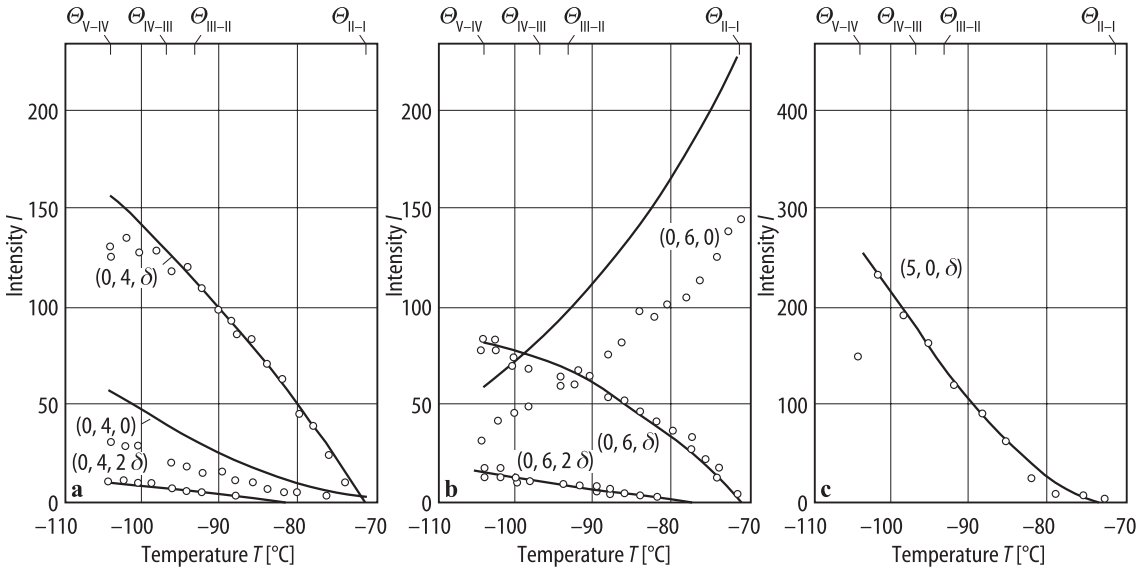

Fig. 50A-1-108. SC(NH$_2$)$_2$. $I_{(h\,k\,\zeta)}$ vs. T [71Shi]. $I_{(h\,k\,\zeta)}$: integrated intensity of X-ray diffraction peak at (h k ζ) in reciprocal space. Usual Bragg reflection corresponds to (hk0) and satellite scattering due to structural modulation to (h k ζ) with $\zeta = \delta$ or 2δ. δ: reduced wave vector of lattice modulation. (**a**) $I_{(0,4,0)}$, $I_{(0,4,\delta)}$, $I_{(0,4,2\delta)}$; (**b**) $I_{(0,6,0)}$, $I_{(0,6,\delta)}$, $I_{(0,6,2\delta)}$; (**c**) $I_{(5,0,\delta)}$.

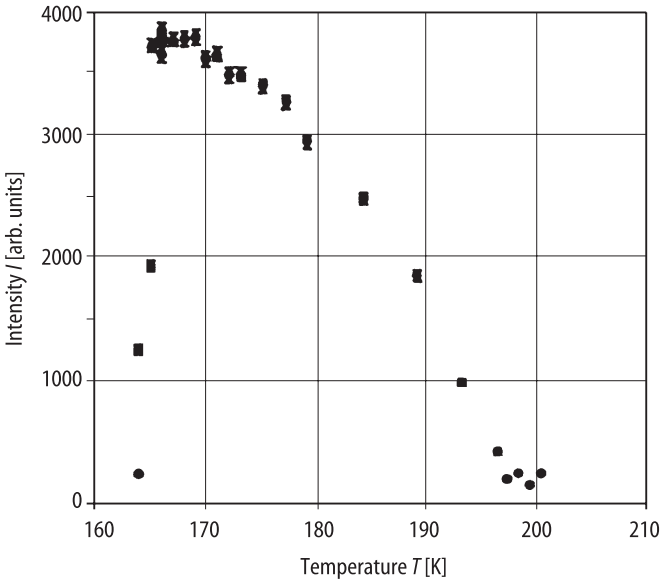

Fig. 50A-1-109. SC(NH$_2$)$_2$. $I_{(1,\,1,\,2+3\delta)}$ vs. T [89Zun]. δ: reduced wave vector of modulation.

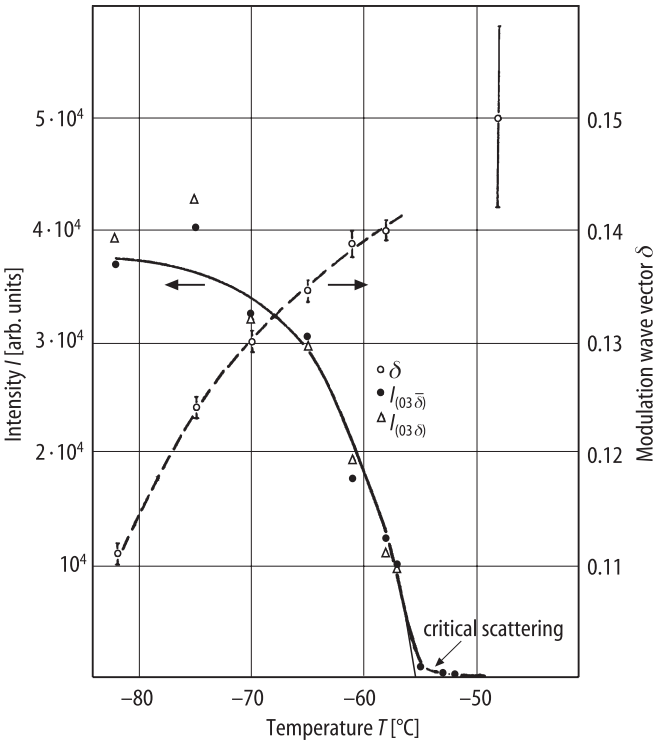

Fig. 50A-1-110. $SC(ND_2)_2$. I vs. T, and δ vs. T [78Mou1]. $I_{(0,3,\pm\delta)}$: elastic neutron scattering intensity at $(0, 3, \pm\delta)$. δ: modulation wave vector.

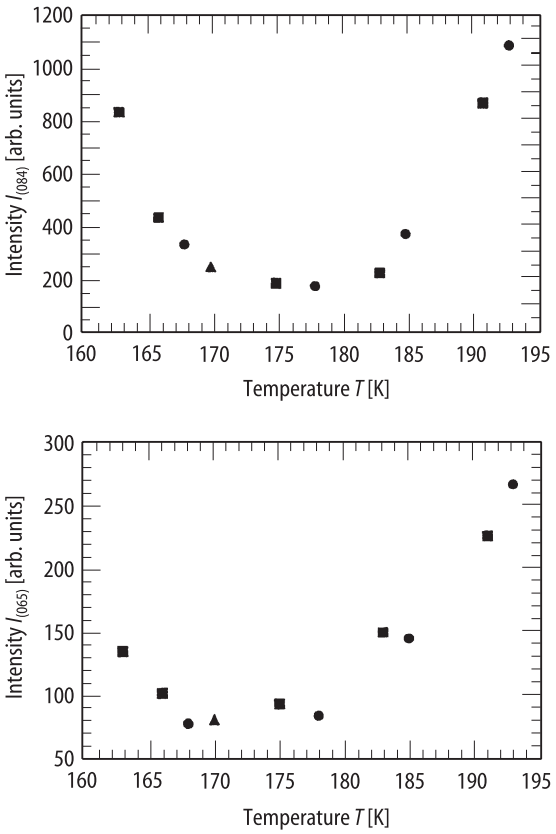

Fig. 50A-1-111. $SC(NH_2)_2$. $I_{(084)}$, $I_{(065)}$ vs. T [97Ara]. Different symbols show the different independent measurements, respectively.

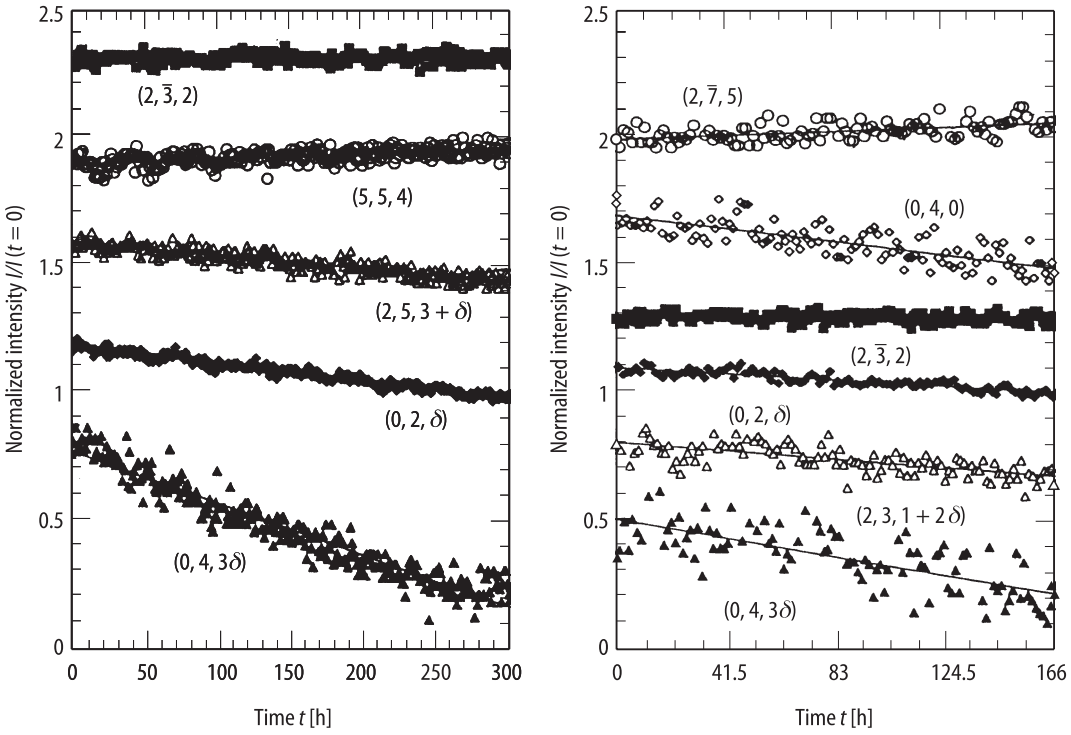

Fig. 50A-1-112. $SC(NH_2)_2$. Time evolution of integrated intensities of X-ray Bragg reflections; $I/I(t = 0)$ vs. t [96Ara]. $T = 170.0(2)$ K. $\delta = 0.116$. The intensities are normalized with respect to their value at $t = 0$.

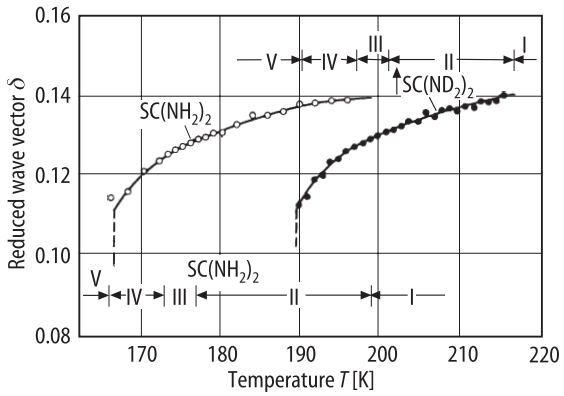

Fig. 50A-1-113. $SC(NH_2)_2$, $SC(ND_2)_2$. δ vs. T [77Iiz]. δ: reduced wave vector of lattice modulation.

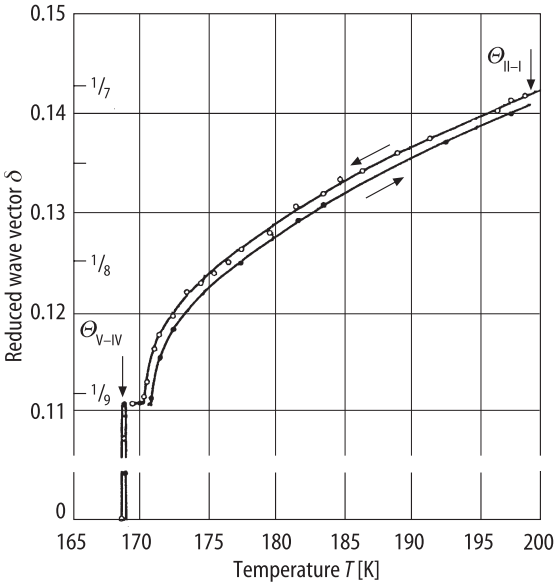

Fig. 50A-1-114. $SC(NH_2)_2$. δ vs. T [85Dur]. δ: reduced wave vector of lattice modulation.

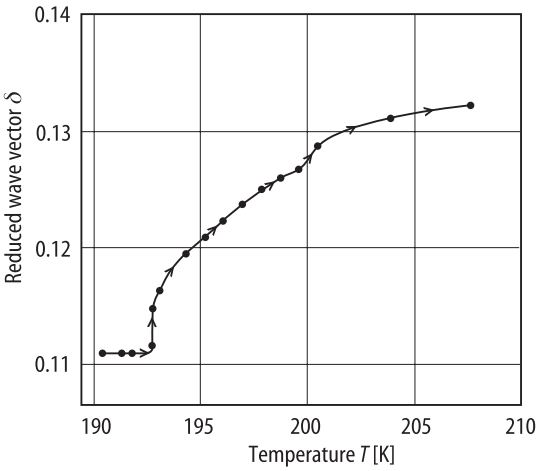

Fig. 50A-1-115. $SC(ND_2)_2$. δ vs. T [79Mou]. δ: reduced wave vector of lattice modulation. Measured at (3, 0, 3δ).

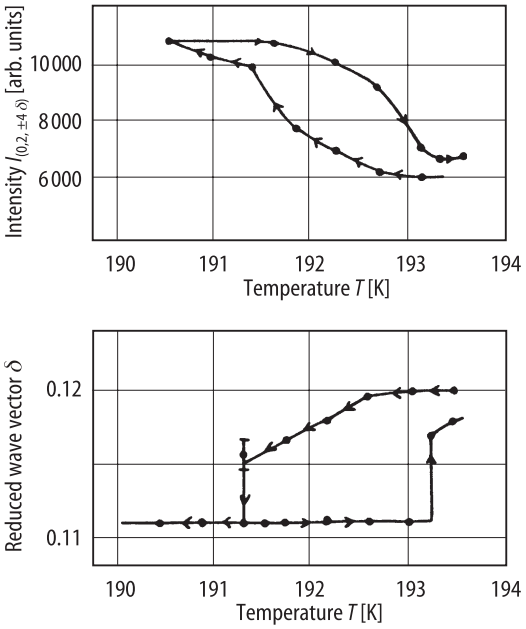

Fig. 50A-1-116. $SC(ND_2)_2$. $I_{(0,2,\pm4\delta)}$ vs. T, and δ vs. T [79Mou]. $I_{(0,2,\pm4\delta)}$: elastic neutron scattering intensity at $(0, 2, \pm4\delta)$. δ: reduced wave vector of lattice modulation.

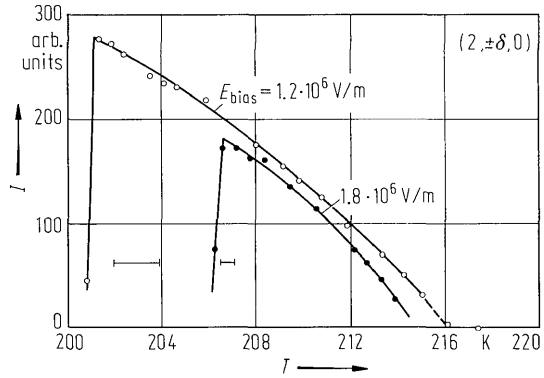

Fig. 50A-1-117. $SC(ND_2)_2$. $I_{(2,\pm\delta,0)}$ vs. T [84Dur]. Parameter: E_{bias}. $I_{(2,\pm\delta,0)}$: neutron satellite intensity. The horizontal bar attached to each curve indicates the temperature range of the phase III (δ = 1/8). Used crystallographic axes are ($\boldsymbol{a}'$, $\boldsymbol{b}'$, $\boldsymbol{c}'$), the case 2 in 1b.

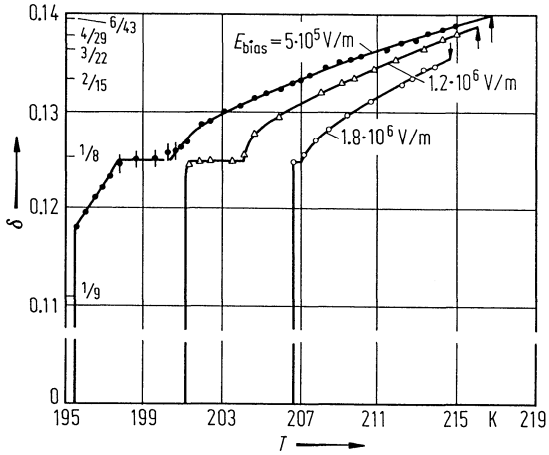

Fig. 50A-1-118. SC(NH$_2$)$_2$. δ vs. T [84Dur]. Parameter: E_{bias} . δ: reduced wave vector of lattice modulation. Arrows attached to each curve indicate $\Theta_{II–I}$.

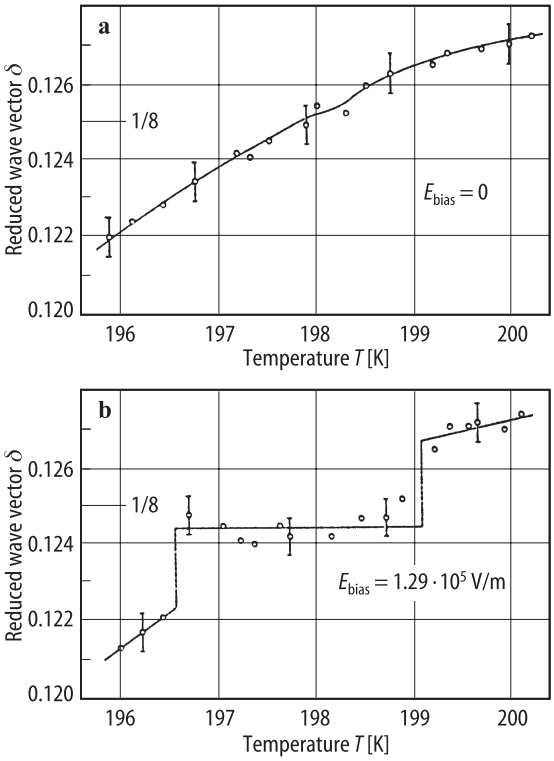

Fig. 50A-1-119. SC(ND$_2$)$_2$. δ vs. T around phase III [82Ges2]. (**a**) E_{bias} = 0, (**b**) E_{bias} = $1.29 \cdot 10^5$ V m^{-1}. δ: reduced wave vector of lattice modulation.

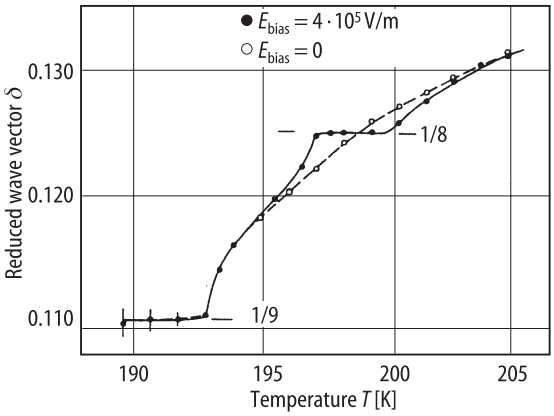

Fig. 50A-1-120. $SC(ND_2)_2$. δ vs. T [82Mou]. Parameter: E_{bias}. δ: reduced wave vector of lattice modulation.

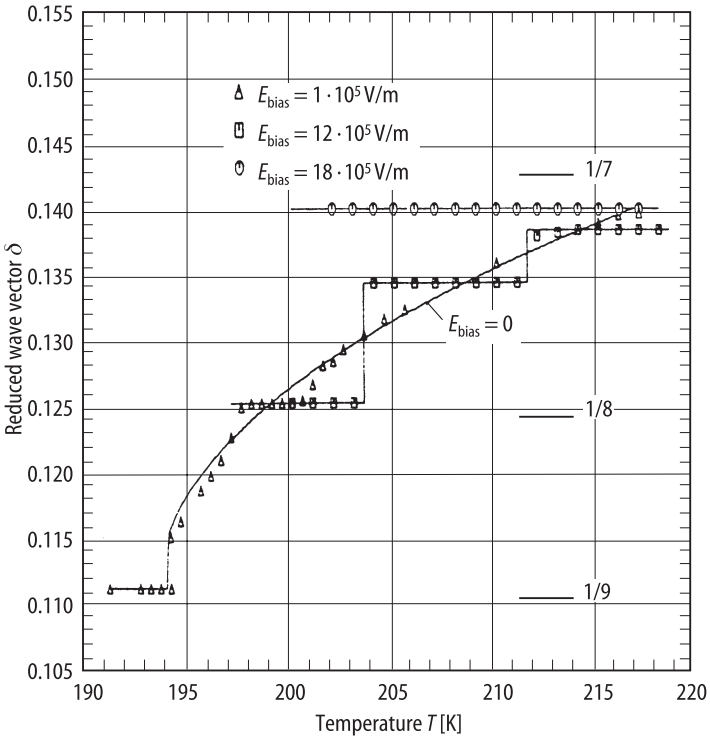

Fig. 50A-1-121. $SC(ND_2)_2$. δ vs. T [83Mou]. Parameter: E_{bias}. δ: reduced wave vector of lattice modulation.

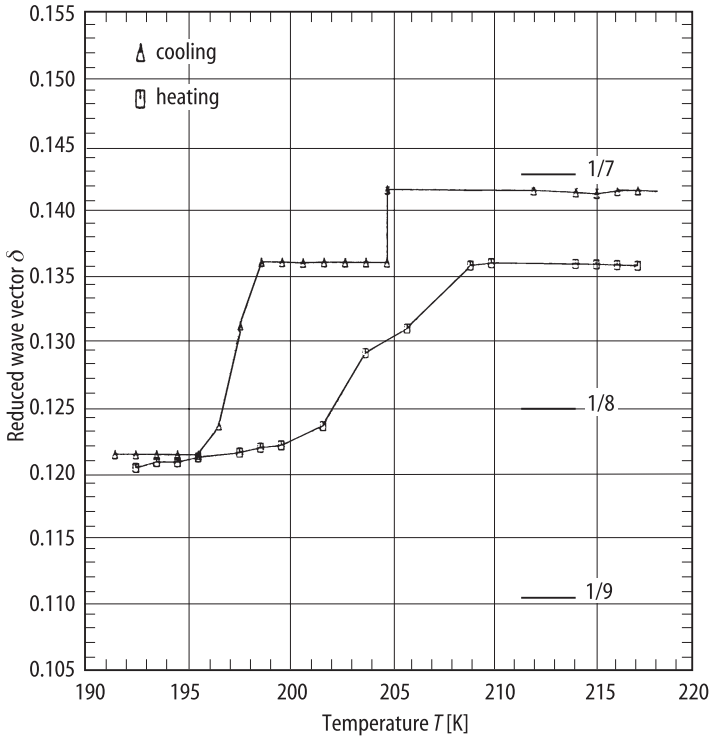

Fig. 50A-1-122. $SC(ND_2)_2$. δ vs. T [83Mou]. Under an applied field $E_{bias} = 1.8 \cdot 10^6$ V m^{-1} sample was cooled from high temperature to $T = 217$ K, then the field was removed. After the process, the measurements of cooling run and of heating run were made. δ: reduced wave vector of lattice modulation.

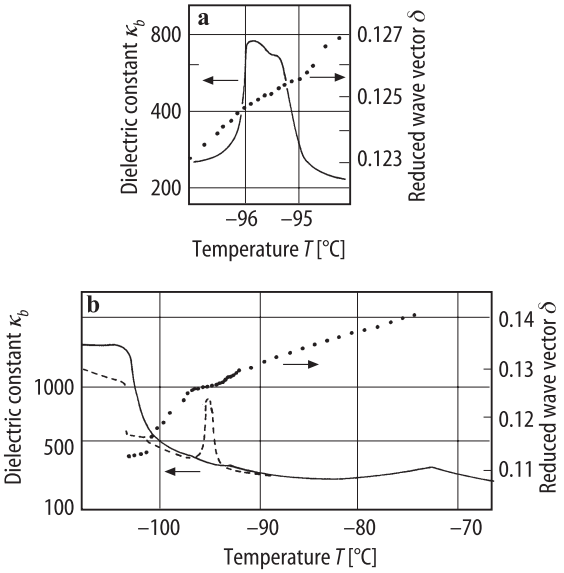

Fig. 50A-1-123. $SC(NH_2)_2$. δ, κ_b vs. T [89Mas]. (**a**) cooling run, (**b**) heating run after cooled from –65 °C to –130 °C applying $E_{bias} = 2.5 \cdot 10^6$ V m^{-1}. The broken line in (b) shows κ_b without E_{bias} on cooling. δ: reduced wave vector of lattice modulation.

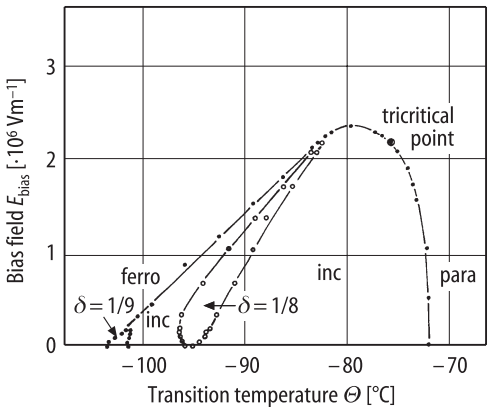

Fig. 50A-1-124. $SC(NH_2)_2$. Θ vs. E_{bias} determined by X-ray measurements [89Mas]. inc: incommensurate phase.

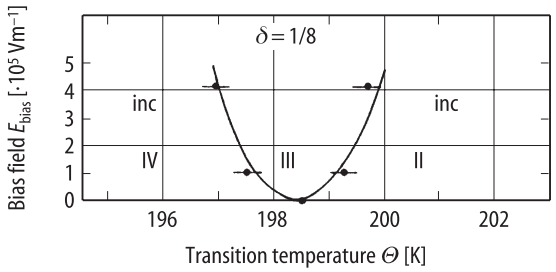

Fig. 50A-1-125. $SC(ND_2)_2$. Θ vs. E_{bias} in the vicinity of phase III [82Mou]. inc: incommensurate phase.

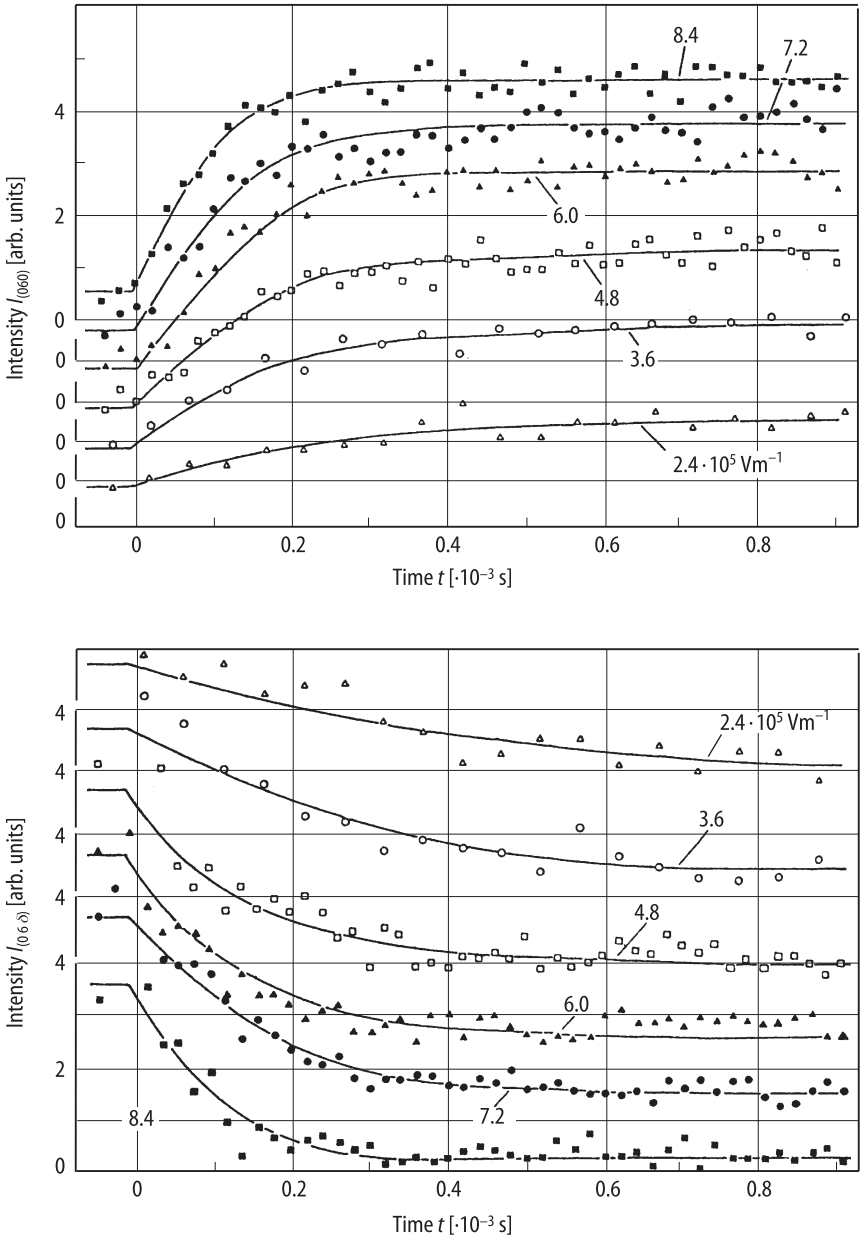

Fig. 50A-1-126. SC(NH$_2$)$_2$. $I_{(060)}$, $I_{(06\delta)}$ vs. t at $T = \Theta_{VI-V}$ + 1 K [89Kom]. t: time after the onset of the electric field. Parameter: E_{bias}. δ: reduced wave vector of lattice modulation.

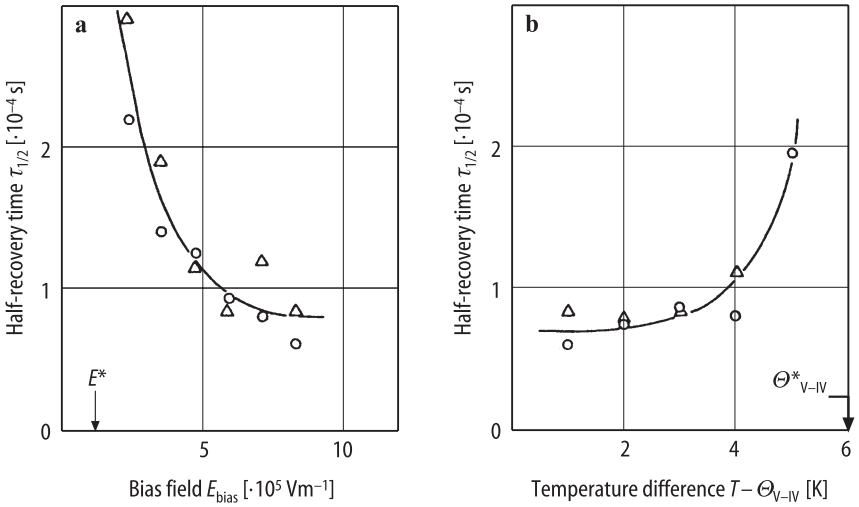

Fig. 50A-1-127. $SC(NH_2)_2$. Electric field and temperature dependence of the half-recovery time $\tau_{1/2}$ [89Kom]. (**a**) $\tau_{1/2}$ vs. E_{bias} at $T = \Theta_{V-IV} + 1$ K, (**b**) $\tau_{1/2}$ vs. $(T - \Theta_{V-IV})$ at $E_{bias} = 8.4 \cdot 10^5$ V m^{-1}. $\tau_{1/2}$ is defined by $I(\tau_{1/2}) = \frac{1}{2}(I(0) + I(\infty))$. E^*: electric field which induces V–IV phase transition at Θ_{V-IV} + 1K. Θ^*_{V-IV}: V–IV transition temperature at $E_{bias} = 8.4 \cdot 10^5$ V m^{-1}.

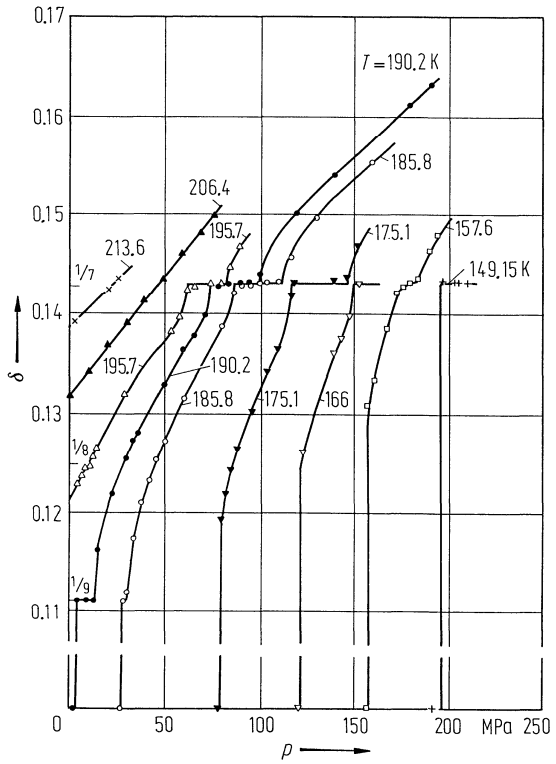

Fig. 50A-1-128. $SC(ND_2)_2$. δ vs. p [82Den]. Parameter: T. δ: reduced wave vector of lattice modulation.

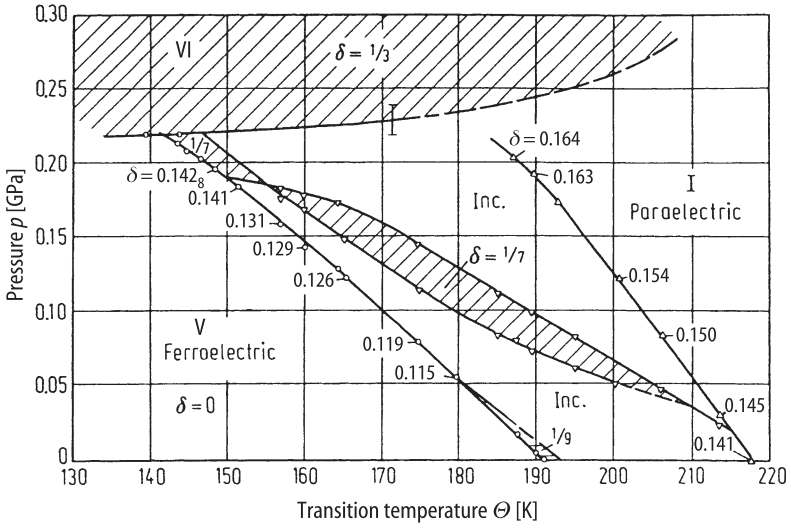

Fig. 50A-1-129. $SC(ND_2)_2$. p–Θ phase diagram with reduced wave vector δ of lattice modulation [82Den]. Values of δ are indicated on the phase boundaries. Inc.: incommensurate phase. Hatched area: commensurate phase.

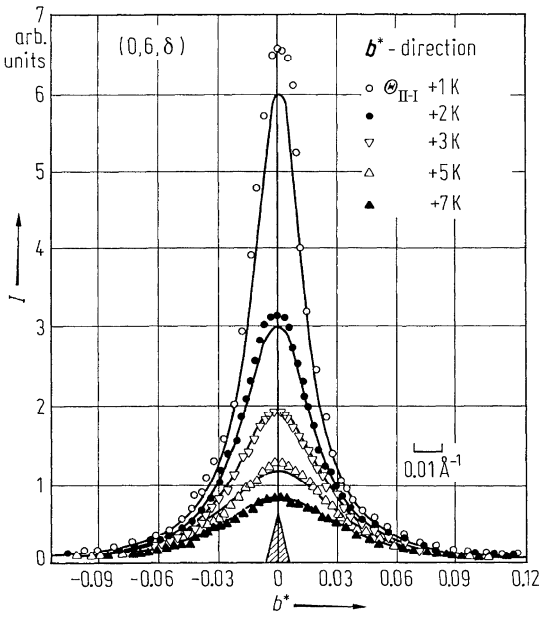

Fig. 50A-1-130. $SC(NH_2)_2$. X-ray diffuse scattering around (0, 6, δ) reciprocal lattice point in phase I [79Tak]. I vs. b^*. Θ_{II-I} = 202 K. δ: position where the first satellite scattering appears. Hatched triangle in the figure (at $b^* = 0$) indicates the size of resolution.

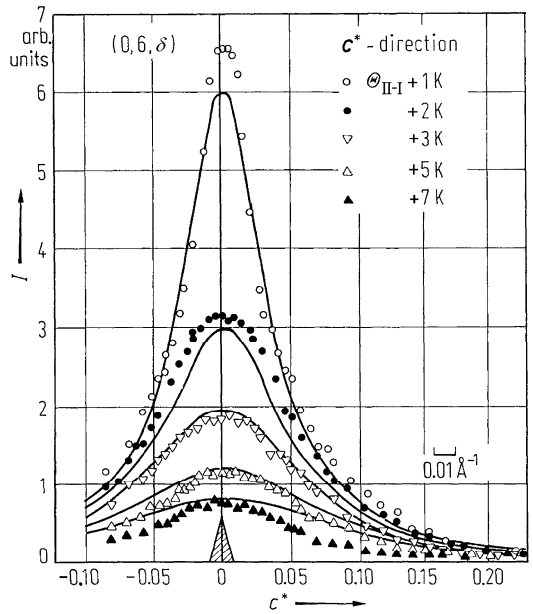

Fig. 50A-1-131. $SC(NH_2)_2$. X-ray diffuse scattering around (0, 6, δ) reciprocal lattice point in phase I [79Tak]. I vs. c^*. Θ_{II-I} = 202 K. δ: position where the first satellite scattering appears. Hatched triangle in the figure (at c^* = 0) indicates the size of resolution.

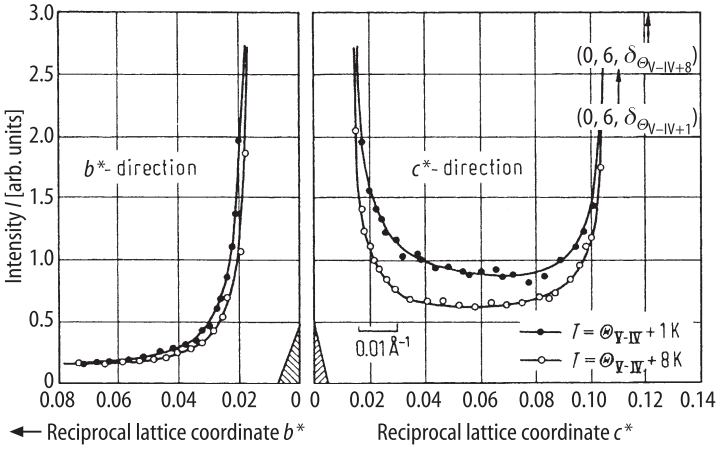

Fig. 50A-1-132. $SC(NH_2)_2$. X-ray diffuse scattering around (0, 6, 0) in phase IV [79Tak]. I vs. b^* and c^*. Θ_{V-IV} = 169 K. Hatched triangle indicates the size of resolution.

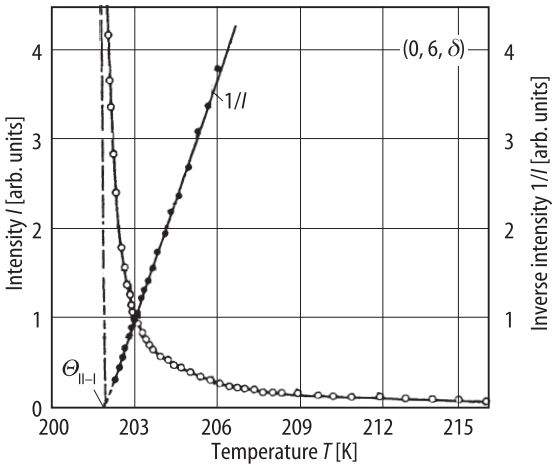

Fig. 50A-1-133. $SC(NH_2)_2$. X-ray diffuse scattering at (0, 6, δ) reciprocal lattice point in phase I [79Tak]. I and $1/I$ vs. T. I: intensity of X-ray diffuse scattering. $\Theta_{II–I}$ = 202 K. δ: position where the first satellite scattering appears.

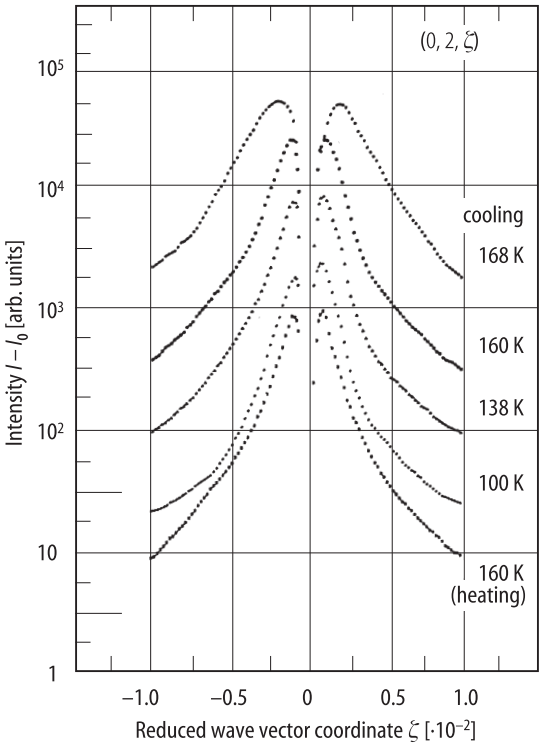

Fig. 50A-1-134. $SC(NH_2)_2$. Excess diffuse scattering around the Bragg reflection 020. ($I - I_0$) vs. ζ [91Mas]. Parameter: T. I_0: intensity at 170 K. ζ: reduced wave vector coordinate in units of $1/c$.

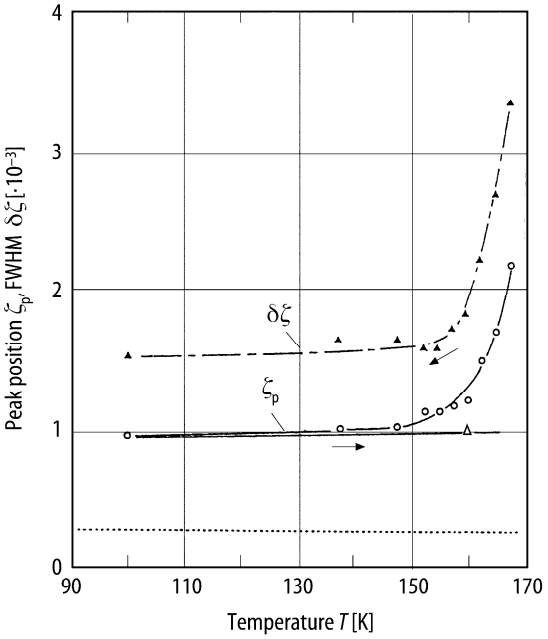

Fig. 50A-1-135. $SC(NH_2)_2$. ζ_p and $\delta\zeta$ vs. T [91Mas]. ζ_p: peak position of the diffuse scattering 02ζ (open circle: cooling, open triangle: heating). $\delta\zeta$: full width at half maximum (FWHM) of the diffuse scattering (full triangle). ζ: reduced wave vector coordinate in units of $1/c$. FWHM of the Bragg reflection 020 is indicated by a dotted line.

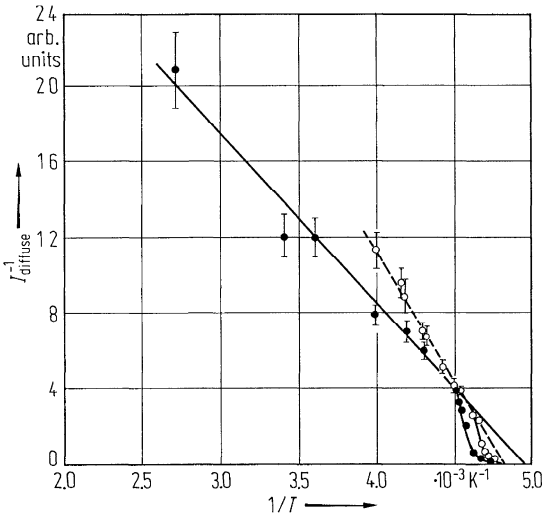

Fig. 50A-1-136. $SC(ND_2)_2$. $I^{-1}_{diffuse}$ vs. T^{-1} [75McK1]. $I_{diffuse}$: neutron diffuse scattering intensity at (0, 4.175, 5). Open and full circles correspond to experiments carried out on different spectrometers. Used crystallographic axes are (***a′***, ***b′***, ***c′***), the case 2 in 1b.

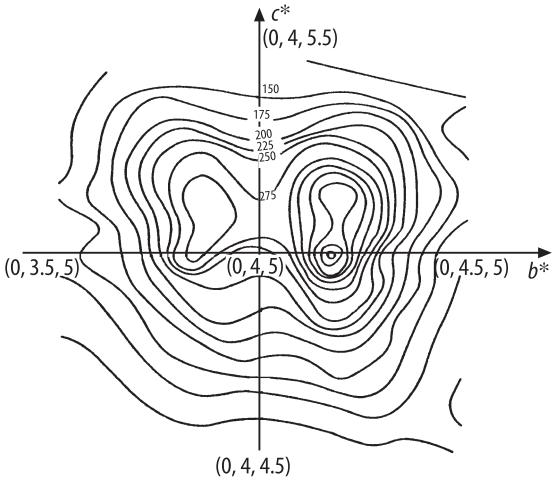

Fig. 50A-1-137. $SC(ND_2)_2$. Distribution of diffusely scattered thermal neutrons around $(0,4,5)$ [75McK1]. T = 225 K. Used crystallographic axes are (***a′***, ***b′***, ***c′***), the case 2 in 1b.

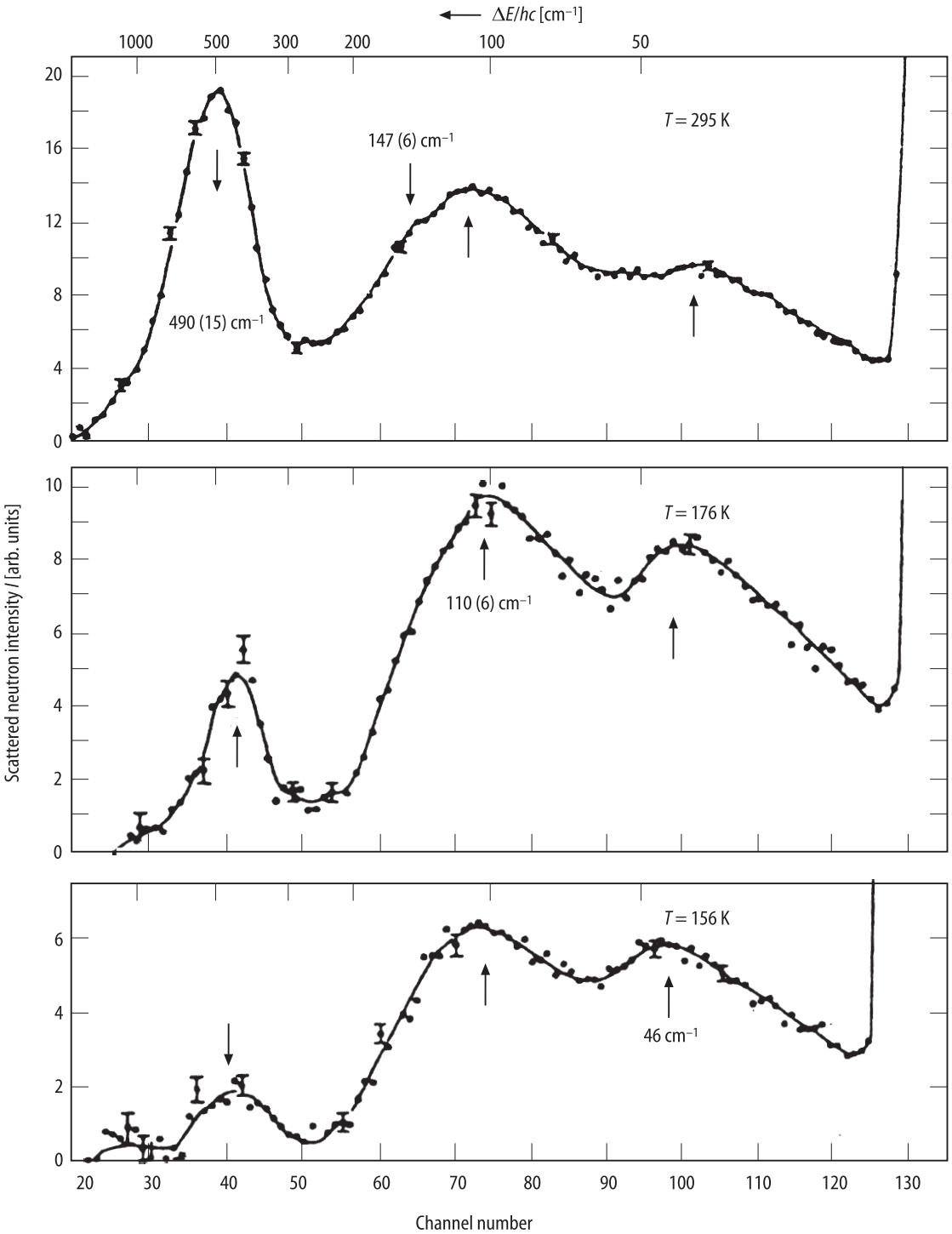

Fig. 50A-1-138. $SC(NH_2)_2$. Time of flight spectra of inelastically scattered neutrons [67Rus]. *I*: scattered neutron intensity. Parameter: *T*. Peak positions are indicated by arrows. Scattered angle = 60°. Polycrystalline sample. Effective mean energy of incident neutrons was 3.5 meV (28 cm^{-1}). Channel width: 25 µs per channel number.

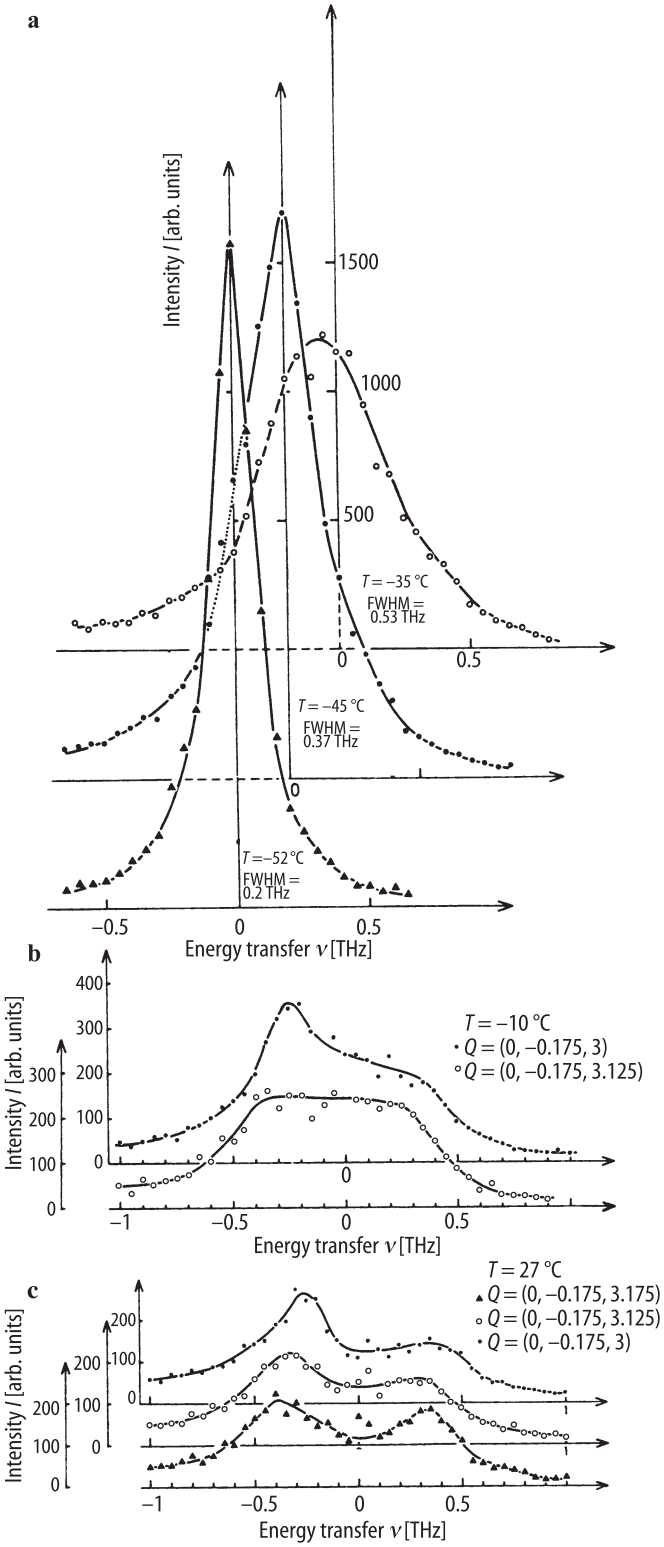

Fig. 50A-1-139. $SC(ND_2)_2$. I vs. ν [78Mou1]. I: inelastically scattered thermal neutrons measured by constant $\boldsymbol{Q}$ method. ν: energy transfer. Parameter: T. Used crystallographic axes are ($\boldsymbol{a}'$, $\boldsymbol{b}'$, $\boldsymbol{c}'$), the case 2 in 1b.

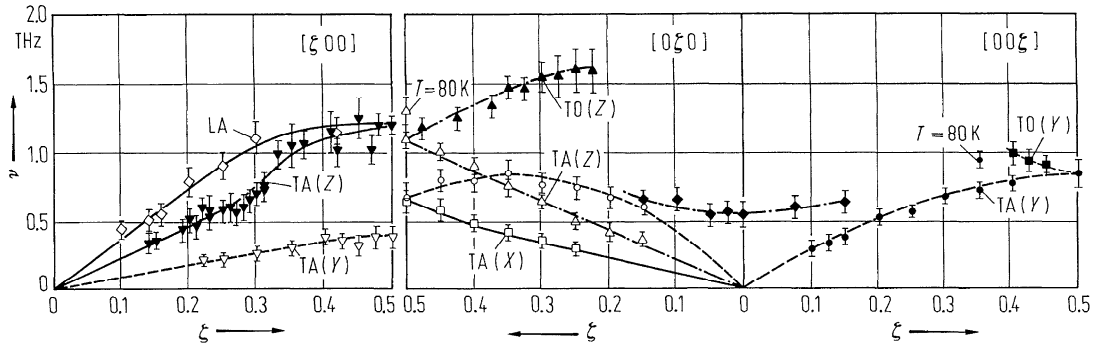

Fig. 50A-1-140. $SC(ND_2)_2$. ν vs. ζ [75McK2]. ν: phonon frequency observed by neutron inelastic scattering. ζ: reduced wave vector coordinate. TA(Z), TA(Y), …: $\boldsymbol{e}$ ∥ [001], $\boldsymbol{e}$ ∥ [010], …, where $\boldsymbol{e}$ denotes polarization of phonon. Mode assignments for open circle, full lozenge were not made. Used crystallographic axes are ($\boldsymbol{a}'$, $\boldsymbol{b}'$, $\boldsymbol{c}'$), the case 2 in 1b.

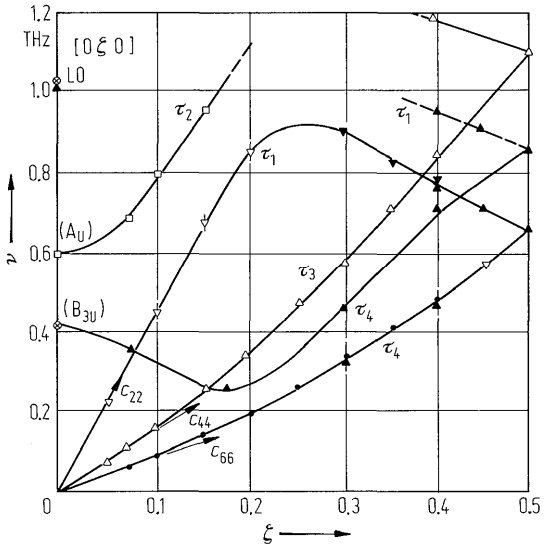

Fig. 50A-1-141. $SC(ND_2)_2$. Dispersion curves of lattice vibration along the direction of structural modulation, ν vs. ζ [80Mou2]. T = 300 K. Used crystallographic axes are ($\boldsymbol{a}'$, $\boldsymbol{b}'$, $\boldsymbol{c}'$), the case 2 in 1b. ζ: reduced wave vector coordinate. Open square: (043), open downside triangle: (040), full downside triangle: (400), open upside triangle: (002), full upside triangle: (003), full circle: (030), circle with cross: IR.

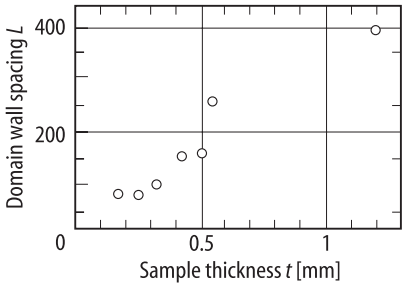

Fig. 50A-1-142. $SC(NH_2)_2$. L vs. t just below Θ_{V-IV} [94Mas]. L: domain wall spacing in units of c. t: sample thickness.

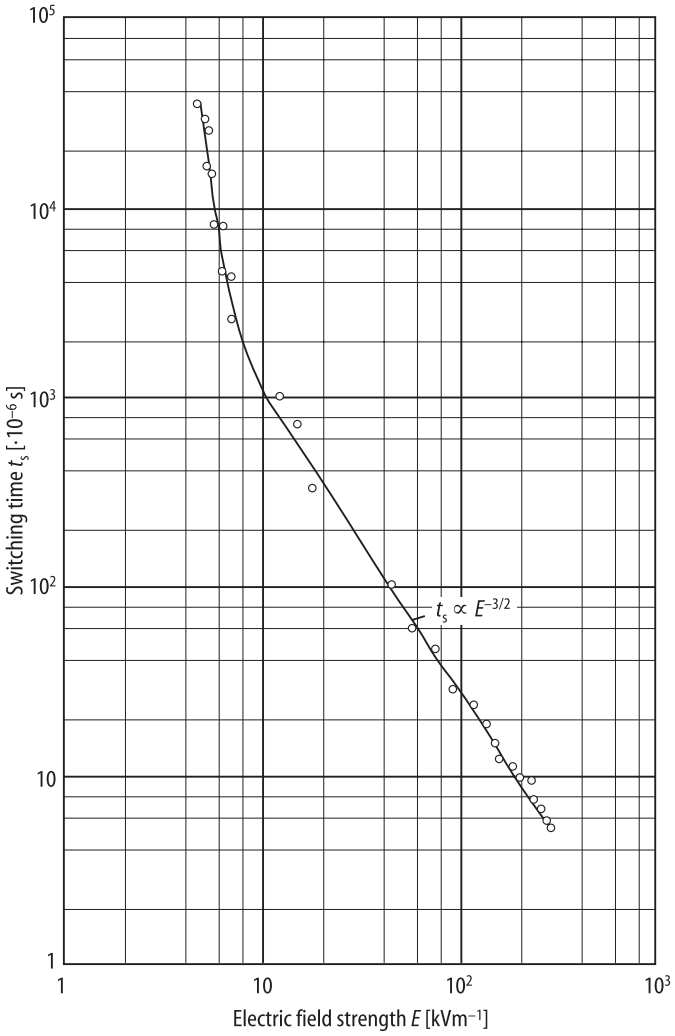

Fig. 50A-1-143. $SC(NH_2)_2$. t_s vs. E [59Gol]. t_s: switching time. T = 150 K.

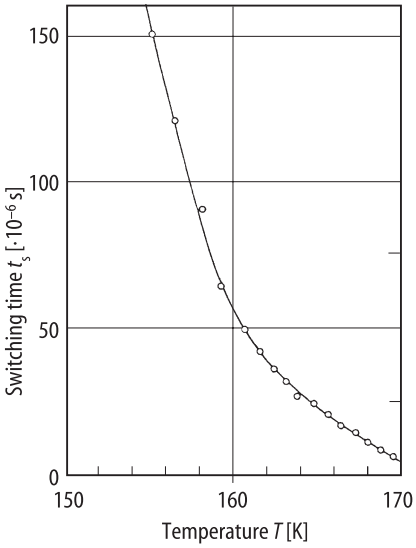

Fig. 50A-1-144. $SC(NH_2)_2$. t_s vs. T [90Ham]. t_s: switching time. E = 7.6 kV m^{-1}.

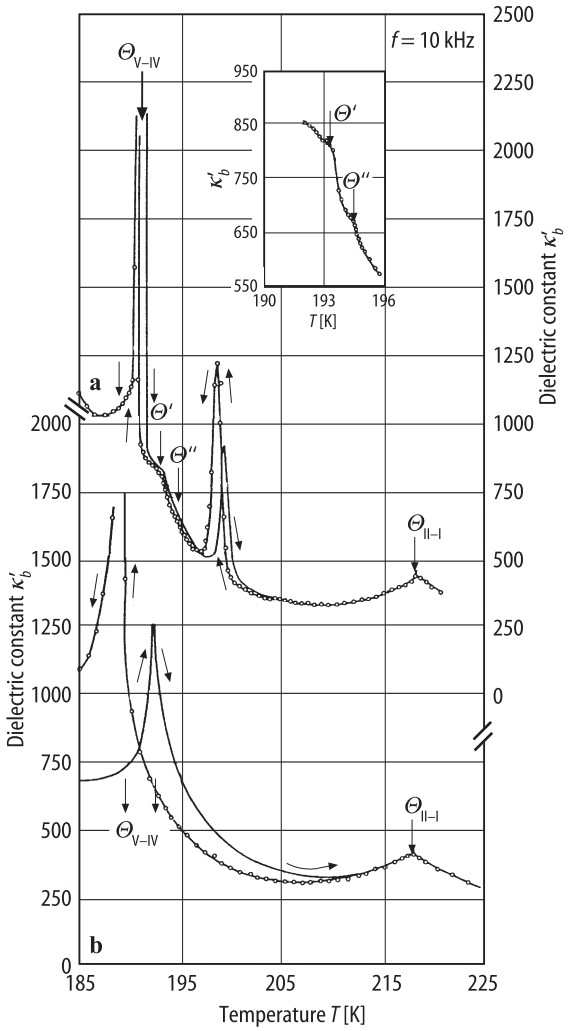

Fig. 50A-1-145. $SC(ND_2)_2$. Radiation damage effect [87And]. κ'_b vs. T at f = 10 kHz. (**a**) dosage 0, (**b**) after $90 \cdot 10^4$ Gy X-ray exposure.

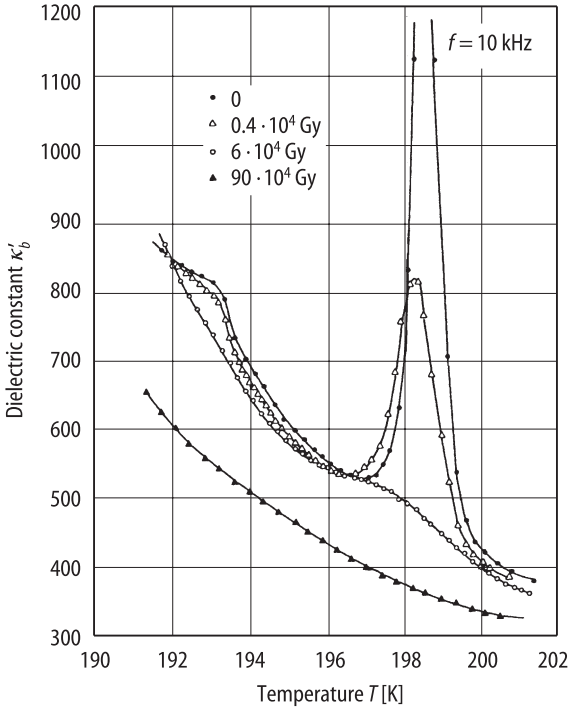

Fig. 50A-1-146. SC(ND_2)$_2$. Radiation damage effect [87And]. κ'_b vs. T at f = 10 kHz. Parameter: X-ray dosage.

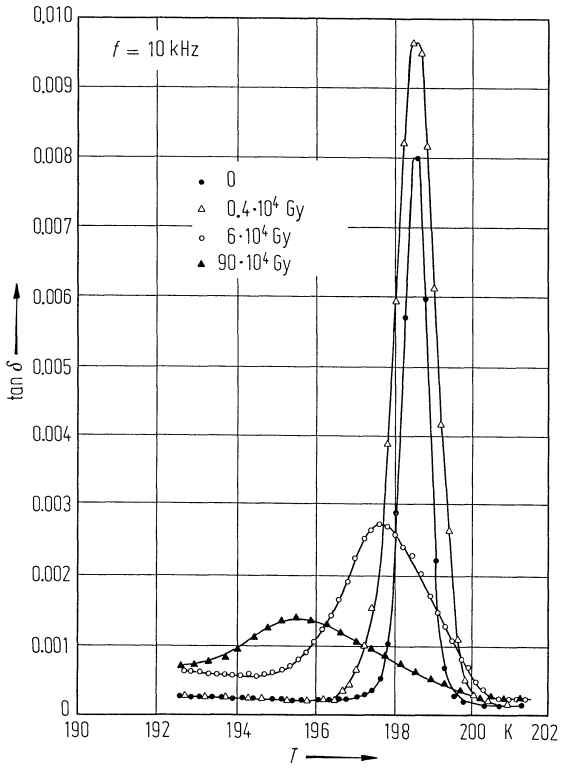

Fig. 50A-1-147. SC(ND_2)$_2$. Radiation damage effect [87And]. tan δ vs. T at f = 10 kHz. Parameter: X-ray dosage.

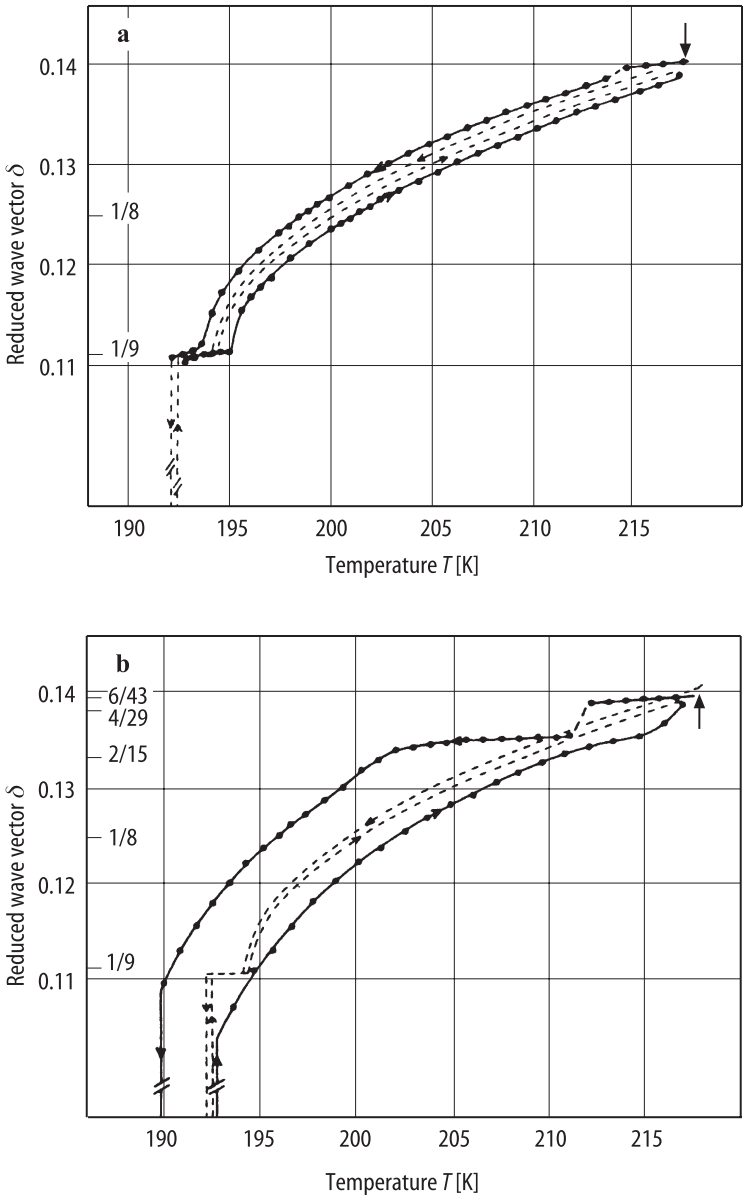

Fig. 50A-1-148. $SC(ND_2)_2$. δ vs. T [87And]. δ: reduced wave vector of lattice modulation. (**a**) before irradiation (dashed lines) and after a 10 Mrad X-ray irradiation (solid lines). (**b**) after a 100 Mrad X-ray irradiation (solid lines). The dashed lines in (b) are the same as in (a). Vertical arrows indicate I–II transition.

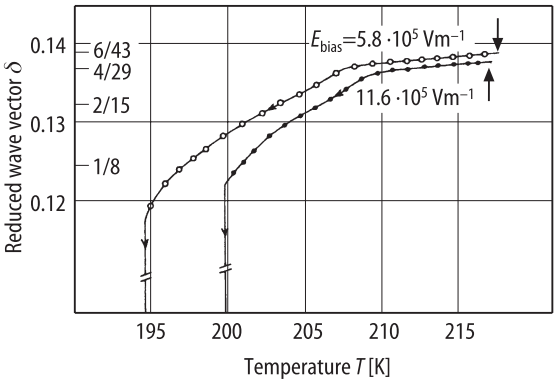

Fig. 50A-1-149. $SC(ND_2)_2$. δ vs. T [87And]. Parameter: E_{bias}. δ: reduced wave vector of lattice modulation. X-ray irradiated sample with 100 Mrad dosage.

References

10Gro Groth, P.: Chemische Kristallographie, Teil 3, Leipzig: Wilhelm Engelman, 1910.
28Dem Demeny, L., Nitta, I.: Bull. Chem. Soc. Jpn. **3** (1928) 128.
28Hen Hendricks, S.B.: J. Am. Chem. Soc. **50** (1928) 2455.
32Wyc Wyckoff, R.W.G., Corey, R.B.: Z. Kristallogr. **81** (1932) 386.
38Bri Bridgman, P.W.: Proc. Am. Acad. Arts Sci. **72** (1938) 226.
54Win Winchell, A.N.: The Optical Properties of Organic Compounds, New York: Academic Press, 1954.
56Sol Solomon, A.L.: Phys. Rev. **104** (1956) 1191.
58Kun Kunchur, N.R., Truter, M.R.: J. Chem. Soc. **517** (1958) 2551.
59Gol Goldsmith, G.J., White, J.G.: J. Chem. Phys. **31** (1959) 1175.
60Dvo Dvoryankin, V.F., Vainshtein, B.K.: Kristallografiya **5** (1960) 589.
61Ems1 Emsley, J.W., Smith, J.A.S.: Trans. Faraday Soc. **57** (1961) 893.
61Ems2 Emsley, J.W., Smith, J.A.S.: Trans. Faraday Soc. **57** (1961) 1233.
61Kab Kabalkina, S.S.: Zh. Fiz. Khim **35** (1961) 276; Russ. J. Phys. Chem. (English Transl.) **35** (1961) 133.
61Vai Vainshtein, B.K., Dvoryankin, V.F.: Dokl. Akad. Nauk SSSR **140** (1961) 111; Sov. Phys. Dokl. (English Transl.) **6** (1962) 747.
62Fut Futama, H.: J. Phys. Soc. Jpn. **17** (1962) 434.
63Cha Chang, E., Westrum Jr., E.F.: Unpublished data cited in [63Fox].
63Fox Fox, D., Labes, M.M., Weissenberger, A.: Physics and Chemistry of Organic Solid State, Vol. 1, New York/London: Interscience Publishers, A Division of John Wiley & Sons, 1963.
63Leo Leonidova, G.G.: Fiz. Tverd. Tela **5** (1963) 3430; Sov. Phys. Solid State (English Transl.) **5** (1964) 2519.
63Nak Nakagawa, T., Sawada, S., Kawakubo, T., Nomura, S.: J. Phys. Soc. Jpn. **18** (1963) 1227.
64Smi Smith, D.H., Cotts, R.M.: J. Chem. Phys. **41** (1964) 2403.
65Kop Koptsik, V.A., Toshev, S.D.: Izv. Akad. Nauk SSSR, Ser. Fiz. **29** (1965) 956; Bull. Acad. Sci. USSR, Phys. Ser. (English Transl.) **29** (1965) 960.
67Fut Futama, H., Shiozaki, Y., Chiba, A., Tanaka, E., Mitsui, T., Furuichi, J.: Phys. Lett. A **25** (1967) 8.
67Rus Rush, J.J.: J. Chem. Phys. **47** (1967) 4278.
67Sug Sugai, S., Mochizuki, J., Futama, H.: Unpublished work (1967).
67Tak Takahashi, H., Schrader, B., Meier, W., Gottlieb, K.: J. Chem. Phys. **47** (1967) 3842.
67Tru Truter, M.R.: Acta Crystallogr. **22** (1967) 556.
68Elc Elcombe, M.M., Taylor, J.C.: Acta Crystallogr. Sect. A **24** (1968) 410.
69Ges Gesi, K.: J. Phys. Soc. Jpn. **26** (1969) 107.
70McK McKenzie, D.R., Ham, N.S., Whitfield, H.J.: Solid State Commun. **8** (1970) 2059.
70Yog Yoganarasimhan, S.R., Sood, R.K.: Philos. Mag. [8] **22** (1970) 1075.
71Jef Jeffery, J.W.: J. Appl. Crystallogr. **4** (1971) 334.
71ORe O'Reilly, D.E., Peterson, E.M., El Saffar, Z.M.: J. Chem. Phys. **54** (1971) 1304.
71Shi Shiozaki, Y.: Ferroelectrics **2** (1971) 245.
72Ban Bandy, A., Cossac, G.L., Lippincott, E.R.: Spectrochim. Acta A **28** (1972) 1807.
72Kla1 Klapper, H.: J. Cryst. Growth **15** (1972) 281.
72Kla2 Klapper, H.: Phys. Status Solidi (a) **14** (1972) 443.
72Lau Laulicht, I., Pellach, E., Brith, M.: J. Chem. Phys. **57** (1972) 2857.
73Fle Fleming, J.W., Siapkas, D., Lewis, J., Wilkinson, G.R.: High-Freq. Dielectr. Meas., Tutorial Conf. (1972), Guildford: IPC Sci. Technol. Press, 1973.
73Hat Hatano, J., Suda, F., Futama, H.: Jpn. J. Appl. Phys. **12** (1973) 1644.
73McK McKenzie, D.R., Dryden, J.S.: J. Phys. C **6** (1973) 767.
73Tsu Tsunekawa, S., Ishibashi, Y., Takagi, Y.: J. Phys. Soc. Jpn. **34** (1973) 470.
74Ben Benoit, J.P., Chapelle, J.P.: Solid State Commun. **14** (1974) 883.
74Ruc Rucci, A., Serpi, A., Serpi Macciotta, P.: Phys. Status Solidi (a) **25** (1974) K191.
75Cza Czapla, Z., Kolodziej, H.A., Sobczyk, L.: J. Chem. Soc., Faraday Trans. II **71** (1975) 763.

75Del Delahaigue, A., Khelifa, B., Jouve, P.: Phys. Status Solidi (b) **72** (1975) 585.
75Fig Figuiere, P., Ghelfenstein, M., Szwarc, H.: Chem. Phys. Lett. **33** (1975) 99.
75Kli Klimowski, J., Wanarski, W., Ozgo, D.: Acta Phys. Pol. A **48** (1975) 307.
75Mac Macciotta Serpi, P., Rucci, A., Serpi, A.: J. Lumin. **9** (1975) 488.
75McK1 McKenzie, D.R.: J. Phys. C **8** (1975) 1607.
75McK2 McKenzie, D.R.: J. Phys. C **8** (1975) 2003.
76Bre Brehat, F., Claudel, J., Strimer, P., Hadni, A.: J. Phys. (Paris) Lett. **37** (1976) L229.
76Iqb Iqbal, Z., Christoe, C.W.: Chem. Phys. Lett. **37** (1976) 460.
76Kla Klapper, H.: J. Appl. Crystallogr. **9** (1976) 310.
76Kli Klimowski, J., Wanarski, W., Ozgo, D.: Phys. Status Solidi (a) **34** (1976) 697.
76Toe Toepfer, K.-D., Helberg, H.W.: Phys. Status Solidi (a) **35** (1976) 131.
77Iiz Iizumi, M., Gesi, K.: Unpublished work (1977).
77Khe Khelifa, B., Delahaigue, A., Jouve, P.: Phys. Status Solidi (b) **83** (1977) 139.
78Jak Jakubowski, B., Rohleder, J.W.: Mol. Cryst. Liq. Cryst. **46** (1978) 157.
78Mou1 Moudden, A.H., Denoyer, F., Benoit, J.P., Fitzgerald, W.: Solid State Commun. **28** (1978) 575.
78Mou2 Moudden, A.H., Denoyer, F., Lambert, M.: J. Phys. (Paris) **39** (1978) 1323.
78Mul1 Mullen, D., Heger, G., Treutmann, W.: Z. Kristallogr. **148** (1978) 95.
78Mul2 Mullen, D., Hellner, E.: Acta Crystallogr. Sect. B **34** (1978) 2789.
78Wad Wada, M., Sawada, A., Ishibashi, Y., Takagi, Y.: J. Phys. Soc. Jpn. **45** (1978) 1905.
79Cao Cao, A.X., Benoit, J.P., Hauret, G., Chapelle, J.P.: Solid State Commun. **31** (1979) 581.
79Mou Moudden, A.H., Denoyer, F., Lambert, M., Fitzgerald, W.: Solid State Commun. **32** (1979) 933.
79Tak Takenaka, H., Terauchi, H., Kawamori, A.: J. Phys. Soc. Jpn. **46** (1979) 914.
79Wan Wanarski, W.: Acta Phys. Pol. A **56** (1979) 197.
80Den Denoyer, F., Moudden, A.H., Lambert, M.: Ferroelectrics **24** (1980) 43.
80Kli Klimowski, J.: Phys. Status Solidi (a) **59** (1980) K39.
80Mou1 Moudden, A.H., Gatebois, L., Denoyer, F., Lambert, M.: Rev. Sci. Instrum. **51** (1980) 836.
80Mou2 Moudden, A.H.: Thesis, Université Paris-Sud, Orsay, 1980.
80Sia Siapkas, D.I.: Ferroelectrics **29** (1980) 29.
80Vol Volkov, A.A., Ishihashi, Y., Kozlov, G.V., Lebedev, S.P., Petzelt, J., Prokhorov, A.M.: J. Phys. Soc. Jpn. **49** (1980) Suppl. B, 78.
80Win1 Winterfeldt, V., Schaack, G.: Z. Phys. B **36** (1980) 303.
80Win2 Winterfeldt, V., Schaack, G.: Z. Phys. B **36** (1980) 311.
81Den Denoyer, F., Moudden, A.H., Bellamy, A., Currat, R., Vettier, C., Lambert, M.: C. R. Acad. Sci. (Paris), Ser. II **292** (1981) 13.
81Jam Jamet, J.P.: J. Phys. (Paris) Lett. **42** (1981) L123.
82Cao Cao, A.X., Krichene, S., Hauret, G., Benoit, J.P., Chapelle, J.P.: Solid State Commun. **43** (1982) 933.
82Den Denoyer, F., Moudden, A.H., Currat, R., Vettier, C., Bellamy, A., Lambert, M.: Phys. Rev. B **25** (1982) 1697.
82Ges1 Gesi, K.: J. Phys. Soc. Jpn. **51** (1982) 701.
82Ges2 Gesi, K., Iizumi, M.: J. Phys. Soc. Jpn. **50** (1982) 1047.
82Jam Jamet, J.P., Lederer, P., Moudden, A.H.: Phys. Rev. Lett. **48** (1982) 442.
82Kut Kutoglu, A., Scheringer, C., Meyer, H., Schweig, A.: Acta Crystallogr. Sect. B **38** (1982) 2626.
82Mou Moudden, A.H., Svensson, E.C., Shirane, G.: Phys. Rev. Lett. **49** (1982) 557.
82Mul Mullen, D.: Acta Crystallogr. Sect. B **38** (1982) 2620.
82Ori Orihara, H., Ishidate, T., Sawada, A., Ishibashi, Y.: J. Phys. Soc. Jpn. **51** (1982) 1216.
82Reh Rehwald, W., Vonlanthen, A.: J. Phys. C **15** (1982) 5361.
82Vol Volkov, A.A., Kozlov, G.V., Lebedev, S.P., Petzelt, J., Ishibashi, Y.: Ferroelectrics **45** (1982) 157.
83Bar Barreto, M.N., Lederer, P., Jamet, J.P.: Phys. Rev. B **28** (1983) 3994.
83Ben Benoit, J.P., Thomas, F., Berger, J.: J. Phys. (Paris) **44** (1983) 841.
83Mou Moudden, A.H., Moncton, D.E., Axe, J.D.: Phys. Rev. Lett. **51** (1983) 2390.
84Ben Benoit, J.P., Berger, J.: Ferroelectrics **53** (1984) 235.
84Dur Durand, D., Dénoyer, F., Currat, R., Vettier, C.: Phys. Rev. B **30** (1984) 1112.
85Dur Durand, D., Dénoyer, F., Moussa, F.: Cited in [86Den].

85Far Farhi, R., Moch, P.: J. Phys. C **18** (1985) 925.

85Hat Hatano, J., Kume, N., Kubota, K., Tsukamoto, T., Futama, H., Gesi, K.: Jpn. J. Appl. Phys. **24** (1985) Suppl. 24-2, 844.

86Bli Blinc, R., Levanyuk, A.P. (eds.): Incommensurate Phases in Dielectrics. 2. Materials. Modern Problems in Condensed Matter Sciences, Vol. 14.2, Amsterdam: Elsevier Science Publishers B.V. (North-Holland), 1986.

86Den Dénoyer, F., Currat, R.: Modulated Phases in Thiourea, pp. 129-160, cited in [86Bli].

86Hau Haussühl, S., Pähl, M.: Z. Kristallogr. **176** (1986) 147.

86Led Lederer, P., Jamet, J.P., Montambaux, G.: Ferroelectrics **66** (1986) 25.

87And Andre, G., Durand, D., Denoyer, F., Currat, R., Moussa, F.: Phys. Rev. B **35** (1987) 2909.

87Bou Boudot, C., Mangin, J., Durand, D.: Phase Transitions **9** (1987) 163.

87Tak Takahashi, I., Onodera, A., Shiozaki, Y.: Phys. Rev. B **36** (1987) 7008.

88Gao Gao, Y., Gajhede, M., Mallinson, P., Petricek, V., Coppens, P.: Phys. Rev. B **37** (1988) 1825.

88Kim Kim, K.-T., Kim, J.-J.: J. Phys. Soc. Jpn. **57** (1988) 2213.

88Sim Simonson, T., Dénoyer, F., Currat, R., Vettier, C.: J. Phys. (Paris) **49** (1988) 471.

88Tak Takahashi, I., Onodera, A., Shiozaki, Y.: J. Phys. C **21** (1988) 5699.

88Tan Tanisaki, S., Mashiyama, H., Hasebe, K.: Acta Crystallogr. Sect. B **44** (1988) 441.

89Ham Hamano, K., Sakata, H., Maruyama, H., Ema, K.: Ferroelectrics **96** (1989) 139.

89Kim Kim, K.-T., Kim, J.: J. Phys. Condens. Matter **1** (1989) 7957.

89Kom Komori, S., Hayase, S., Terauchi, H.: J. Phys. Condens. Matter **1** (1989) 3789.

89Lee Lee, S.-M., Kwun, S.-I.: J. Korean Phys. Soc. **22** (1989) 336.

89Mas Mashiyama, H., Jida, S., Tanisaki, S.: Ferroelectrics **96** (1989) 133.

89Zun Zuñiga, F.J., Madariaga, G., Paciorek, W.A., Pérez-Mato, J.M., Ezpeleta, J.M., Etxebarria, I.: Acta Crystallogr. Sect. B **45** (1989) 566.

90Far Farhi, R., Schäfer, F.-J., Kleemann, W.: Ferroelectrics **105** (1990) 255.

90Ham Hamano, K., Sugiyama, T., Sakata, H.: J. Phys. Soc. Jpn. **59** (1990) 4476.

90Mad Madariaga, G., Zuñiga, F.J., Paciorek, W.A., Pérez-Mato, J.M., Ezpeleta, J.M., Etxebarria, I.: Ferroelectrics **105** (1990) 309.

90Mas Mashiyama, H., Sakamoto, M., Jida, S.: Ferroelectrics **105** (1990) 273.

90Ono Onodera, A., Fujiwara, Y., Kato, Y., Takahashi, I., Shiozaki, Y.: Ferroelectrics **105** (1990) 231.

90Tak Takahashi, I., Onodera, A., Shiozaki, Y.: Acta. Crystallogr. Sect. B **46** (1990) 661.

90Yam Yamashita, H., Yagi, T., Onodera, A., Shiozaki, Y.: J. Phys. Soc. Jpn. **59** (1990) 2293.

91Hol Holderna-Matushkiewich, K., Klimowski, J.: Izv. Akad. Nauk SSSR, Ser. Fiz. **55** (1991) 526; Bull. Acad. Sci. USSR, Phys. Ser. (English Transl.) **55** (1991) 106.

91Mas Mashiyama, H., Sakamoto, M., Nakamura, H., Kasano, H., Asahi, T., Hasebe, K., Kishimoto, S.: J. Phys. Soc. Jpn. **60** (1991) 1755.

92Aoy Aoyama, J., Suzuki, S., Takagi, M.: J. Phys. Soc. Jpn. **61** (1992) 3613.

92Che Chen, X.K., Li, G., Du, W.M., Cummins, H.Z.: Ferroelectrics **137** (1992) 251.

92Gla Gladkii, V.V., Kirikov, V.A., Ivanova, E.S., Kallaev, S.N.: Fiz. Tverd. Tela **34** (1992) 3170; Sov. Phys. Solid State (English Transl.) **34** (1992) 1695.

93Iga Igaruta, J.M., Lopez-Echarri, A., Breczewski, T., Ruiz-Larrea, I.: Phase Transitions **46** (1993) 47.

93Kan Kang, S.-Y., Kim, J.-J.: Phys. Rev. B **47** (1993) 12263.

94Bag Bagautdinov, B.Sh., Shmyt'ko, I.M.: Pis'ma Zh. Eksp. Teor. Fiz. **59** (1994) 171; JETP Lett. (English Transl.) **59** (1994) 182.

94Bil Billesbach, D.P., Ullman, F.G.: Ferroelectrics **155** (1994) 221.

94Kan Kang, S.-Y., Kim, J.-J.: Ferroelectrics **155** (1994) 263.

94Mas Mashiyama, H., Mizota, N., Tsubouchi, A.: Ferroelectrics **157** (1994) 81.

94Ono1 Onodera, A., Watanabe, O., Yamashita, H., Haga, H., Shiozaki, Y.: Ferroelectrics **155** (1994) 311.

94Ono2 Onodera, A., Haga, H., Denoyer, F., Godart, J., Shiozaki, Y.: Ferroelectrics **155** (1994) 305.

94Tak Takagi, M., Suzuki, S.: J. Phys. Soc. Jpn. **63** (1994) 1580.

96Ara Aramburu, I., Madariaga, G., Pérez-Mato, J.M., Breczewski, T.: Acta Crystallogr. Sect. A **52** (1996) 203.

96Mag Magataev, V.K., Glushkov, V.F., Gladkii, V.V., Zheludev, I.S.: Kristallografiya **41** (1996) 116; Crystallogr. Rep. (English Transl.) **41** (1996) 108.

96Noz Nozaki, R., Nakano, H., Noda, N., Haga, H., Shiozaki, Y.: J. Korean Phys. Soc. **29** (1996) S736.
97Ara Aramburu, I., Madariaga, G., Pérez-Mato, J.M.: Acta Crystallogr. Sect. A **53** (1997) 329.